IntechOpen

Power Plants in the Industry

Edited by Tolga Taner

POWER PLANTS IN THE INDUSTRY

Edited by **Tolga Taner**

Power Plants in the Industry
http://dx.doi.org/10.5772/intechopen.73347
Edited by Tolga Taner

Contributors

Valentina Evgenievna Zavalova, Alexei Shurupov, Alexander Kozlov, Mihail Shurupov, Nina Shurupova, Vladimir Fortov, Tat-Hean Gan, Anurag Dhutti, Jihong Wang, Decai Li, Wenbin Zhang, Shutaro Takeda, Richard Pearson, Adelaida Mihaela Duinea, Junio Damasceno, Eduarda Nascimento, Sabrinne Kelly Souza, Tolga Taner

Notice

First published in London, United Kingdom, 2019 by IntechOpen
eBook (PDF) Published by IntechOpen, 2019
IntechOpen is the global imprint of INTECHOPEN LIMITED, registered in England and Wales, registration number: 11086078, The Shard, 25th floor, 32 London Bridge Street
London, SE19SG – United Kingdom
Printed in Croatia

British Library Cataloguing-in-Publication Data
A catalogue record for this book is available from the British Library

Additional hard and PDF copies can be obtained from orders@intechopen.com

Power Plants in the Industry
Edited by Tolga Taner

p. cm.

Print ISBN 978-1-78985-083-3

Online ISBN 978-1-78985-084-0

eBook (PDF) ISBN 978-1-83962-008-9

Meet the editor

Tolga Taner is the Head of the Department of Motor Vehicles and Transportation Technology at the Aksaray University since 2012. He received his B.S. degree in Mechanical Engineering in 1998; his M.S. degree in Mechanical Engineering from Pamukkale University, Denizli, Turkey, in 2002 and his Ph.D. degree in Mechanical Engineering from the Gazi University of Engineering Faculty, Ankara, Turkey, in 2013. In 2018, Inter-University Council (UAK) awarded him the title of Associate Professor. He also worked as a Lecturer (Part-Time) in the Department of Technical Programs, Middle East Technical in 2003-2006. His current research interests include exergy, renewable energy, and PEM fuel cells. He has published many scientific conference papers and books. In addition, he has been a manager and researcher in many research projects.

Contents

Preface

This is a book based on knowledge of power plants in the industry. In addition, the research of power plants can be the answer to many critical problems for energy production. Moreover, power plants with different fuels are also researched in this book.

This book will encourage both academic research and industrial application processes. From concept to publication, this book took approximately one year to complete. I thank the publisher, Intech, in particular the Author Service Manager, Ms. Sara Debeuc for her support, help, and guidance. I also thank all of the chapter authors for their huge efforts. Finally, I thank my family, my wife Öznur, and my daughter Özüm for their support.

I hope that this book will be helpful and that this book will make a scientific contribution to power plant workers, researchers, academics, MSc and PhD students, and other scientists in both the present and future.

Associate Professor Dr. Tolga Taner, PhD
Department of Motor Vehicles and Transportation Technology
Aksaray University
Aksaray, Turkey

Section 1

Power Plants and Technical Details

Chapter 1

Introductory Chapter: Application of Power Plants in the Industry

Tolga Taner and Mecit Sivrioglu

Additional information is available at the end of the chapter

http://dx.doi.org/10.5772/intechopen.82406

1. Introduction

Power plants are very significant for all industry sectors that depend on exergy processes. Since many factories use such energies for their major processes, they have installed power plants on account of their factories. Installing power plants can gain their energy in an efficient way for the factory. This book poses exergy and application technology to energy processes. This book impresses on the exergy with an overview of all of the energy systems. Energy and exergy efficiencies related to thermodynamic laws are carried out for the power plant and technology. All processes depend on energy that is used more than other similar factories.

These calculations can be determined by thermodynamics laws and their general and specific formulas. Using a Rankine Cycle is more effective than the other thermodynamic cycles. In addition, it includes mass and energy conversion according to a dead state. All these formulas and calculations pose energy and exergy efficiencies.

This book poses energy and exergy efficiency of energy systems and industry about several different factories. Technoeconomic analysis is carried out for the energy and exergy efficiency progresses that should be applied in power plant of factory, which is the center of a factory. In addition, power plant can be an essential influence for factories' lucrativeness. Hence, process stream for the factory energy solutions can be determined energy and exergy efficiencies. This application also can be used for energy saving by power plant's exergy. This book aims to define a comprehensive overview of the application of power plants. In conclusion, this book aims to demonstrate the efficiency of energy and new technological developments in many different areas for power plants.

2. A brief of power plants

This book covers energy and exergy efficiency of power plants in the industry. Technoeconomic analysis is carried out for the energy and exergy efficiency progresses that should be applied in power plant of many different factories, which are the center of a factory. In addition, power plant can be an essential influence for factory profit. For this reason, the process flow in the factory energy solution, the energy and exergy efficiencies contained in the Thermodynamic Law can be determined [1]. This application can be used for energy saving by the power plant. Moreover, there are Thermodynamic Laws in nuclear energy studies [2]. Energy and exergy analysis studies are also applied in wind energy [3]. Different topics and advantages such as solar energy and fuel cell energy and exergy analyses are emphasized from renewable energy sources [4-6]. Energy production also plays a major role in the power plants with fluid bed boiler [7-9]. Power plants are very significant for all industry sectors that depend on exergy processes. Since many factories use such energies for their major processes, they have installed power plants on account of their factories. Installing power plants can gain their energy in an efficient way for the factory. This book explores the view of general exergy that is valid for all energy systems. In this way, the cost of thermoeconomic, energy and exergy is known as exergoeconomic (technoeconomic) [10, 11]. These data can be analyzed by sensitivity, uncertainty, and other data analysis methods [1, 2, 4, 6, 12, 13]. Power plants are very significant for all industry sectors that depend on exergy processes. Since many factories use such energies for their major processes, they have installed power plants on account of their factories [14]. Installing power plants can gain their energy in an efficient way for the factory. These calculations are based on the laws of Thermodynamics and their general and special formulas.

2.1. Methods, calculations, and Rankine cycle

Using general cycle Rankine cycle that is more effective cycle than the other thermodynamic cycles. The Rankine cycle for the steam power plant is given in **Figure 1**. Boiler feed water is pumped to the economizer. From here, the pressure-reducing valve is sent to the boiler. In detail, energy calculations are made according to the input and output data from 6 points of Rankine cycle [1].

The temperature-entropy diagram in the Rankine cycle used for the steam power plant cycle is shown in **Figure 2**.

Rankine cycle calculations are calculated according to the following formulas. Thermodynamic vapour tables are used in calculations. The turbine dryness fraction is calculated from Eq. (1) as below [1]:

$$x_{t6,o} = (s_{t5,i} - s_{c1,i})/s_{c1,fg} \tag{1}$$

where $x_{t6,o}$—turbine dryness fraction output, [−]; $s_{t5,i}$—turbine entropy input, [kJ/kg K]; $s_{c1,i}$—condenser entropy input, [kJ/kg K]; and $s_{c1,fg}$—condenser entropy (difference between saturated liquid and steam), [kJ/kg K].

http://dx.doi.org/10.5772/intechopen.82406

The turbine enthalpy output is calculated from Eq. (2) as follows [1]:

$$h_{t6,o} = h_{t6f,o} + x_{t6,o}.h_{t6fg,o} \quad (2)$$

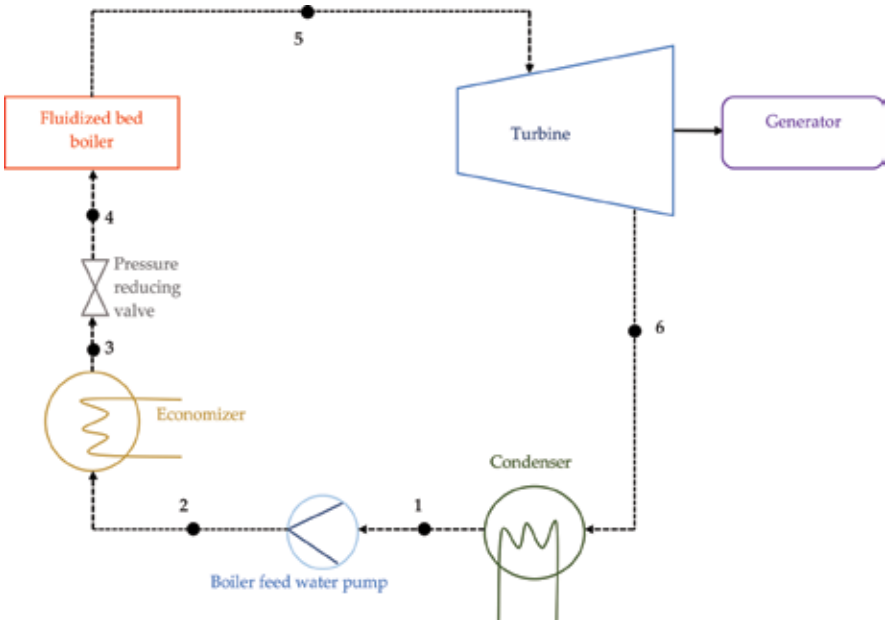

Figure 1. Steam power plant, Rankine cycle [1].

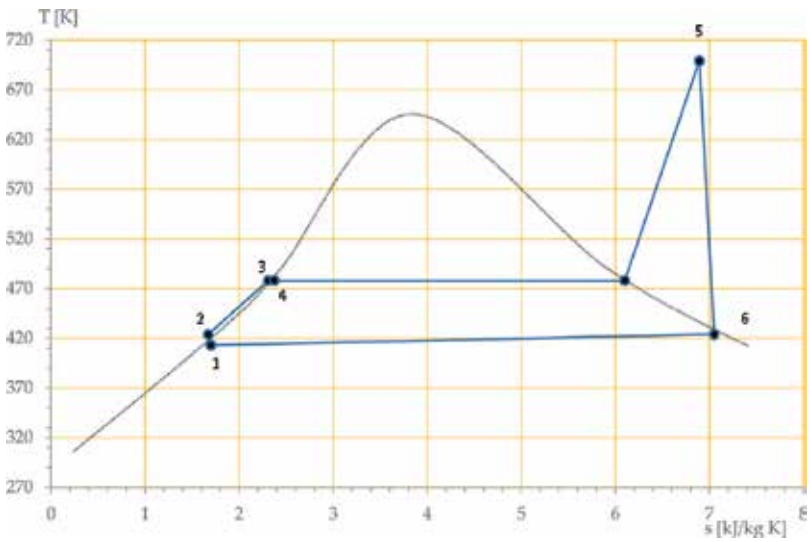

Figure 2. Steam power plant, Rankine cycle T-S diagram [1].

where $h_{t6,o}$—turbine enthalpy output, [kJ/kg]; $h_{t6f,o}$—turbine-saturated fluid enthalpy output, [kJ/kg]; and $h_{t6fg,o}$—urbine-saturated liquid and vapor enthalpy output, [kJ/kg].

Boiler feed water pump work calculations are presented in the following equation Eq. (3) [1]:

$$w_{pp} = \left[v_{pp,f} \times \left(P_2 - P_1\right)_{pp}\right] / \eta_{pp} \tag{3}$$

where w_{pp}—pump work, [kJ/kg]; $v_{pp,f}$—specific volume of saturated liquid of feed pump, [m^3/kg]; $(P_2 - P_1)_{pp}$—supply pump pressure difference, [kPa]; and η_{pp}—pump efficiency is accepted as 80% [1].

The heat input to the fluidized bed boiler is found in the following equation Eq. (4) [1]:

$$q_{k4,i} = \left(h_{k5,o} - h_{v4,o}\right) \tag{4}$$

where $q_{k4,i}$—boiler heat input, [kJ/kg]; $h_{k5,o}$—boiler enthalpy output, [kJ/kg]; and $h_{v4,o}$—pressure-reducing valve enthalpy outlet, [kJ/kg].

Turbine work can be given in Eq. (5) as follows [1]:

$$w_t = \eta_t \, \eta_j \left(h_{t5,i} - h_{t6fg,o}\right) \tag{5}$$

where w_t—turbine work [kJ/kg]; η_t—turbine yield was accepted as 85% [1]; and η_j—generator efficiency is accepted as 95% [1].

Net work (The amount of energy production) is found in the following equation Eq. (6) as follows [1]:

$$w_{net} = w_t - w_{pp} \tag{6}$$

where w_{net}—net work, [kJ/kg]; w_t—turbine work, [kJ/kg]; and w_{pp}—pump work, [kJ/kg].

Thermal efficiency can be given in equal Eq. (7) as follows [1]:

$$\eta_{th} = w_{net} / q_{k4,i} \tag{7}$$

where $q_{k4,i}$—boiler heat input, [kJ/kg]; η_{th}—thermal efficiency, [%]; and w_{net}—net work, [kJ/kg].

Irreversibility equation can be defined by Eq. (8) as follows [1]:

$$I = \left[T_\infty \, x\left(\left(s_{k5,o} - s_{pp,f}\right) + \left(-q_{k4,i} / T_{k4,i}\right)\right)\right] + \left[T_\infty \, x\left(\left(s_{pp,f} - s_{t6,o}\right) + \left(q_{k4,o} / T_\infty\right)\right)\right] \tag{8}$$

where I—irreversibility, [kJ/kg]; $s_{k5,o}$—boiler entropy output, [kJ/kg K]; $s_{t6,o}$—turbine entropy output, [kJ/kg K]; $s_{pp,f}$—feed-pump-saturated liquid entropy output, [kJ/kg K]; and T_∞—dead state temperature, [K].

Exergy lost can be given in equal Eq. (7) as follows [1]:

$$E_{x\ell} = (h_{t5,i} - h_{pp2,o}) - [T_{\infty} \times (s_{t5,i} - s_{pp2,o})] \quad (9)$$

where Ex_{ℓ}—exergy lost, [kJ/kg]; $h_{t5,i}$—turbine enthalpy input, [kJ/kg]; $h_{pp2,o}$—feed pump enthalpy output, [kJ/kg]; $s_{t5,i}$—turbine entropy input, [kJ/kg K]; and $s_{pp2,o}$—feed pump entropy output,[kJ/kg K].

The application of net energy transfer can be calculated from Eq. (10) as follows [1]:

$$En_{net} = w_t + h_{t6,o} - h_{k4,i} \quad (10)$$

where En_{net}:—net energy transfer, [kJ/kg]; w_t—turbine work, [kJ/kg]; $h_{t6,o}$—turbine enthalpy output, [kJ/kg]; and $h_{k4,i}$—boiler enthalpy input, [kJ/kg].

2.2. Lime production energy and exergy calculation

According to the data obtained from the factory, the energy and exergy calculations of the lime from the fluid boiler were made according to the following formulas.

Accordingly, the amount of CaO can be found from Eq. (11) as follows [1, 9]:

$$m_{CaO} = m_{Ca(OH)_2} \% \text{ CaO} \quad (11)$$

where m_{CaO}—lime (CaO) mass flow rate, [kg/h]; $m_{Ca(OH)_2}$—$Ca(OH)_2$ mass flow rate, [kg/h]; and % CaO—lime percentage, [%].

The energy of lime (CaO) is found in the following equation Eq. (12) as follows [1, 9]:

$$En_{CaO} = m_{CaO} \times h_{CaO} \quad (12)$$

where En_{CaO}—lime energy, [W]; m_{CaO}—lime (CaO) mass flow rate, [kg/h]; and h_{CaO}—lime enthalpy, [kJ/kg].

The lime (CaO) exergy can be found in the following Eq. (13) as follows [1, 9]:

$$Ex_{CaO} = m_{CaO} \times \psi_{CaO} \quad (13)$$

where Ex_{CaO}—lime exergy, [W]; m_{CaO}—lime (CaO) mass flow rate, [kg/h]; and ψ_{CaO}—lime-specific exergy, [kJ/kg].

The energy consumption per lime production is found in the following equation Eq. (14) as follows [1, 9]:

$$en = En/m_{CaO} \quad (14)$$

where CaO is lime and en_{CaO} is the energy consumption per lime production, [kJ/kg].

Lime energy quality can be found in the following Eq. (15) as follows [1, 9]:

$$\Theta_{CaO} = Ex_{CaO}/En_{CaO} \tag{15}$$

where Θ_{CaO} is the lime energy quality, [%].

2.3. Thermal energy efficiency calculations of fluidized bed boiler

The following formulas are used for the calculation of the factory thermal boiler energy efficiency.

The energy input amount of the boiler is calculated from Eq. (16) as follows [1]:

$$q_{k,i} = m_{k,i}\, C_p\, (T_{k,o} - T_{k,i}) \tag{16}$$

where $q_{k,i}$—amount of energy entering the boiler, [kW]; $m_{k,i}$—water flow rate, [kg/h]; $T_{k,i}$—fluid boiler water inlet temperature, [°C]; $T_{k,o}$—fluid boiler water outlet temperature, [°C]; and C_p—specific thermal capacity, [kJ/kg K].

The heat transfer resulting from combustion in the boiler is calculated from Eq. (17) as follows [1]:

$$q_{k,o} = m_y\, H_u \tag{17}$$

where m_y—fuel flow in the boiler, [kg/h]; and H_u—combustion temperature (thermal value), [kJ/kg].

Accordingly, the efficiency of the boiler (ηk) is calculated from Eq. (18) as follows [1]:

$$\eta_k = q_{k,i}/q_{k,o} \tag{18}$$

The energy and exergy analysis in the fluidized bed boiler is easily calculated from all these formulas. In addition, lime energy can also be included in the calculations.

3. Conclusion

This book poses application of a power plant technology in terms of calculation with thermodynamic laws. In addition, this chapter indicates energy and exergy efficiency of power plants in the industry. Technoeconomic analysis is carried out for the energy and exergy efficiency progresses that should be applied in power plant of sugar factory, which is the center of a factory. In addition, power plant can be an essential influence for factory profit. It is concluded that the laws and properties of thermodynamics should be the result-oriented, especially for power plants. This application can be used for energy savings by the power plant.

http://dx.doi.org/10.5772/intechopen.82406

Power plants are very significant for all industry sectors that depend on exergy processes. Since many factories use such energies for their major processes, they have installed power plants on account of their factories. Installing power plants can gain their energy in an efficient way for the factory. This book poses exergy and application technology to energy processes. This book impresses on the importance of an exergy with an overview of all of the energy systems. Energy and exergy efficiencies related to thermodynamic laws are carried out for the power plant and technology.

All processes depend on energy that is used more than the other similar factories. These calculations can be determined by thermodynamics laws and their general and specific formulas. Using a general cycle, Rankine cycle, is a more effective cycle than the other thermodynamic cycles. In addition, it includes mass and energy conversion according to a dead state. All these formulas and calculations pose energy and exergy efficiencies.

This book poses energy and exergy efficiency of energy systems and industry about several different factories. Technoeconomic analysis is carried out for the energy and exergy efficiency progresses that should be applied in power plant of factory, which is the center of a factory.

As a result, power plants can play an effective role in increasing the profitability of factories. For this reason, energy and exergy efficiencies can be determined by thermodynamic laws in order to make the process flow of the plants more efficient in energy solutions. In this way, power generation in power plants can be made more useful by identifying energy and exergy efficiencies.

Nomenclature

% CaO	lime percentage, [%]
ΘCaO	lime energy quality, [%]
$(P\,2 - P\,1)_{pp}$	supply pump pressure difference, [kPa]
h_{∞}	dead state enthalpy, kJ/kg
h_{i}	enthalpy input, kJ/kg
$h_{k5,o}$	boiler enthalpy output, [kJ/kg]
h_{o}	enthalpy output, kJ/kg
$h_{t6,o}$	turbine enthalpy output, [kJ/kg]
$h_{t6f,o}$	turbine-saturated fluid enthalpy output, [kJ/kg]
$h_{t6fg,o}$	turbine-saturated liquid and vapour enthalpy output, [kJ/kg]
$h_{v4,o}$	pressure-reducing valve enthalpy outlet, [kJ/kg]
$m_{Ca(OH)\,2}$	Ca (OH) 2mass flow rate, [kg/h]
$q_{k4,i}$	boiler heat input, [kJ/kg]

$q_{k4,i}$	boiler heat input, [kJ/kg]
s_{∞}	dead state entropy, kJ/kg K
$s_{c1,fg}$	condenser entropy (difference between saturated liquid and steam), [kJ/kg K]
$s_{c1,i}$	condenser entropy input, [kJ/kg K]
s_{i}	entropy input, kJ/kg K
$s_{k5,o}$	boiler entropy output, [kJ/kg K]
s_{o}	entropy output, kJ/kg K
$s_{pp,f}$	feed pump-saturated liquid entropy output, [kJ/kg K]
$s_{t5,i}$	turbine entropy input, [kJ/kg K]
$s_{t6,o}$	turbine entropy output, [kJ/kg K]
T_{∞}	dead state temperature, K
$v_{pp,f}$	specific volume of saturated liquid of feed pump, [m^3/kg]
w_{net}	net work, [kJ/kg]
w_{net}	net work, [kJ/kg]
w_{pp}	pump work, [kJ/kg]
w_{pp}	pump work, [kJ/kg]
w_{t}	turbine work [kJ/kg]
w_{t}	turbine work, [kJ/kg]
$x_{t6.o}$	turbine dryness fraction output, [−]
η_{ex}	exergy efficiency, %
η_{j}	generator efficiency is accepted as 95% [1]
η_{pp}	pump efficiency is accepted as 80% [1]
η_{t}	turbine yield was accepted as 85% [1]
η_{th}	thermal efficiency, [%]
∞	dead state
CaO	lime
C_p	specific thermal capacity, [kJ/kg K]
en_{CaO}	energy consumption per lime production, [kJ/kg]
En_{CaO}	lime energy, [W]
En_{net}	net energy transfer, [kJ/kg]

http://dx.doi.org/10.5772/intechopen.82406

Ex_{CaO}	lime exergy, [W]
Ex_{ℓ}	exergy lost, [kJ/kg]
h	specific air or steam enthalpy, kJ/kg
h_{CaO}	lime enthalpy, [kJ/kg]
$h_{k4,i}$	boiler enthalpy input, [kJ/kg]
$h_{pp2,o}$	feed pump enthalpy output, [kJ/kg]
$h_{t5,i}$	turbine enthalpy input, [kJ/kg]
$h_{t6,o}$	turbine enthalpy output, [kJ/kg]
H_u	combustion temperature (thermal value), [kJ/kg]
i	input (Inlet)
I	irreversibility, kJ/kg
m_{CaO}	lime (CaO) mass flow rate, [kg/h]
m_{CaO}	lime (CaO) mass flow rate, [kg/h]
m_{CaO}	lime (CaO) mass flow rate, [kg/h]
$m_{k,i}$	water flow rate, [kg/h]
m_y	fuel flow in the boiler, [kg/h]
n	amortization period, year
o	output (Outlet)
$q_{k,i}$	amount of energy entering the boiler, [kW]
s	specific, air or steam entropy, kJ/kg K
$s_{pp2,o}$	feed pump entropy output,[kJ/kg K]
$s_{t5,i}$	turbine entropy input, [kJ/kg K]
T	sugar temperature, K
$T_{k,i}$	fluid boiler water inlet temperature, [°C]
$T_{k,o}$	fluid boiler water outlet temperature, [°C]
v_i	fluid inlet velocity, m/s
v_o	fluid outlet velocity, m/s
w_t	turbine work, [kJ/kg]
Ψ	specific air or steam-specific flow exergy, kJ/kg
ψ_{CaO}	lime-specific exergy, [kJ/kg]

Author details

Tolga Taner[1]* and Mecit Sivrioglu[2]

*Address all correspondence to: tolgataner@aksaray.edu.tr

1 Department of Motor Vehicles and Transportation Technology, Aksaray University, Aksaray, Turkey

2 Department of Mechanical Engineering, Gazi University, Ankara, Turkey

References

[1] Taner T. Food industry energy efficiency and energy management: The case of sugar factory [dissertation]. Ankara: Gazi University; 2013. Available from: www.fbetezbankasi.gazi.edu.tr

[2] Taner T. Economic analysis of a wind power plant: A case study for the Cappadocia region. Journal of Mechanical Science and Technology. 2018;**32**(3):1379-1389. DOI: 10.1007/s12206-018-0241-6

[3] Taner T, Demirci OK. Energy and economic analysis of the wind turbine plant's draft for the Aksaray City. Applied Ecology and Environmental Sciences. 2014;**2**(3):82-85. DOI: 10.12691/aees-2-3-2

[4] Taner T. Alternative energy of the future: A technical note of PEM fuel cell water. Fundamentals of Renewable Energy and Applications. 2015;**5**(3):1-4/1000163. DOI: 10.4172/20904541.1000163

[5] Taner T. Energy and exergy analyze of PEM fuel cell: A case study of modelling and simulations. Energy. 2018;**143**:284-294. DOI: 10.1016/j.energy.2017.10.102

[6] Taner T. The micro-scale modeling by experimental study in PEM fuel cell. Journal of Thermal Engineering. 2017;**3**(6):1515-1526. DOI: 10.18186/journal-of-thermal-engineering.331755

[7] Taner T. Optimisation processes of energy efficiency for a drying plant: A case of study for Turkey. Applied Thermal Engineering. 2015;**80**:247-260. DOI: 10.1016/j.applthermaleng.2015.01.076

[8] Taner T. Energy-exergy analysis and optimisation of a model sugar factory in Turkey. Energy. 2015;**93**:641-654. DOI: 10.1016/j.energy.2015.09.007

[9] Taner T, Sivrioglu M. A lime production of the fludized bed boiler's energy and exergy analyse. Journal of Thermal Engineering. 2017;**3**(3):1271-1274. DOI: 10.18186/journal-of-thermal-engineering.323393

[10] Taner T, Sivrioglu M. A techno-economic & cost analysis of a turbine power plant: A case study for sugar plant. Renewable and Sustainable Energy Reviews. 2017;**78**:722-730. DOI: 10.1016/j.rser.2017.04.104

[11] Taner T, Sivrioglu M. Thermoeconomic analysis for the power plants of sugar factories. Journal of the Faculty of Engineering and Architecture of Gazi University. 2014;**29**(2): 407-414. DOI: 10.17341/gummfd.73993

[12] Topal H, Taner T, Naqvi SAH, Altinsoy Y, Amirabedin E, Ozkaymak M. Exergy analysis of a circulating fluidized bed power plant co-firing with olive pits: A case study of power plant in Turkey. Energy. 2017;**140**:40-46. DOI: 10.1016/j.energy.2017.08.042

[13] Topal H, Taner T, Altinci Y, Amirabedin E. Application of trigeneration with direct co-combustion of poultry waste and coal: A case study in the poultry industry from Turkey. Thermal Science. 2017;**137**. DOI: 10.2298/TSCI170210137T: In Press

[14] Taner T, Sivrioglu M, Topal H, Dalkilic AS, Wongwises S. A model of energy management analysis, case study of a sugar factory in Turkey. Sadhana. 2018;**43**(42):1-20. DOI: 10.1007/s12046-018-0793-2

Chapter 2

Modernization and Development Scenarios of the Power Plants in the Present Energy Market Context

Adelaida Mihaela Duinea

Additional information is available at the end of the chapter

http://dx.doi.org/10.5772/intechopen.80887

Abstract

The aim of this study is to analyze several possible hypotheses for the development of a power plant in the context of the local electricity and heat market. The energy market may be constraint by the probable cessation of the activity of the most important customer in the industrial market, hereinafter referred to as "strategic customer." Stopping its activity would deprive the power plant of an annual electricity supply of 28.02% of the electricity production estimated in the "continuity" hypothesis with the strategic customer, namely an annual heat of 78.19% of the heat output of the same alternative. It is very clear that stopping the activity of the company constitutes a disability for the power plant, whose magnitude has been highlighted by the comparative analysis of several possible scenarios of modernization, modernization-development, and development. As far as the electricity market is concerned, the power plant belongs to the area that is strongly equipped with sources of electricity production. With regard to the thermal energy market, the power plant, following the decoupling of the strategic customer, loses an important and stable consumer and stays only with the production of heat for heating the buildings and the preparation of domestic hot water for the residents of the city. The study's result is the hierarchy of the proposed technical scenarios from the point of view of the necessary investment, the variation of the electricity tariff on the market, and the environmental impact.

Keywords: energy market, optimization, power plant, steam generator

1. Introduction

The energy system and the related market have gone a long way, from the vertically integrated model to a decentralized system, from centralized programming to obtaining the right to produce through the bidding process, the daily bidding process referring to 24 hour the next

day. The opening of the electricity market fundamentally altered the trading environment, with a residual energy demand at regulated prices. This is mainly due to the fact that small companies and residential consumers have low volumes, and the costs of changing the vendor may indicate that the decision is uneconomic [1, 2]. The fundamental position in the development of a power plant is to minimize the risks (in the case of PPP—public-private partnership projects) ensuring that in the sizing of the transaction and in the market activity, each risk is identified and allocated to the entity capable of administering, diminishing, or supporting it [3, 4]. Main risks in the development of a power plant are considered to be:

- The overall risk of the deregulated market—appears to be a challenge to all electricity producers, except for the "must run" type. In a deregulated market, the most common ways to significantly reduce this risk are bilateral physical contracts and hedging contracts.
- Risk of nonscrutiny—can be contracted through contracts, or if possible, export contracts.
- General regulatory risk—applies to any manufacturer; keeping it at an acceptable level is achieved through the knowledge of long-term energy policy and political stability.
- The risk of regulating the environmental impact—the most difficult to appreciate and manage; shall apply in the same amount to all competitors, who produce electricity using the same type of fuel.
- Risk of noncredulity—a robust economic and financial analysis to persuade the banks on the feasibility of the project substantially reduces this risk.
- Fuel price risk—one of the most visible risks. Even if it is difficult to quantify, it is obvious that the trend for the price of fuel, especially hydrocarbons, is on the rise.

The power plant has as its activity, the production of electric and thermal energy (steam and hot water), for industrial and urban consumers in the city. The plant has the following capacities installed: steam generators of 420°t/h, 140 bar, 540°C operating with primary fuel—lignite and support fuel—HFO for the flame and 50 and 25 MW turbo generators. The evacuation of the produced electric power is done through the 110 kV connection substation to the National Energy System. The evacuation of thermal energy to its main consumer, the industrial and urban consumers in the city, is achieved through technological and heating networks.

2. Current position of the power plant in the energy market

2.1. Electricity market

The plant's electricity production is based on the existence of traditional consumers such as the most important economic agent, the "strategic customer" and the adjacent locality.

Although the share in total deliveries differs considerably between consumers, the customer portfolio is characterized by the fact that:

- SEN is an important customer, requesting 75% of the total deliveries.
- The economic agent is a strategic customer, considering the level of safety in the electricity supply.

The strategic customer's consumption was approximately constant; the electricity production increased with the optimization of the operation of the power plant.

In **Tables 1–3,** the values resulting from the statistical processing of the average monthly powers are presented.

It is noted that unlike other consumers, the strategic customer records consumption averages close to the maximum/minimum values, emphasizing the continuity of the power supply. During the operation of the power plant, it has emphasized "minor" energy exchanges: consumers connected directly, termed third parties—0.11% of total deliveries made to the contour of the power plant.

Clearly, the future of the power plant depends on the evolution of the demand for electricity, primarily in the area, but also on the entire national market and export prospects, respectively.

Parameter, UM	Condensation	Heat	Total
Maximal peak power, extrapolated, MW_e	145.008	139.111	272.126
Weighted average multiannual power, MW_e	72.923	75.021	147.944
Minimum average monthly power, MW_e	18.062	23.108	51.582
Average standard deviation, MWe	34.054	31.799	53.583

Table 1. The "raw" energy production.

Parameter, UM	TOS	Deliveries	Total
Maximal peak power, extrapolated, MW_e	43.112	221.932	262.989
Weighted average multiannual power, MW_e	27.993	120.101	148.667
Minimum average monthly power, MW_e	13.307	42.105	55.309
Average standard deviation, MWe	8.021	46.988	54.860

Table 2. Technological consumptions and energy supply.

Parameter, UM	Strategic customer	NES	Deliveries
Maximal peak power, extrapolated, MW_e	32.014	190.996	222.072
Weighted average multiannual power, MW_e	29.987	90.012	120.126
Minimum average monthly power, MW_e	23.026	10.877	42.396
Average standard deviation, MWe	1.563	47.084	47.424

Table 3. Energy supply to strategic customer and to the NES.

Of great importance is the existence of eligible consumers in the area, who can conclude contracts at longer intervals. Their motivation may be: a certain tradition of previous collaboration with the power plant, the possibility of negotiating convenient clauses, an advantageous price due to the low transport and distribution tariff, and preferential financial arrangements including price variations in time that share the risk of variations of high fuel prices.

2.2. Thermal energy market

The portfolio of consumers active on the power plant's thermal energy market has a less disadvantageous structure, given that the strategic customer has a significant share. The power plant produces heat and delivers heat using thermal agents: industrial steam at a pressure of 40 bar for the strategic customer, industrial steam at a pressure of 13 bar for the strategic customer, and hot water for "urban" consumers in the locality. The disappearance of the strategic consumer will dictate decisively the structure of the plant's operating scheme. In terms of supplying the city with thermal energy, it is made through a branched type hot water network. The thermal power to cover the current heat demand is approximately 154 MWt for the maximum winter regime and 15 MWt for maximum summer mode when intermittent hot water is delivered.

Maintaining the current centralized heating system from a cogeneration source is appropriate due to the absence of a viable technical and economic alternative in the medium term; the town is not connected to the natural gas network. This makes it impossible to replace the cogeneration source with quaternary, block, or apartment heating plants. Individual stove heating is excluded in condominiums. **Tables 4** and **5** synthesize the data related to thermal energy production and supply corresponding to various thermal levels and to various types of consumers.

Parameter, UM	Max.	Monthly averages	Socket	SRR
Maximal peak power, extrapolated, MW_t	99.38	98.86	89.18	50.67
Weighted average multi annual power, MW_t	87.92	85.04	66.92	19.83
Minimum average monthly power, MW_t	52.01	50.11	37.89	0.00
Average standard deviation, MW_t	7.06	7.37	15.62	13.94

Table 4. Characteristic values of 40 bar technological steam deliveries.

Parameter, UM	Steam, 13 bar	District heating	Deliveries to TP
Maximal peak power, extrapolated, MW_t	192.01	155.32	95.57
Weighted average multiannual power, MW_t	127.43	66.98	37.29
Minimum average monthly power, MW_t	73.88	10.92	1.08
Average standard deviation, MW_t	25.68	49.31	34.83

Table 5. Characteristic values of 13 bar technological steam and hot water supply.

http://dx.doi.org/10.5772/intechopen.80887

Compared to the electricity market, which has at least national coverage, thermal energy has, for obvious technical reasons, a strictly local character. The eventual disappearance of the major thermal consumer creates relatively pessimistic premises in terms of the potential for the evolution of demand for thermal energy and its exploitation.

Even if the power plant currently occupies a strong position in the energy market, its evolution may change either through the development of the most important economic agent or through the predictable development of the city.

The existence of eligible customers is very important for the evolution of power plant. They can conclude contracts on the long terms—their competitive strength depends on their own development programs and financing schemes.

At the same time, it is estimated that in about several years, the city will be connected to the natural gas network, which may lead to disconnections of urban consumers, respectively, a decrease of the demand for heat by 3–5%. To this can be added the self-limiting trends of the consumption of heat and hot water, which will be manifested with the development of measurement systems and the "individualization" of invoices due to the generalization of the thermal points and the blocks or stairs, the introduction of hot water meters and using thermostatic valves and cost allocators.

However, there are number of directions for increasing the area in terms of the development of the thermal energy market using hot water: development of a new housing district—an average consumption of 32% (10.5 MWt) of the current average annual urban consumption of about 35 MWt is estimated. The development of greenhouses at the outskirts of the city will increase the average annual heat supply in the hot water network by 7.2 MWt (16%). These, summed up at the peak of winter with the current thermal load, outline an increase of about 52% of peak demand for thermal energy.

3. Technical analysis for modernization and development of the power plant

The following evolving alternatives for the power plant are developed:

- Modernization alternatives (AM), which will keep the plant's current architecture and add a DKAR 22 turbine and desulphurization plant.
- Modernization-development alternatives (AMD), which will keep part of the current scheme of the boiler plant, namely the cogeneration stage that provides the heating and domestic hot water needs of the city.
- Alternative of development (AD), which relies on closing the existing power plant and building/installing new groups.

The "development" groups can keep current energy conversion technology, the Rankine-Hirn water-steam cycle, or they can work on mixed water-steam cycle technology. In both cases, the

required heat demand for the city is met and the fossil fuel energy is converted into electricity and heat at higher yields than the current scheme. The fuels to be used are lignite (L), coal (H), and natural gas (G).

3.1. Modernization alternatives

3.1.1. Modernization of the existing facilities with existing fuels and strategic customer operation, A_1-AM_1

This is the "continuity" alternative, involving the commissioning of the steam counter pressure at 22 bar turbine, nominal parameters 135 bar, 535°C. The plant will consume primary energy generated by the combustion of 9,402,028 MWh/year fuels, lignite, and a combustion support fuel, delivering to the fence an amount of electricity of 1,697,729 MWh/year and thermal energy, 36 bar industrial steam, 16 bar industrial steam, and hot water, respectively 2,970,201 MWh/year.

3.1.2. Modernization of existing fuel exchanges and strategic customer operation, A_2-AM_2

The alternative consists of the change of lignite fuel in coal to reduce fuel/ash flows and the costs of transporting, handling, and storing them. The power plant will consume primary energy generated by the combustion of 9,205,007 MWh/year fuels, delivering 1,766,108 MWh/year to the fence. The amount of annual heat is the same as in the previous case.

3.1.3. Modernization of existing facilities with existing fuel and without the strategic customer, A_3-AM_3

In this hypothesis, the plant will consume primary energy generated by the combustion of 5,591,227 MWh/year fuels, delivering to the fence an amount of electricity of 1,189,662 MWh/year and thermal energy from the hot water, respectively 1,008,164 MWh/year.

3.1.4. Modernization of existing facilities with fuel change and without strategic customer, A_4-AM_4

This alternative is similar to A_3-AM_3 and consists of the change of lignite fuel in coal based on the same boiler and turbine equipping schemes as in the previous case.

Thus, the power plant will consume primary energy generated by the combustion of 5,385,005 MWh/year fuels, delivering to the fence an amount of electricity of 1,301,104 MWh/year. The amount of annual thermal energy is the same as in the previous case.

3.2. Modernization-development alternatives

3.2.1. Modernization of existing installations and development with a new unit of 100 MW, without changing the conversion technology, A_5-AMD_1

It is a development modernization solution, which consists of coupling a 420 t/h steam generator with a simple cycle turbine, new investment, to increase the electric energy output from the power plant.

The plant will consume primary energy generated by the combustion of 8,262,441 MWh/year fuels, delivering to the fence an amount of electric energy of 1,981,112 MWh/year. In this and in the previous case, the amount of annual thermal energy is the same.

3.2.2. Modernization of existing installations and development with a new 100 MW unit without changing the conversion technology with fuel change, A_6-AMD_2

The alternative is similar to the one above, except that there is a change of solid, lignite-fired fuel into coal.

3.2.3. Modernization of existing installations and development with a new 220 MW with intermediate overheating, without changing the conversion technology, A_7-AMD_3

It is a modernization solution consisting of the transformation of two (three) boilers for intermediate overheating, in the 2 × 50% scheme, with a new 220 MW turbine. The power will be 343 MW in winter mode and 297 MW in summer mode.

In this hypothesis, the power plant will consume primary energy generated by the combustion of 8,901,121 MWh/year fuels, delivering to the fence an amount of electric energy of 2,1981,787 MWh/year to the fence.

It is the scenario with the largest amount of electric energy.

3.2.4. Modernization of existing installations and development with a new 200 MW unit without changing the conversion technology with fuel change, A_8-AMD_4

The hypothesis is similar to the one above, except that the shift of solid lignite fuel into coal, with additional investment, is also emerging.

3.2.5. Modernization of existing installations and development with a new unit with conversion technology change—CCGA 110 MW single shaft, A_9-AMD_5

This alternative preserves some of the existing capacities of the lignite energy conversion technology, introducing in addition a combined gas-steam cycle. The plant will consume primary energy generated by combustion of 6,401,117 MWh/year fuels, delivering to the fence a quantity of electric energy 1,911,027 MWh/year.

3.2.6. Modernization of existing facilities and development with a new unit changing conversion technology—CCGA 110 MW single shaft and fuel, A_{10}-AMD_6

The scenario is similar to the one above, except that the shift of solid lignite fuel into coal, with additional investment, is also emerging.

3.3. Scenarios of development

3.3.1. Development with a new 225 MW with intermediate overheating without changing conversion technology, A_{11}-AD_1

The current equipment with turbines is abandoned and a new group with intermediate overheating and urban outlet is installed, operating on two existing boilers and delivering in the system a maximum power of 190 MW in winter and 220 MW in summer. The plant will consume primary energy generated by the combustion of 5,552,219 MWh/year fuels, to the

fence a quantity of electric energy 1,397,782 MWh/year to the fence. The amount of annual thermal energy is the same as in the previous case.

3.3.2. New 225 MW with intermediate overheating without change of conversion technology with fuel change, A_{12}-AD_2

The alternative is similar to the one above, except that the change of solid, lignite-fired, coal-powered fuel with supplementary investment increases.

3.3.3. Development with a new unit and change of conversion technology—CCGA 220 MW triple shaft, A_{13}-AD_3

This scenario completely abandons the equipment of today's turbines and installs a mixed gas-steam cycle consisting of 273 MW gas turbines, a rehabilitation boiler, and a 68 MW steam turbine running on natural gas.

The power plant will consume primary energy generated by combustion of 3,567,884 MWh/year, delivering to the fence an amount of electric energy of 1,698,117 MWh/year. In this and in the previous case, the amount of annual thermal energy is the same.

4. Technical and economic analyzes of hierarchy of proposed technical scenarios

The purpose of the economic analysis is to:

- identify and assess the costs and revenues of the various scenarios of developing and/or upgrading the power plant in order to optimize the production of electric and thermal energy;
- compare costs and revenues for the proposed scenarios;
- establish a ranking of the proposed scenarios based on the technical and economic efficiency achieved with the help of the established performance indicators;
- perform the sensitivity analysis of the main performance indicators on changes in the economic input data, validating the proposed scenario ranking.

The forecast for financial flows is based on direct costs (which may be associated with the production of electricity and heat) and revenues.

Thus:

- Direct costs include entries calculated based on material costs, staff costs, overhead costs, and maintenance costs.
- The investment includes engineering costs, equipment costs, construction and assembly costs, and design and study costs.

The total investments for each scenario are shown in **Table 6**.

The most important observations regarding the values presented are: switching from lignite to charcoal operation entails very high costs, which create discrepancies between solutions of the same type in terms of investment; the most expensive solution turns out to be the A_8-AMD_4 scenario, and the cheapest is maintaining the current profile with the introduction of desulphurization facilities.

It noted the presence in the first four scenarios of three solutions based on the use of lignite, even if it is not about the evaluation of operating costs, where the price of fuel would be preponderant.

4.1. Economic performance indicators

The economic analysis involves calculating the financial indicators of the projects. For this purpose, the updated financial flow method was used in line with internationally accepted standards. For the calculation of performance indicators, the updated financial flow also includes the amount of the investment [3, 5, 6].

The project performance evaluation criteria are: net income, NI; internal return rate, IRR; and updated recovery period of invested capital, Ta.

Net income is calculated based on the annual financial flow (At), which takes into account investment expenses, operating expenses, and revenues. Future annual flows generated by the investment are updated at the time of commissioning of new plants. The viability of the project is established if the net income, calculated over the entire analysis period (t), is positive for an update rate (a) considered. The relationship for the net income estimation is:

No	Alternative	Investments (mil. Euro)
1	A_3-AM_3	75
2	A_4-AM_4	135
3	A_5-AMD_1	134
4	A_6-AMD_2	207
5	A_7-AMD_3	198
6	A_8-AMD_4	271
7	A_9-AMD_5	170
8	A_{10}-AMD_6	228
9	A_{11}-AD_1	151
10	A_{12}-AD_2	181
11	A_{13}-AD_3	171

Table 6. Estimates of investments by objective.

$$NI = \sum_{t=1}^{n} \frac{A_t}{(1+a)^t} \tag{1}$$

The net income reported under the project to the updated investment is the "net income rate, $R_{NI,}$" expressed in $USD_{NI}/USD_{investment}$.

$$R_{NI} = \frac{NI}{\sum_{t=1}^{PIF} \frac{IE_t}{(1+a)^t}} \tag{2}$$

This efficiency indicator derives from the "3e" rule - identifies the financial efficiency as an effect/effort ratio. It allows not only the appreciation of the project itself (for which R_{NI} higher than one is recommended) but also the comparison of several technical and economic variants (which entail considerably different investment costs).

The internal ratio (IRR) is also based on the updated cash flow and represents the "update" rate for which net income becomes zero. This is an indicator of the maximum interest rate at which borrowings can be made to finance the capital investment. The calculation relation for determining the internal ratio is:

$$\sum_{t=1}^{n} \frac{A_t}{(1+r)^t} = 0 \tag{3}$$

Upgraded recovery time (Ta) is a superior net income concept, especially for large-scale businesses. The method updates the net earnings, recorded each year, determining the period of recovery of the invested capital. It is a clear criterion for accepting projects.

The acceptability criterion is that the recovery period is less than the normal use period. This period corresponds to the moment when the cumulative net cumulative revenue becomes zero:

$$\sum_{t=1}^{T_a} \frac{A_t}{(1+a)^t} = 0 \tag{4}$$

The economic analysis, expressed by the updated net income, internal rate update, and refund time in update values gives the results presented in **Table 7**.

As can be seen from table, the most economically viable comparisons from the economic point of view are: the A_{11}-AD_1 solution presents the best value for economic efficiency indicators; A_3-AM_3 is ranked second; the A_7-AMD_3 solution is ranked third, following the economic analysis.

It is, however, observed that, in the assumptions considered, none of the solutions analyzed leads to positive net income values under the reference prices considered.

No	Alternative	Investment, mil. Euro	NI, mil. Euro	The internal rate of return, %
1	A_3-AM_3	−1.007	0.63	—
2	A_4-AM_4	−6.107	—	—
3	A_5-AMD_1	−1.912	0.20	—
4	A_6-AMD_2	−9.348	—	—
5	A_7-AMD_3	−1.831	2.66	—
6	A_8-AMD_4	−9.799	—	—
7	A_9-AMD_5	−4.015	—	—
8	A_{10}-AMD_6	−8.346	—	—
9	A_{11}-AD_1	−899	6.33	—
10	A_{12}-AD_2	−5.637	—	—
11	A_{13}-AD_3	−5.548	—	—

Table 7. Values of economic criteria for proposed scenarios.

From these results, there is a group of solutions that are more effective (in relative terms) than the rest of the proposed scenarios. Solutions that involve running on coal cannot be an option for the development of the boiler because of the very high investment involved in boiler modification. Also, solutions that propose natural gas operation do not provide special economic performance, mainly due to the high price of this fuel.

As regards the internal return rate of the investment, in none of the projects it exceeds the discount rate of 10%. In conclusion, none of the projects is profitable, all are accompanied by losses. Solutions selected to be the subject of financial analysis are those that occupy the top four positions of the rankings, namely, A_3-AM_3, A_5-AMD_1, A_7-AMD_3, A_{11}-AD_1 **Table 8**.

It can be concluded that the plant must continue to operate on lignite. The installation of new groups, in parallel or not with the modernization of existing ones, will be decided by the price of capitalizing the electricity that will be produced. With faster growth than the forecasted price of electricity, the solutions will be favored, which increase the installed power of the plant and the annual amount of electricity produced and delivered.

No	Alternative	VNA, mil. Euro	RIR, %	TRA, years
1	A_{11}-AD_1	−899	6.33	—
2	A_3-AM_3	−1.007	0.63	—
3	A_7-AMD_3	−1.831	2.66	—
4	A_5-AMD_1	−1.912	0.20	—

Table 8. Solutions selected to be the subject of financial analysis.

4.2. Sensitivity analysis

The aim of the sensitivity analysis is to determine the variation of the economic indicators values when certain parameters are changing and to check the ranking obtained from the economic analysis for various scenarios [7].

The most important parameter at which the sensitivity of economic indicators is checked is the slope of increasing electricity price. This increase was considered, as a reference value, to be 10% per year [8, 9]. The sensitivity of economic efficiency (expressed by net income variation) was studied to change this growth slope from 5 to 15%. The values obtained from the calculation for the four proposed scenarios are presented in **Table 9**.

The conclusions resulted from this sensitivity analysis are:

- The efficiency of the project is extremely sensitive to the change in the price of energy recovery; any change in the slope of growth in the next few years may even change the order of the proposed scenarios;
- If there is not an annual increase of at least 10% of the electricity price, the continuity solution with the modernization of the existing equipment is the only one eligible; the conclusion is logical because in the absence of industrial heat consumption and a favorable evolution of the price of energy recovery, it is not efficient to make new investments.
- On the contrary, with an increase of the electric energy tariff up to 15%/year, the A_7-AMD_3 solution becomes the most efficient proposal because it is the project that offers the highest annual electricity for sale. In addition, the solution becomes economically efficient, with a positive NI value.

From the point of view of the variation of the electricity tariff on the market, these simulations were made in the assumption of an annual increase of electricity tariff of 10%/year. When this increase is higher (15%/year), the order is preserved, even NI for the first rank is positive because this is the project that offers the largest annual amount of electricity for sale. When this increase is lower (5%/year), the continuity scenario, A_3-AM_3, is on the first place because,

Alternative	Slope variation of increase of electricity price		
	5%	10% (ref)	15%
A_{11}-AD_1	−2.011	−899	231
A_3-AM_3	−1.982	−1.007	−33
A_7-AMD_3	−3.593	−1.831	−68
A_5-AMD_1	−3.435	−1.912	−390

Table 9. Sensitivity of NI (millions Euro) to the change in the slope of the electricity price increase.

in the absence of industrial heat consumption and a favorable evolution of the energy recovery tariff, it is not efficient to make new investments [10].

5. Environmental impact

Primary fuel used is Oltenia lignite, support fuel—oil. **Table 10** shows the energy characteristics of fuel use. An environmental impact assessment was conducted for each energy solution, by taking into consideration the energy generators functioning on lignite and fuel oil as support fuel amounting to a 6% heating contribution, respectively; the amount of solid particles issued, the amount—concentration of CO_2, SO_2, and NO_x.

The environmental impact assessment is analyzed on four technical options, all without the main economic agent, namely: A_3-AM_3—equipment: actual—new type turbine, fuel type: 95% coal, 5% liquid fuel support, energy with fuel: coal 5,301,116 MWh/year and liquid fuel 340,006 MWh/year, A_5-AMD_1—equipment: actual—new type turbine—100, fuel type: 95% coal, 5% liquid fuel support, energy with fuel: coal 7,880,065 MWh/year and liquid fuel 498,963 MWh/year, A_7-AMD_3—equipment: actual—new type turbine - 200, fuel type: 95% coal, 5% liquid fuel support, energy with fuel: coal 8,401,060 MWh/year and liquid fuel 528,714 MWh/year and A_{11}-AD_1—equipment: new group with intermediate superheating and urban connection, fuel type: 93% coal +7% liquid fuel support, energy with fuel: coal 5.046.869 MWh/year and liquid fuel 376,981 MWh/year [11].

The calculations impose, in a first stage, the determination of the chemical composition to the equivalent fuel, the coal-HFO mixture. The recurrence relationship is:

$$X = m_c X^i + m_{HFO} X_{HFO} \tag{5}$$

Energy characteristic		Primary fuel	Support fuel
Chemical composition,%	C^i	23.10	87.15
	H^i	1.80	10.70
	O^i	9.60	0.70
	S_c^i	1.50	1.00
	N^i	0.63	0.15
	A^i	21.60	0.20
	W_t^i	41.77	0.10
Low calorific power, H_i, kJ/kg		7753.60	40,595

Table 10. Energy characteristics of fuels.

where m_c, m_{HFO} is the mass participation of the coal and the HFO in the mixture, and X^i, X_{HFO} is the percentage participation of the element in the coal composition, respectively, in HFO composition, to the initial state.

The second stage aims at determining the combustion products [12–15]. Therefore, is determined [16]:

- theoretical amount of oxygen required for combustion, Nm^3/kg:

$$V_{O2}^0 = 1.867\frac{C}{100} + 5.6\frac{H}{100} + 0.7\frac{S_c}{100} - 0.7\frac{O}{100} \tag{6}$$

- theoretical volume of dry air required for combustion, Nm^3/kg:

$$V_a^0 = \frac{1}{0.21}\left(1.867\frac{C}{100} + 5.6\frac{H}{100} + 0.7\frac{S_c}{100} - 0.7\frac{O}{100}\right) \tag{7}$$

- theoretical volume of humid air needed for combustion, Nm^3/kg:

$$V_{aum}^0 = 1.0161V_a^0 \tag{8}$$

- theoretical volume of triatomic gases, Nm^3/kg:

$$\mathrm{V}_{\mathrm{RO2}}^0 = 1.867\frac{C + 0.375S_c}{100} \tag{9}$$

- theoretical volume of diatomic gases, Nm^3/kg:

$$V_{N2}^0 = 0.79V_a^0 + 0.8\frac{N}{100} \tag{10}$$

- theoretical volume of water vapor, Nm^3/kg:

$$V_{H2O}^0 = 0.112H + 0.01244W_t + 0.00161 \cdot x \cdot V_a^0 \tag{11}$$

- theoretical volume of dry combustion gases, Nm^3/kg:

$$V_{gu}^0 = V_{RO2}^0 + V_{N2}^0 \tag{12}$$

- theoretical volume of the combustion gases, Nm^3/kg:

$$V_{ga}^0 = V_{gu}^0 + V_{H2O}^0 \tag{13}$$

- real volume of the combustion gases, Nm^3/kg:

$$V_{ga} = V_{ga}^0 + (\lambda - 1)V_{aum}^0 \tag{14}$$

- actual flow of the combustion gases:

$$D_{gN} = B_{ech} \cdot V_g(\lambda) \tag{15}$$

Table 11 shows the calculation of the enthalpy of the combustion gases according to the temperature and the coefficient of excess air.

The scheme for calculation of the combustion and the exit temperature of gases in the furnace has been carried out using Matlab-Simulink software [12–15]. In **Figure 1**, the scheme for combustion calculation is given.

Figure 2 shows the scheme for the determination of the equivalent fuel chemical composition.

The amount of particulate matter emitted is given by, [g/s]:

$$M_c = 10\left(A + q_m \frac{H_i}{32700}\right)\alpha_c B \tag{16}$$

and the ash concentration before the electrostatic precipitator, $[mg/Nm^3]$:

$$c_c = \frac{M_c}{D_{gN}} \tag{17}$$

t [°C]	I_g^0	I_a	I^0_{aum}	$I_g = I_g^0 + I_a + (\lambda\text{-}1)I^0_{aum}$	
				$\lambda_f = 1.2$	$\lambda_f = 1.4$
100	434.90	15.24	318.1	514.2	576.9
200	883.04	31.97	638.9	1041.8	1171.3
400	1815.93	69.11	1299.7	2143.9	2402.1
800	3845.12	148.3	2710.2	4541.7	5080.04
1000	4930.64	193.1	3456.8	5811.6	6501.6
1400	7203.18	312.7	4994.8	8506.2	9507.9
1600	8392.33	382.4	5772.5	9912.7	11048.2

Table 11. Enthalpy-temperature—Coal-HFO mixture, q_{HFO} = 6%.

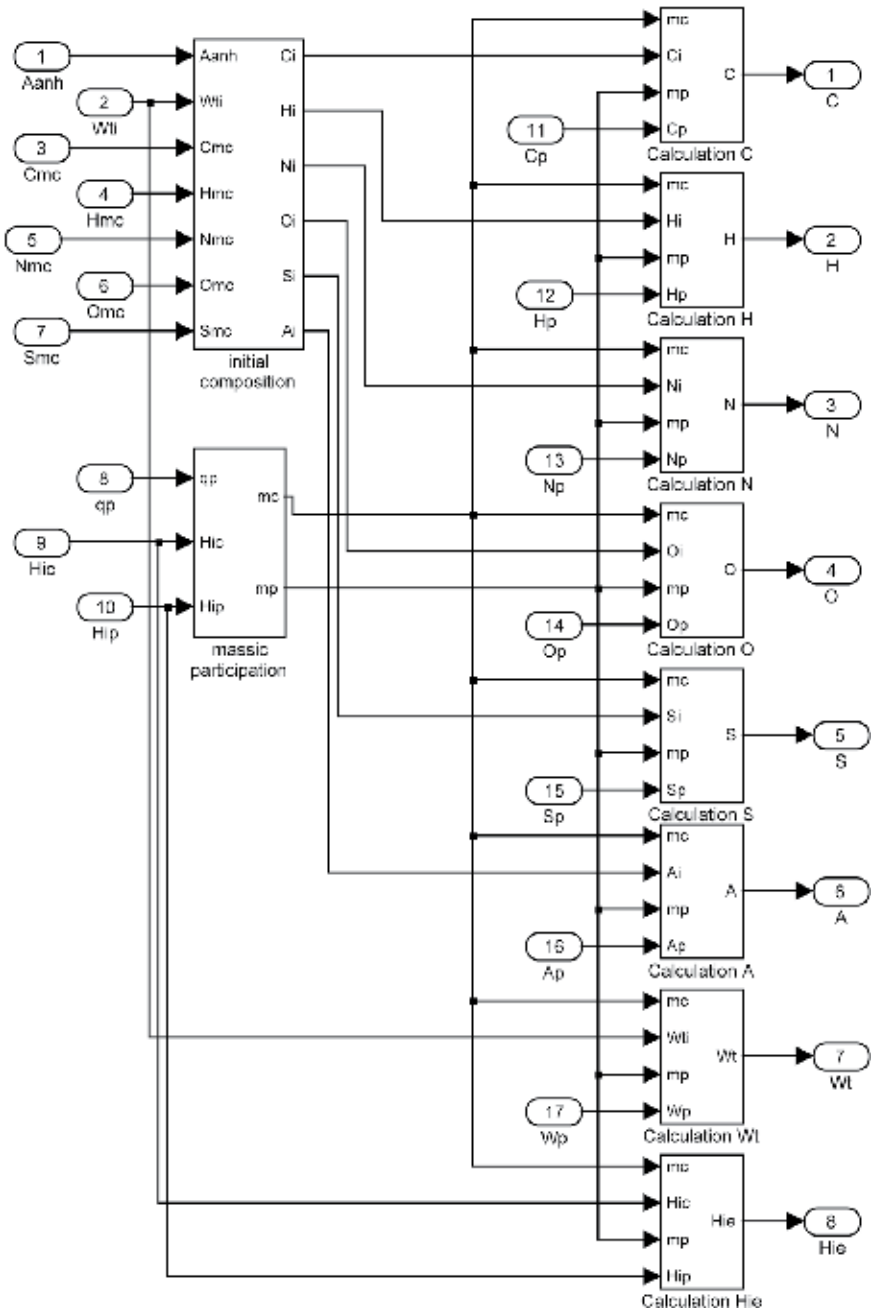

Figure 1. Scheme for determining the equivalent fuel chemical composition [12–15].

http://dx.doi.org/10.5772/intechopen.80887

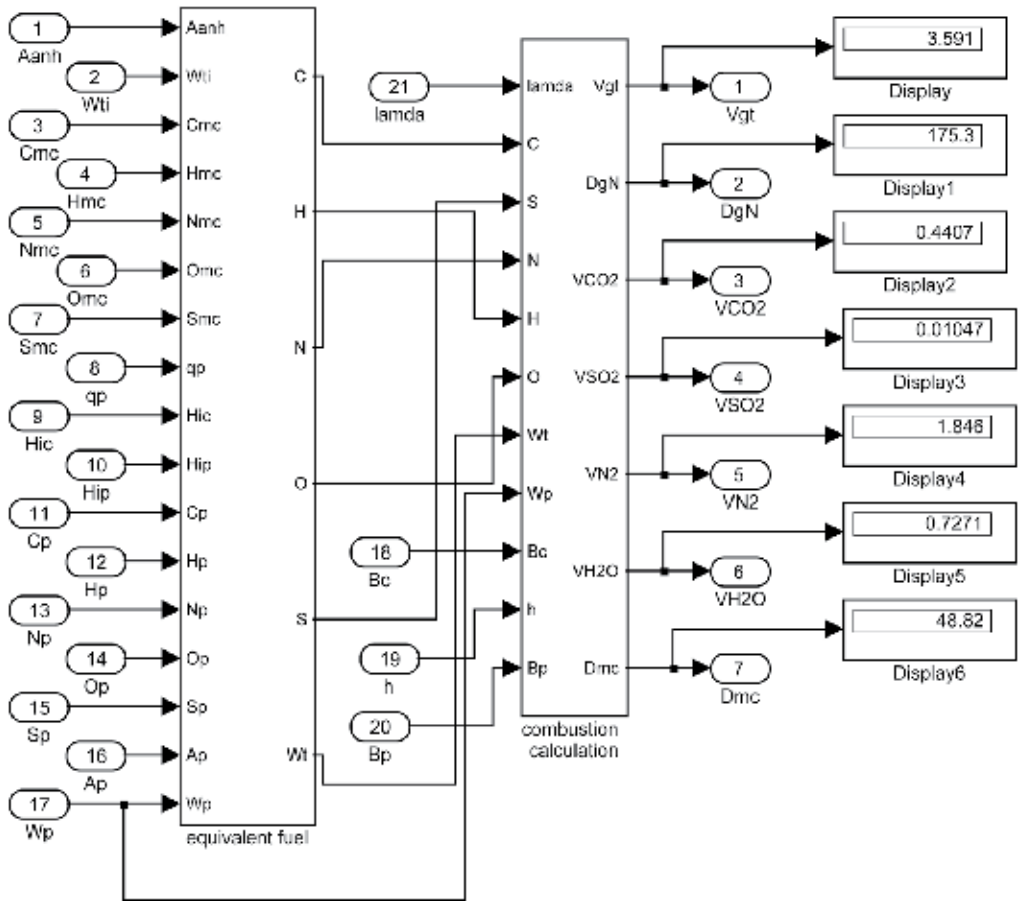

Figure 2. Scheme for the calculation of the combustion products [12–15].

The amount and concentration of CO_2 are:

$$M_{CO2} = 36.66 \cdot C \cdot B \tag{18}$$

$$c_{CO2} = \frac{M_{CO2}}{D_{gN}} \tag{19}$$

The concentration of SO_2 before the desulphurization installation (with $\eta = 0.94$ in order to respect the limit 400 mg/Nm^3) is:

$$c_{SO2} = \frac{M_{SO2}}{D_{gN}} \tag{20}$$

The amount and the concentration of NO_2 are:

$$M_{NO2} = B \cdot H_i \cdot k_{NO2} \tag{21}$$

$$c_{NO2} = \frac{M_{NO2}}{D_{gN}} \tag{22}$$

In order to lower the c_{NO2} value below the regulated one, a primary method of reducing the concentration of NO_2 may be used. For example: low excess air, reducing the preheating temperature of the air, and low NOx burners. Environmental conditions imposed can only be met by imposing minimum technical measures, whatever the scenario being analyzed. **Table 12** shows these measures, namely, efficiency of the electrostatic precipitator, efficiency of the wet scrubber, primary method of NO_x reduction, and reduction of the rate of excess air upon exhaust (to approximately 1.4).

Comparing the four technical scenarios analyzed, it is noted that the most environmentally friendly are in order: the development scenario with a 200 MW group and the continuity scenario in the current scheme.

No	Parameter	A_3-AM_3	A_5-AMD_1	A_7-AMD_3	A_{11}-AD_3
1	Coal flow, t/h	263.66	422.39	447.98	274.03
2	HFO flow, t/h	4.00	5.69	6.10	4.45
3	Combustion gases flow, m^3_N/h	1124.46	1677.38	1775.87	1084.02
4	Amount retained slag and ash, t/year	522,550	794,122	822,550	510,310
5	Amount CO_2 produced, t/year	2,119,006	3,158,961	3,352,088	2,041,116
6	NOx reduction method	primary	primary	primary	primary
7	Needed limescale, t/year	105,000	159,000	167,144	101,020
8	Production of dry gypsum, t/year	141,011	220,191	224,998	137,200
9	Electrofilter efficiency, %	99.9	99.9	99.9	99.9
10	Wet scrubber efficiency, t/year	93	93	93	93

Table 12. Minimum technical measures require.

6. Result and discussion

The possible cessation of strategic customer activity will drastically reduce the plant's operational efficiency and compromise further participation in its energy market, whatever the scenario under consideration. The only ways to survive the power plant are:

- Administrative integration of the power plant with the mining units so that the lignite price is less than 8 Euro/MWht. In **Figure 3**, one can see the tendency of variation in the operational cost of energy (electrical + thermal) for the four scenarios, compared to the continuity scenario characterized by the maintenance of the strategic client.

http://dx.doi.org/10.5772/intechopen.80887

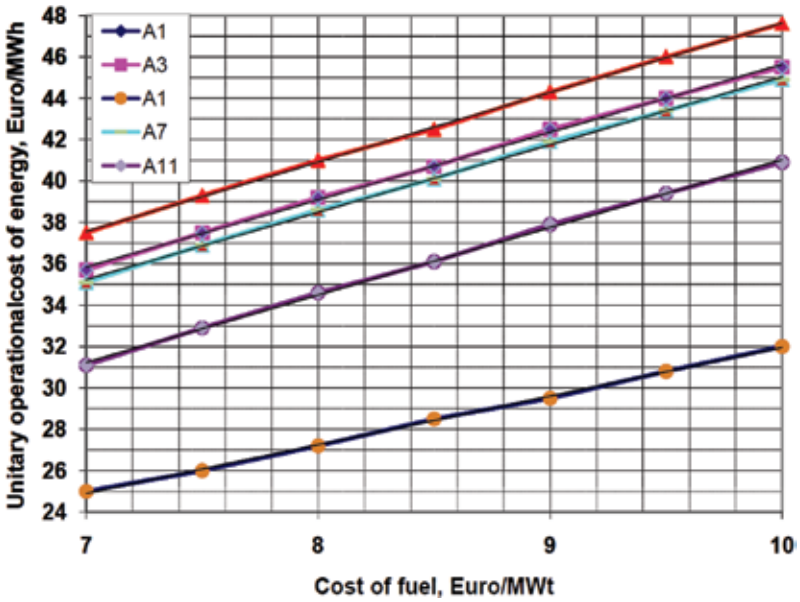

Figure 3. Variation of the specific energy cost depending on the lignite price [10].

The calculation was based on the situation, where the weight of the fuel of 8.5 Euro/MWht is 70% in the total expenses of the boiler plant. The lowest cost is given by the current scheme in operation with the most important customer. The next scenario is the development with a 200 MW group.

- Conclusion of long-term electricity contracts at prices slightly above the market price.
- Efficiency of branch activity by increasing the share of fuel in electricity from 70 to 80–85%.
- Finding an industrial steam consumer to replace the current one in the thermal balance of the power plant.
- Increasing the thermal energy delivered in cogeneration by finding low-level heat consumers (greenhouses); in this case, the operation of the plant can only be profitable in seasonal mode (15 October–15 March).

7. Conclusions

The plant will only be able to operate on scenarios that use primary fuel, lignite. The choice of one or the other of the existing solutions will be based solely on the analysis of the evolution of the price of electricity utilization. If this parameter has an annual growth slope of more than 10%, projects involving the increase of installed power, A_3-AM_3, are preferred and should be taken into account. However, if, in the coming years, there is a slower increase in the price of

electricity used, caution should be exercised when making a decision on new investments in the increase of installed power.

Author details

Adelaida Mihaela Duinea

Address all correspondence to: adelaida.duinea@incesa.ro

Faculty of Electrical Engineering, University of Craiova, Craiova, Romania

References

[1] Workshop Clean Air for Europe (Programul CAFÉ) – EURELECTRIC/VGB; December; 2015. Available from: www.eurelectric.org

[2] Pop O, Radu I, Arama S. Attracting Investors in Conversion Projects on Coal for Hydrocarbon Groups, Round Table: Fossil Fuels in Romania: Present and Future; 30 March 2016

[3] Taner T, Sivrioglu M. A techno-economic & cost analysis of a turbine power plant: A case study for sugar plant. Renewable and Sustainable Energy Reviews. 2017;**78**:722-730. DOI: 10.1016/j.rser.2017.04.104

[4] Hunton & Williams – Proposed privatization Strategy for Turceni and Rovinari Thermal Power Plants. Final report prepared for USAID and Ministry of Economy and commerce. Bucharest; 2013

[5] Esen H, Esen M, Inalli M, Pihtili K. Energy and exergy analysis of a ground-coupled heat pump system with two horizontal ground heat exchangers. Building and Environment. 2007;**42**(10):3606-3615

[6] Tolga T, Mecit S. Energy-exergy analysis and optimisation of a model sugar factory in Turkey. Energy. 2015;**93**(1):641-654. DOI: 10.1016/j.energy.2015.09.007

[7] Esen H, Esen M, Inalli M. Technoeconomic appraisal of a ground source heat pump system for a heating season in eastern Turkey. Energy Conversion and Management. 2006;**47**(9–10):1281-1297

[8] Tolga T. Energy and exergy analyze of PEM fuel cell: A case study of modeling and simulations. Energy. 2018;**143**:284-294. DOI: 10.1016/j.energy.2017.10.102

[9] Tolga T. Optimisation processes of energy efficiency for a drying plant: A case of study for Turkey. Applied Thermal Engineering. 2015;**80**:247-260. DOI: 10.1016/j.applthermaleng.2015.01.076

[10] Duinea AM. About the development strategies of power plant in energy market. AIP Conference Proceedings. 2017;**1918**:020012. DOI: 10.1063/1.5018507

[11] Duinea AM, Ciontu M, Bratu C. Some considerations about the hierarchy of the technical solutions for the modernization of power plants. In: Proceedings of the International Conference on Energy, Environment Development and Economics (EEDE'16); 14–17 July 2016; Corfu. Greece; 2016

[12] Duinea AM, Mircea PM. Issues regarding the furnace operation of the steam generator in dynamic regime. Journal of Sustainable Energy. **V**(2):31-34. ISSN 2067-5534

[13] Duinea AM. Analysis, Modeling and Simulations of Heat Exchange Surfaces of Steam Generators. Craiova: Sitech; 2015

[14] Duinea AM. Advances in modeling and simulation of steam generators in power plants. In: Schellenberg C, editor. Design, Types and Applications. 2017. ISBN: 978-1-53612-510-8

[15] Duinea A. Contributions for computerized management of energy facilities operation [thesis]. University of Craiova; 2009

[16] Lazaroiu G. Programming Systems from Modeling and Simulation. Bucureşti: Publishing Politehnica Press; 2005

Chapter 3

Pipeline Health Monitoring to Optimise Plant Efficiency

Anurag Dhutti and Tat-Hean Gan

Additional information is available at the end of the chapter

http://dx.doi.org/10.5772/intechopen.80844

Abstract

This chapter presents technological innovations that support asset integrity management—a crucial activity for optimising plant efficiency. In ageing thermal and geothermal power plants, critical assets such as steam piping are subject to high pressures and temperatures that accelerate damage mechanisms. Traditionally, the critical locations of these assets undergo routine inspection which is both costly and time consuming and affects the plant reliability and energy availability. There is an increasing trend in the application of non-destructive testing (NDT) and information technologies to in-service monitoring of these assets. The aim of this chapter is to provide a comprehensive overview of the state-of-the-art monitoring technologies for *steamlines*, with a focus on high temperature ultrasonic guided wave techniques. The enabling technologies, which include high temperature sensors, diagnostic data analysis algorithms and their monitoring performances, are reviewed. These technological advancements enable inspection without interruption of plant operations, and provide diagnosis and prognosis data for condition-based maintenance, increasing plant safety and its operational efficiency.

Keywords: thermal power plant, steamlines, non-destructive testing, ultrasonic guided waves, structural health monitoring, temperature compensation, monitoring data analysis, defect detection, optimised maintenance planning

1. Introduction

Thermal power plants (fossil fuel: coal, natural gas, oil; nuclear; and biomass) are critical to the global security of supply, accounting for 80% of global electricity [1], and provide flexibility in capability and availability to meet increasing electricity demand. To remain competitive in emerging utilities markets, the costs of power production need to be reduced. To

achieve this, utilities have two key objectives: to reduce capital costs by deferring replacement and life extension of expensive components; and to reduce operating and maintenance (O&M) costs by optimising operations, inspection and maintenance procedures. The need for reduced CO_2 emissions, improved plant efficiency and availability also drives harsher (high process temperatures and pressures) and cyclic duty schedules, resulting in accelerated and severe creep-fatigue damage. This demands increased attention on the critical components. However, reduction of O&M costs may promote fewer, shorter, substandard maintenance and inspection outages, thus placing the critical infrastructure at a greater risk of failure.

In recent years, there has been an increased emphasis on the development of damage prognosis systems that can inform the operators of a structure's health and developing damage, and can provide an estimate of its remaining useful life. These systems have the potential to transform maintenance procedures from schedule-driven to condition-based implementation, thus cutting the time for which the structures are offline, reducing life-cycle costs and decreasing labour requirements. Structural health monitoring (SHM) is an essential component of any damage prognosis system. It allows in-service monitoring of a structure for damage and provides information about any anomalies detected.

This chapter is devoted to high temperature pipelines (HTPs) which are critical components in a thermal power plant (TPP), providing connections between the feed water pumps, the boiler or heat exchanger and the turbine. Each plant has several kilometres of HTP carrying steam under extreme temperature and pressure conditions. At present, the majority of TPPs have an average operating age of over 30 years and HTP failure is listed among the major causes of ageing TPP outages. HTPs suffer continuous cyclic loading and extreme temperature and pressures, and are known to develop defects through a range of mechanisms—creep, fatigue [2], creep-fatigue [3] and thermal fatigue [4], and corrosion [5]. Root-cause analyses of super-heated boiler-tube failure [6] indicate thermal shock and differential thermal expansion are also responsible for defect development. High pH values for steam have been reported to cause stress corrosion cracking (SCC) in heat-affected zones (HAZs) [7].

Failure to detect such defects in HTPs have resulted in catastrophic failures (examples in **Figure 1**) every year or two, causing loss of life and widespread power cuts, with environmental damage and negative financial consequences.

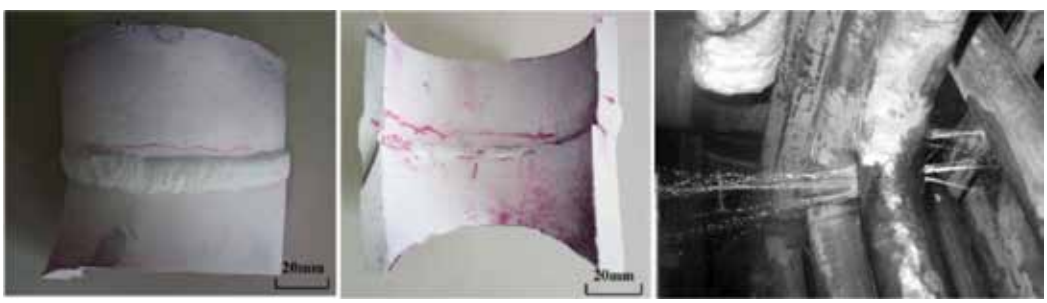

Figure 1. Crack appearance on the outer and inner walls of a furnace tube [7].

High resolution non-destructive testing (NDT) technologies such as X-ray and ultrasonic testing (UT) are state-of-the-art for periodic inspection and can detect cracks and wall thickness reduction. These techniques, however, present many challenges, such as over-heating equipment, personnel risks of heat exhaustion or burns, and the difficulty of accessing the pipe surfaces and are therefore only employed during planned maintenance outages. These traditional NDT techniques can provide only local condition information and thus require access to the pipe by, e.g., erection of kilometres of scaffolding and extensive lagging removal, which is expensive and time consuming. The guided wave testing (GWT) approach, on the other hand, provides a non-invasive remote solution with the ability to screen long lengths of pipe and provides 100% cross section area coverage from a single test point; it is also ideal for road crossings and buried pipes. GWT has been widely adopted by the Oil and Gas Industry and, until recently, this approach was used periodically for routine off-load inspections with re-deployable, detachable sensor systems. Repeated access to pipes for re-deployment, however, can be costly and time-consuming, and only possible for HTPs during outages. There are many current commercial systems (for example, see [8, 9]) used in the Oil & Gas Industry, but their operational temperature limits prevent their use on HTP.

This chapter first describes the underlining background of guided wave testing and its influence by temperature. Then recent developments on high temperature transducer design, coupling and data analytics relevant for the application will be discussed. The chapter can serve to provide guidelines for future developments of GWT-based SHM systems for HTP.

2. Background of ultrasonic guided wave technology

2.1. Ultrasonic wave theory

The term "ultrasound" refers to the propagation of mechanical stress waves in a medium at frequencies above 20 kHz, i.e. above the human audible range. Like any other wave, these waves have a velocity (c), wavelength (λ) and frequency (f) which are defined by Filipczynski [10] and related by Eq. (1).

$$c = f\lambda \tag{1}$$

An infinite medium supports two possible wave modes: compression and shear. The particle displacement for these wave modes and the direction of propagation are shown in **Figure 2**.

Compression waves are made up of particles vibrating in the same direction as the propagation of the wave. They can propagate in solids, liquids and gases. Shear (also known as transverse) waves vibrate perpendicular to the direction of propagation and can exist only in materials with shear "stiffness" (solids and viscous liquids). Compression and shear waves travel at different velocities but are constant in most materials at a constant temperature. The propagation velocities of compression waves (c_c) and shear waves (c_s) are related to the material's density (ρ), Poisson ratio (μ) and Young's modulus (E) or the modulus of rigidity (G) by Eq. (2, 3).

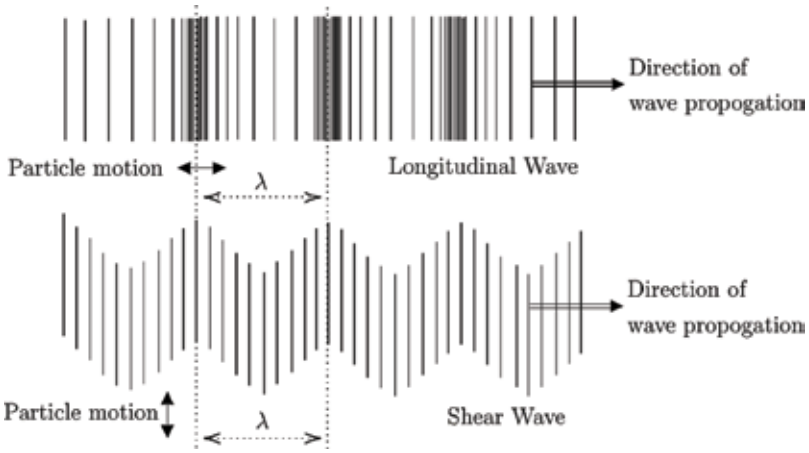

Figure 2. Illustration of particle motion in the two bulk wave modes: longitudinal and shear.

$$C_c = \sqrt{\frac{E(1-\mu)}{\rho(1+\mu)(1-2\mu)}} \tag{2}$$

$$C_s = \sqrt{\frac{E}{2\rho(1+\mu)}} = \sqrt{\frac{G}{\rho}} \tag{3}$$

Acoustic impedance (Z) is used to calculate the reflection and transmission coefficients between two media and is defined as the product of wave velocity (c) and material density (ρ).

$$Z = \rho c \tag{4}$$

Transmission through a finite layer is dependent on the layer's thickness, acoustic impedance and the frequency of the wave. Layers can be acoustically transparent when their thickness is equal to an integral multiple of half wavelengths; due to the formation of standing waves within the layer. This holds when the incident wave is perpendicular to the surface. When the wavelength is much larger than the thickness of the layer, both sides of the layer are approximately in phase so the layer is effectively transparent and these bulk waves travel through a material unaffected by boundaries. Waves that travel along the layers instead of through them are called ultrasonic guided waves (UGW).

Other wave modes such as Rayleigh waves [11] occur due to object boundaries. Rayleigh waves have an elliptical vibration with the major axis of vibration perpendicular to the direction of propagation. These surface waves exist in a half-space, a surface backed by a semi-infinite volume, and can penetrate to a 1.5λ depth below the surface. In contrast, Lamb waves fill the entire volume, provided its thickness is less than 2λ. These were first analysed on plates by Horace Lamb [12] and can be considered as Rayleigh waves bounded by two parallel edges. The fundamental theory of Lamb waves and a review of their applications for long-range inspection of different structures have been reviewed [13].

Just as with plates, hollow tubes have a thin cross section and are bounded by two surfaces. Guided waves in hollow cylinders and thin walled tubes have thus been explored [14] and are also termed Lamb waves. Lamb wave theory assumes an infinite rectangular plate as the medium, but in a hollow cylinder, the circumferential curvature results in a continuous (periodic) boundary condition in distinction to a plate's infinite edge. Therefore the propagation of Lamb waves in tubes is more complex and exists in more numerous modes in tubes than in plates. These will be described in the next section.

2.2. Guided waves in pipes

Guided wave propagation in cylindrical structures has been thoroughly investigated by Gazis and Zemanek [15, 16] who showed the presence of three basic families based on their displacement patterns: Axially symmetric wave modes—longitudinal (L) and torsional (T); and non-axially symmetric—flexural (F) modes, as illustrated in **Figure 3**.

Looking along the pipe from one end, the L wave mode can be visualised as a travelling bulge, the F wave as a flexing of the pipe in any number of directions and the T wave as a twisting of the pipe. The wave modes' designations defined by Meitzler [17] include two numbers, for example, T(0, 1), where the first number is the circumferential wavenumber (also known as the order) and the second number denotes the sequential mode. If the order is zero the wave is axially symmetric and the displacement pattern does not vary around the circumference. All torsional and longitudinal wave modes are axially symmetric. If the order is higher than zero, the wave is non-axially symmetric and must be flexural.

The guided wave particle displacement, u (and particle velocity) is a function of frequency, material thickness and the diameter of the pipe with the following relation in Eq. (5) [18].

$$u = A\, e^{i\left(kz + \frac{n\theta}{2\pi} - \omega t\right)} \tag{5}$$

where A is a constant, k is the wavenumber along the axis of the pipe, z is the distance along the pipe, n is the wavenumber around the circumference of the pipe and θ is the angle around

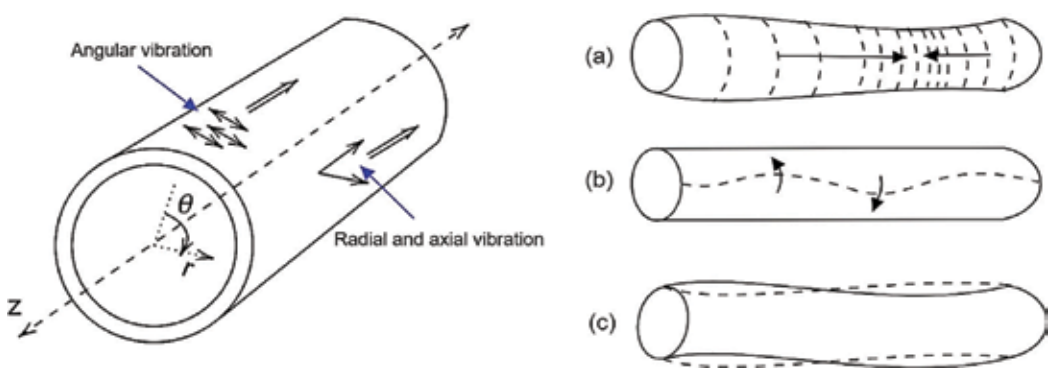

Figure 3. Representation of (a) longitudinal, L (b) torsional, T and (c) flexural, F wave modes in pipes.

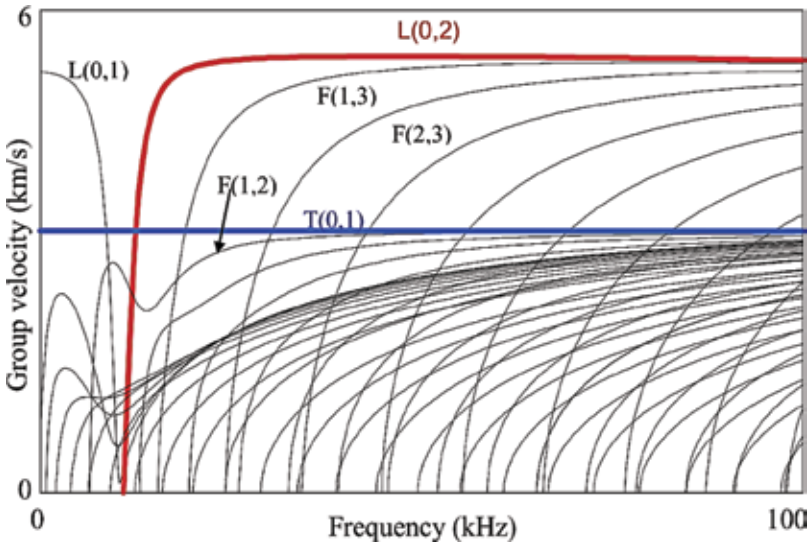

Figure 4. Group velocity dispersion curves for a 6″ schedule *40 steel pipe* [23].

the circumference as defined in **Figure 3**. There are a number of wave modes present at any given frequency. These wave modes can also be described mathematically by the characteristic equation, Eq. (5). The solution of the characteristic equation then provides dispersion curves which are used to illustrate the variation in the wave's phase velocity (v_p) and group velocity (v_g) over a range of frequencies for each wave mode. Commercial software such as *DISPERSE* [19] and *GUIGUW* [20] solve the characteristic equation through iterative computation to generate dispersion curves for multilayer structures.

The group velocity dispersion curve of a 6 inch Schedule 40 steel pipe (**Figure 4**) shows that more than 50 wave modes exist below 100 kHz. For non-dispersive wave modes in a particular frequency range, the phase velocity dispersion curve will be flat with v_p close to v_g [21]. In contrast, dispersive wave modes spread in space over time as they have frequency-dependent velocities and different v_p and v_g. Non-dispersive signals are preferred for ultrasonic testing as dispersion complicates the analysis of signals for flight measurement [22] and reduces the signal to noise ratio. In **Figure 4**, the highlighted fundamental torsional T(0,1) and longitudinal L(0,2) modes are non-dispersive in the frequency range of interest for UGW. These wave modes have been implemented for GWT technique, which will be described now.

2.3. Pipeline inspection using guided wave testing

In conventional UT, high frequency ultrasound is used to measure wall thickness examining the volume of material directly under the test probe location. In contrast, in GWT, an ultrasonic pulse is transmitted along the pipelines via a pulse-echo system (**Figure 5**) which comprises of a pulser-receiver, a laptop PC to control the test and an array of transducers designed to transmit the desired wave mode. Guided waves within pipelines at lower frequencies possess low attenuation and can propagate long distances (tens of meters in each direction). A proportion

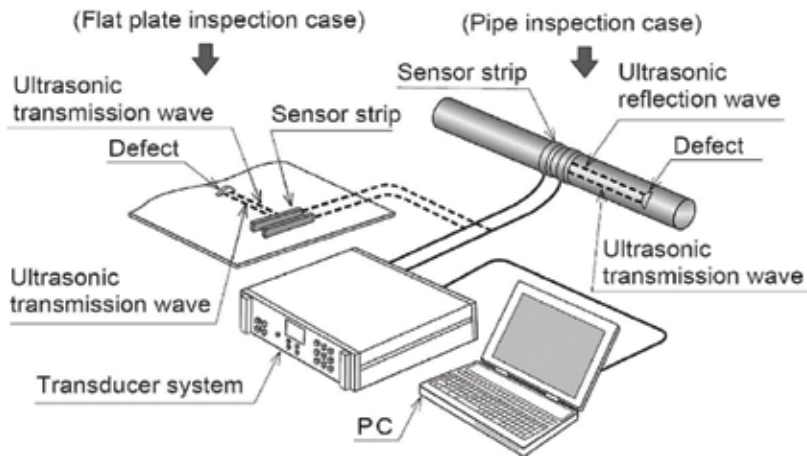

Figure 5. Schematic of guided wave pipe inspection and monitoring system [25].

of the energy contained in the propagating wave front will be reflected back to the tool when an acoustic impedance change occurs due to the presence of a feature or discontinuity in the pipe. It can provide 100% coverage of the cross section of the pipe; detecting and locating both internal and external defects without disrupting operation.

This technology enables rapid screening of long lengths of pipes and is also commonly known as long range ultrasonic testing (LRUT). The definitions and standards for LRUT instrumentation, data collection and analysis have been set in the International Standard ISO 18211:2016 "Nondestructive testing—Long-range inspection of above-ground pipelines and plant piping using guided wave testing with axial propagation" [24].

Initial field trials of this technique were carried out in the mid-1990s [26] where a dry coupled transducer system [27] was used to excite L(0,m) mode and propagation distances approaching 50 m were reported. The same research group began to refine previous findings through their development of a shear transducer and details on responses from a variety of discontinuities found in industrial pipework were reported [28]. This led to the development of several commercial GWT systems [8, 9] which were widely adopted by the Oil and Gas Industry for periodic off-load inspections and have shown reliable defect detection capability for (reducing) defects that remove around 3–9% of the pipe cross section area.

2.3.1. Guided wave mode selection

Dispersion and multiple guided wave modes are the main problems for GWT [29] and excitation of single and non-dispersive wave mode is of practical importance [30] to obtain signals that can be reliably interpreted. The selection of guided wave mode and frequency for GWT depends on properties of the system under inspection (dispersion, attenuation, and sensitivity) and on the transduction system (excitability, detectability and selectivity). Based on these properties, a procedure for identification of suitable modes for a particular inspection task was proposed by Wilcox [31]. T(0,1) and L(0,2) modes are the most attractive modes for GWT

as they are non-dispersive and their mode shape has uniform stress over the whole cross section of the pipe providing 100% coverage.

In GWT, the sensitivity is a function of the signal-to-coherent-noise ratio where the coherent noise is caused by excitation of unwanted modes. It is therefore essential to design the transducer system to excite only the chosen mode. Longitudinal modes may provide ~2.5 times more flaw sensitivity compared to torsional modes [32] but complex signal processing is required due to their dispersive nature. In practice, the torsional mode is more commonly used as it is non-dispersive in the entire frequency range, it does not get influenced by fluid in the pipe unlike longitudinal modes (due to their radial displacement) and is also easier to excite in pure form, which will be described in the next section.

2.3.2. Guided wave excitation

There are several transduction technologies for generation and detection of UGW including electromagnetic acoustic transducers (EMATs) [33], piezocomposite transducers, magnetostrictive devices [34], lasers and the most commercially used piezoelectric transducers. A transducer can excite all the modes that exist within its frequency bandwidth. This can complicate signals and make their interpretation difficult.

Initial development of a piezoelectric transducer system for GWT of pipes [26] reported the use of two circumferential rings of dry coupled shear transducer [27] to obtain unidirectional propagation of L(0,2) mode. The directionality is achieved with the application of time delays and phase manipulation between the rings. However, the second axially symmetric L(0,1) mode is also excited by the two-ring system and can make interpretation of the results less reliable. Additional rings of transducers can be implemented to supress the L(0,1) mode but this adds to the cost of the system, especially for larger diameter pipes. Longitudinal modes are also affected by the fluid in the pipe because of their radial displacement.

The T(0,1) mode, on the other hand, is the only axially symmetric torsional mode in the frequency range of interest. So only two rings of transducers are required to obtain single mode and unidirectional excitation. Torsional forcing can be achieved by simply rotating the shear transducer used for the L(0,2) mode by 90° to apply the force in the circumferential direction rather than axially. A transducer array with an even circumferential spacing between transducers generates signals with high-level mode purity. To cancel the propagation of non-axisymmetric Flexural modes, the number of transducers in the ring should be greater than the highest order of flexural mode present in the chosen frequency range [35].

In terms of excitation input, narrow band signals are generally used, such as several cycles of sine wave modulated with a window function (e.g. Hanning). They provide good signal strength and avoid dispersion while propagating long distances. The choice of central frequency for this excitation is based on the desired mode which should have low dispersion over this narrow band so that all frequencies will travel at the same velocity, minimising errors introduced by dispersion. By exciting all transducers in a ring equally and concurrently, an axially symmetric mode is launched.

2.3.3. Guided wave propagation and reflections

When an axisymmetric mode (T or L) is incident on an axisymmetric feature such as a flange, uniform weld or a square end, axisymmetric modes are reflected. But in the presence of non-axisymmetric features such as corrosion, a non-axisymmetric wave will be reflected back to the transducer rings. A number of studies have explored the interaction of UGW modes with defects [35] and features in pipes such as flanges and pipe supports [28]. For the L(0,2) mode the reflection from defects has been evaluated as a function of defect depth, axial and circumferential extent and of excitation frequency [36]. Likewise the interaction of the T(0,1) mode with pipe defects [37] such as cracks and notches [38] and holes [39]. The presence and axial locations of defects can thus be determined by analysing these reflections and their time of arrival.

2.4. Pipeline monitoring system requirements

SHM using GWT has found a variety of practical applications on the rail, ship hull, aircraft and containment structures [40] and the requirement for continuously assessing the integrity of critical pipelines has fostered activities to develop their monitoring systems. A state-of-the-art review of pipe monitoring technologies can be found in [41] but these are not targeted for HTP. There are pipe monitoring solutions for HTP offered by Ionix [42] and Permasense [43] used for wall thickness monitoring but can only provide local coverage at the installed location. To enable long range inspection using GWT for SHM of pipelines, there is a requirement for permanently installed transducers to repeatedly transmit excitation signals and receive responses which are then analysed for early detection of defects to ensure the integrity of the pipeline. The system should be reliable throughout prolonged exposure to variable environmental and operational conditions. A monitoring solution based on GWT-gPIMS [44] is offered by Guided Ultrasonic Ltd. and its stability and defect detection capabilities have been demonstrated [45]. This is however limited to operate at temperatures below 90°C and hence not applicable for HTPs. The following sections review HT transducer designs and the data analysis for temperature corrections that can enable the application to HTPs.

3. High temperature guided wave transducers

3.1. Piezoelectric transducer design

Piezoelectric sensing is the most promising technique due to its high-temperature stability and reliability, and its cost-effectiveness with simple and light-weight construction [46]. Piezoelectric transducers are constructed using five main components: a face plate, a piezoelectric element, backing/damping block, casing and electrical connections, as illustrated in **Figure 6**.

The electrical connection allows the transfer of an electrical pulse to and from the piezoelectric element. The live connection is generally made with a lead, and earthing is effected via the casing. The casing also provides mechanical support for the whole transducer as well as electrical shielding for the piezoelectric element. The damping or backing block damps the vibration

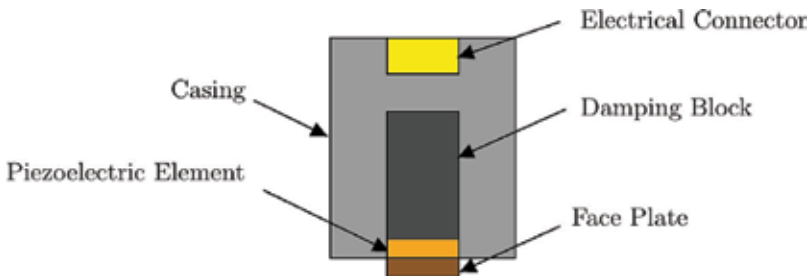

Figure 6. Construction of a generic piezoelectric transducer.

of the piezoelectric element after the excitation pulse has been transmitted. The piezoelectric element generates the mechanical signal from an electrical input—or, conversely, an electrical signal from a mechanical input—enabling transmission and reception of ultrasonic signals, respectively. The face-plate protects the fragile piezoelectric element.

In order to properly design a piezoelectric transducer the following factors must be addressed: (a) all wave modes apart from the one being used for inspection must be suppressed; (b) frequency response should be linear (**Figure 7**) in the region of operation (otherwise neighbouring resonant frequencies may give rise to mode coupling, frequency jumps and performance dips); and (c) the transducer efficiency must be high.

The major challenge for ultrasonic testing at high temperature is to develop transducers that can operate at the target temperatures whilst providing suitable coupling between the transducer and the target material, and provide long term stable performance at the target temperature. This application requires careful selection of materials as presented below.

3.2. High temperature piezoelectric materials

The electromechanical properties that characterise piezoelectric materials are described by a number of interrelated coefficients standardised by the IEEE [47]. These coefficients include

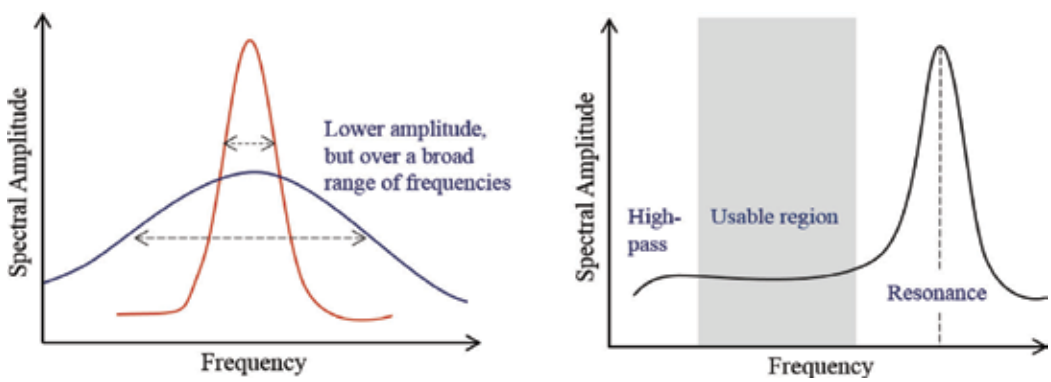

Figure 7. Sketch of a piezoelectric transducer frequency response of a narrow-band (red) and a broadband transducer (blue) (left) and the highlighted region (right) shows the usable region for UGW.

piezoelectric, dielectric and elastic material properties. High temperature piezoelectric materials are being developed for SHM and NDE of the new generation turbines and critical structures in more efficient nuclear/electrical power plants. The temperature limitation of the piezoelectric materials is governed by increased conductivity and mechanical attenuation and variation of the piezoelectric properties with temperature.

There are a number of high temperature materials commercially available and others under development. These are of two types: ferroelectric polycrystalline (such as barium titanate—$BaTiO_3$ and lead zirconate titanate—PZT) and single crystals (such as Quartz—SiO_2 and Lithium Niobate—$LiNbO_3$). The single crystals have high electrical resistivity and low losses, they avoid domain-related ageing behaviour and have an excellent thermal stability. Various piezoelectric materials have been researched for high temperature applications, including quartz, gallium phosphate ($GaPO_4$), langasite ($La_3Ga_5SiO_{14}$), and aluminium nitride (AlN). Each of these materials has unique advantages and drawbacks for use in HTPE transducers and a detailed review of these materials with their properties can be found in [48–50].

A useful guide for the selection of the appropriate piezoelectric material is its figure-of-merit (FOM) depending on the specific application [51]. The FOM for a high temperature transducer is the product of piezoelectric charge and voltage coefficients ($d_{ij} \times g_{ij}$), where a higher value gives a higher electromechanical coupling defining the ratio of stored electrical energy to applied mechanical energy, and *vice versa*. Phase transitions are also an important consideration for material selection, as, beyond specific temperatures, the ferroelectric material may transform from its ferroelectric phase to a high symmetry non-ferroelectric phase. The transition temperature is also referred to as the Curie temperature (T_c) and above this temperature, the material is permanently depolarized and no longer piezoelectric. For high temperature monitoring applications, it is not recommended to use ferroelectric materials at temperatures exceeding $0.5T_c$ [52] in order to minimise thermal ageing and property degradation. **Figure 8** shows the FOM of selected piezoelectric materials for high temperature shear transducer.

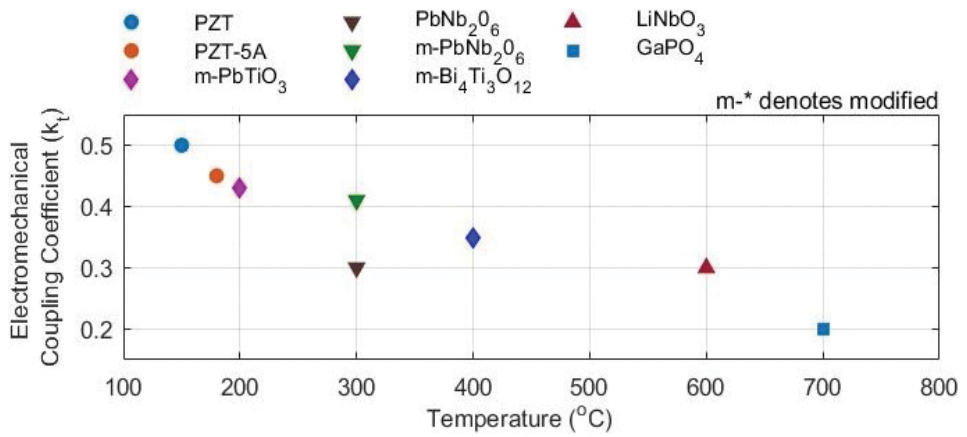

Figure 8. High temperature piezoelectric materials and their maximum operating temperature and electromechanical coupling factor in the thickness mode.

To apply the electric field and to obtain the generated charge signal in the piezoelectric material, thin film electrodes (~100 nm) are commonly applied. Many metallic, metallic alloys and conductive ceramic electrodes have been researched for high temperature applications. The most popular is a platinum thin film electrode (recommended for T < 650°C) with persisting excellent electrical properties, high melting point and resistance to oxidation. Other thin film electrodes for operation at temperatures up to 850°C have been summarised in [53]. The shape of the electrode can also influence the behaviour or mode of vibration as shown in a previous study [54], so FEA modelling is often necessary to achieve the desired displacement patterns.

3.3. High temperature transducer backing

In contrast to bulk resonant transducers which have relatively low internal damping making them very good for producing resonant transducers, piezoelectric materials must be damped heavily to produce broadband, guided-wave transducers.

3.4. Transducer assembly for high temperatures

To assemble the transducer the components in Section 3.1 must be bonded together. There are limitations on how this can be done without damaging the parts—particularly the piezoelectric material. The temperature required for bonding must not be high enough to cause melting and must be below half of the piezoelectric material's Curie temperature. The bond must also remain strong at the operating temperature of the device, as the transducer assembly can suffer permanent damage at high temperatures caused by excessive differential thermal expansion. The pressure used in the bonding process is another key parameter—at too high a pressure there could be damage to the parts. A crack on one part will cause diffraction of the acoustic waves which could seriously affect the performance of the transducer. The bond must also be elastic in order to be able to change shape as the piezoelectric deforms, and as the other parts of the transducer expand or contract due to changes in temperature. Common methods of bonding include the use of high temperature epoxy, which is a thermosetting polymer used as a glue. Also, glass solder can be used up to 500°C, after which it reacts chemically with other components. Other methods include regular soldering, diffusion bonding, ultrasonic welding, cementing, sol–gel and vacuum brazing. A comprehensive review of these bonding techniques and designs of ultrasonic transducers for high temperature can be found in [48].

3.5. Transducer coupling mechanism

The mechanical wave generated within the piezoelectric element has to be coupled into the object to be inspected. There are three different methods of acoustic coupling at high temperatures: dry-coupling (with a high pressure); fluid coupling; and solid coupling. For high frequency UT, the ultrasound propagates through the transducer's face plate to the object through a couplant, generally a gel but an elastomer or water can also be used. However, for UGW shear wave transducers, a coupling with a high modulus of rigidity must be used, which is commonly achieved by dry-coupling. The piezoelectric transducers may be attached to the pipe using adhesives. The effect of adhesive on the ultrasonic vibrations has been

investigated through parametric studies on bonding layer properties such as adhesive thickness and shear modulus [55]. Improperly prepared bonding layers with uneven distribution of adhesives under the transducer can significantly reduce the performance of the transducer. Two methods—electromechanical impedance characterisation and time-domain terahertz spectroscopy [56]—have been previously used to assess the quality of these adhesive bond.

4. Guided wave monitoring data analysis

Once the SHM system is installed on the pipe, regular inspection data is recorded into a monitoring database. The collected UGW data is then processed to provide information regarding the presence of a defect and information regarding its type, location and severity. The performance of defect detection techniques relies on the hypothesis that the recorded signal remains stable if no defect is present. The UGW data is, however, susceptible to changes in environmental and operational conditions (EOCs) such as temperature, humidity, pressure, vibration, flow, etc., influencing the electronic devices, transducer time behaviour and even the structure itself. Of the EOCs, temperature has been shown to be the dominant effect on UGW, often masking the real damage information. This can lead to false diagnostics and prognostics and therefore to ensure the reliability of the SHM system, the data should be corrected for any temperature induced variations. In the following sections, the effect of temperature on the UGW signals will be described and different data correction methodologies are discussed. Thereafter, approaches for defect detection from the corrected data are presented.

4.1. Effect of temperature on ultrasonic guided waves

Propagation of sound depends on the type, temperature and composition of the medium. Several investigations into the effect of temperature on the recorded waveform have been carried out [57] and change of temperature has been shown to be the main source of fluctuations in the received signals [58]. The influence of temperature on GWT of pipes is a combination of effects on the pipe mechanical properties and on ultrasonic transducers and their bonding [59]. However, for small temperature variations of a few degrees, the effect on transducer performance has been shown to be significantly less than that on wave propagation [60].

UGW signals undergo changes in amplitude and phase under the influence of varying temperature. The phase shift in the transducer signals is mainly attributable to the change in wave propagation velocity from changes in the mechanical properties of the pipe [61]. Changes in signal amplitude are attributable to changes in the temperature-dependant properties of the ultrasonic transducer, particularly of the piezoelectric and adhesive materials, as described in Section 3. It is possible through careful selection of adhesives and transducer materials to minimise this variability.

The relevant pipe mechanical properties are the elastic and shear moduli and the density, which relate to the elasto-acoustic properties of the material, acoustical absorption and ultrasonic wave velocity. Thermal expansion changes propagation distance directly and indirectly through changes in the thickness of the pipe. The effects of temperature are also reported to be

increased at greater propagation distance. The relationship between the difference in arrival times of the signal and the change in temperature of the structure can be written as

$$\delta t = \frac{d}{v}(\alpha - \gamma)\delta T \tag{6}$$

Here, δt is the difference in arrival times of signals when the change in temperature of the structure is δT. d is the distance propagated by the wave and v is the wave velocity. α is the coefficient of thermal expansion and γ is the coefficient of change in phase velocity. γ is usually significantly greater than α and hence from Eq.(6), it can be seen that the main contribution to the time shift due to temperature variations is from the change in wave velocity. Also, since the time shift is directly proportional to the propagation distance, the effect of temperature variation increases with propagation distance. The inverse relation to the wave velocity suggests that faster modes will be less affected than slower ones.

4.2. Signal processing for data correction

Temperature-induced variations in UGW signals can adversely affect the defect detection capabilities as observed in a previous study [62] which investigated the effect of temperature variation on Lamb waves from ambient temperatures up to 70°C. The temperature effect (analysed using principal components) was reported much more pronounced than the effect of a drilled damage (hole) with a diameter of 1 mm. There have been several investigations within the SHM research community to address this issue, and a number of temperature-compensation strategies have been proposed. The main objective of temperature compensation is to achieve propagation time and amplitude correction, and these strategies can be divided into two techniques: data driven and analytical physics-based.

For data driven techniques, a large baseline set of transducer measurements from the structure at a different temperature is required. It has been suggested to use a 'bank' of baseline signals for various temperatures and to pick a baseline signal which minimises differences relative to the test signal for that temperature. This method is called optimum baseline selection (OBS) and the selection criteria can be based on mean square deviation [57] or maximum residual amplitude [63]. A large baseline set is not always available and in some cases, the temperature of the selected baseline can be different from the temperature of the test signal. In order to adjust the selected baseline, baseline signal stretch (BSS) was introduced, which in its simplest form only requires a single baseline datum at a reference temperature. BSS is carried out using time domain stretching where local coherence is estimated as a function of time using short time cross-correlation [57]. A combination of BSS and OBS has been applied by [59, 63–65] to provide enhanced temperature compensation while requiring a reduced number of baseline data sets. New methodologies proposed for stretch-based temperature compensation [66] operate on signals in the stretch factor and scale-transform domain and have shown improved computation speed.

The physics-based compensation techniques [57, 67] are based on transducer signal reconstruction at different temperatures based on underlying physical principles as described in Section 4.1. One such technique is proposed in [68] where the changes in elastic modulus and thermal expansion were used to model the varying time-of-flight over a modest temperature range within ±50°C, which gave good agreement with experiments. These analytical solutions

http://dx.doi.org/10.5772/intechopen.80844

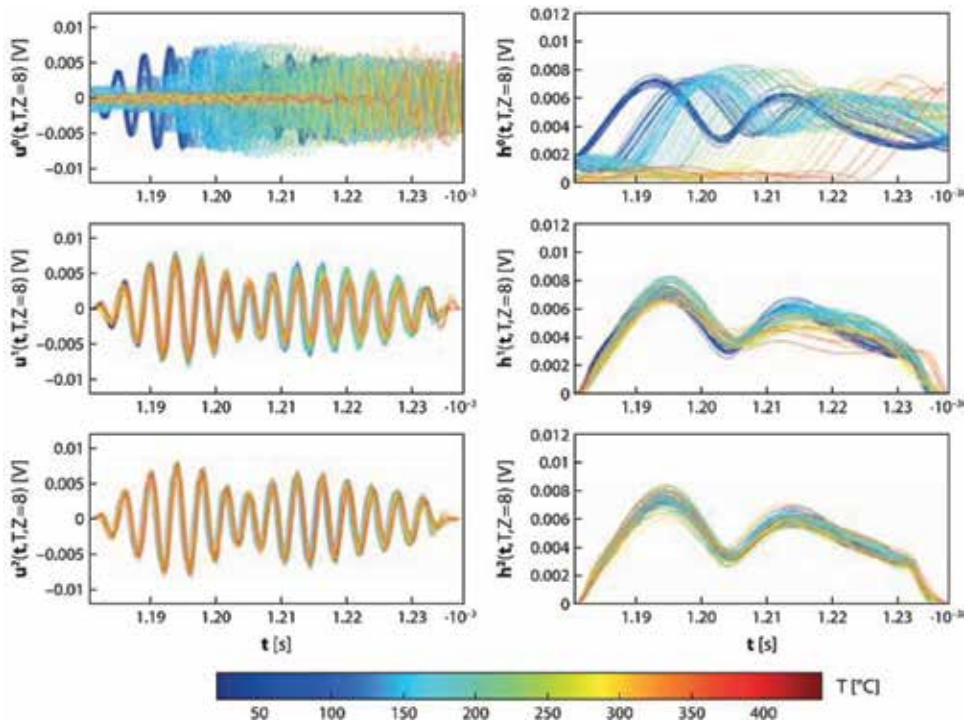

Figure 9. Example results of temperature correction, (top) original signals, signals after (middle) correction in the time domain, and (bottom) phase and amplitude correction [69].

were limited to simple structural geometries and boundary conditions. Analytical models can also be coupled with data-driven strategies, with fewer baseline measurements making this approach efficient, practical and useful (**Figure 9**) as demonstrated in [69].

4.3. Damage detection methodologies

To detect whether the pipeline being inspected has developed damage, a method for damage detection must be applied to the corrected data. Damage detection is generally performed by unsupervised algorithms, as the inspection data corresponding to the damage state is not known *a priori*. One such algorithm is outlier analysis (OA) [70] where damage sensitive features are extracted from the signals, and the aim is to identify if the measured signal has deviated from the baseline distribution by defining a threshold. This threshold depends on the baseline data and its statistical representation. The analysis can be applied as univariate or multivariate depending on the number of features. Root mean square (RMS) value has been successfully used as a damage sensitive feature for detection of notch and hole type defects on a plate [57], and for corrosion type defects on pipes [71] using torsional and flexural modes. For multivariate analysis, a vector of damage index is formed by extracting a number of features and classical methods of multi-variate statistics such as principal component analysis (PCA) is applied to them. For the multi-variate case, OA can be performed using a self-organising mapping technique [72] or Mahalanobis squared distance [70]. An artificial neural network (ANN)

based method was applied in [70] for damage classification and it was able to outperform OA for damage detection with just one feature. However, for implementing an ANN based approach, data from the structure with known types and levels of damage is required.

5. Conclusions

This chapter presents GWT for structural health monitoring of high temperature pipelines to support asset integrity management and condition based maintenance for optimising plant efficiency. To provide the reader with a background on GWT, a comprehensive overview of this technology covered the fundamental theory of guided waves in pipes, GWT system components and the desired input parameters for optimising performance. GWT technology has been widely used in the industry for routine inspection of pipelines. To avoid costs associated with repeated access, monitoring systems have been developed and have demonstrated the improved reliability of information and enhanced defect detection capability. The enabling technologies for HTP monitoring, which include high temperature guided wave transducers, temperature data correction and diagnostic algorithms, are reviewed. These technologies can advance the current GWT-based monitoring systems for application on HTPs. This will provide diagnosis and prognosis data to ensure the integrity of HTPs without interruption of plant operation, thus increasing plant safety and its operational efficiency.

Author details

Anurag Dhutti[1] and Tat-Hean Gan[1,2]*

*Address all correspondence to: tat-hean.gan@brunel.ac.uk

1 Brunel University London, UK

2 TWI Ltd. Granta Park, Cambridge, UK

References

[1] International Energy Agency. Key world energy statistics [Internet]. 2017. Available from: http://www.iea.org/ [Accessed: 02/01/2018]

[2] Bush SH. Failure mechanisms in nuclear power plant piping systems. Journal of Pressure Vessel Technology. 1992;**114**:389-396. DOI: 10.1115/1.2929244

[3] Gaur B, Babakr A. Piping failure in a superheated steam service—A case study. Matériaux & Techniques. 2013;**101**:206. DOI: 10.1051/mattech/2013067

[4] Viswanathan R, Stringer J. Failure mechanisms of high temperature components in power plants. Journal of Engineering Materials and Technology. 2000;**122**:246-255. DOI: 10.1115/1.482794

[5] Sabouri M, Hoseiny H, Faridi HR. Corrosion failure of superheat steam pipes of an ammonia production plant. Vacuum. 2015;**121**:75-80. DOI: 10.1016/j.vacuum.2015.07.022

[6] Naď M, Buzík J, Létal T, Lošák P. Root-cause analysis of superheater-tube failure. Materials and Technology. 2017;**51**:503-507. DOI: 10.17222/mit.2016.204

[7] Xu S, Meng W, Wang C, Sun Z, Zhang Y. Failure analysis of TP304H tubes in the superheated steam section of a reformer furnace. Engineering Failure Analysis. 2017;**79**: 762-772. DOI: 10.1016/j.engfailanal. 2017.05.033

[8] Eddyfi. Long-Range Guided Wave Testing with Teletest Focus+ [Internet]. 2018. Available from: https://www.teletestndt.com/ [Accessed: 06/10/2018]

[9] Guilded Ultrasonic Ltd. Inspection [Internet]. Available from: http://www.guided-ultrasonics.com/inspection/ [Accessed: 06/10/2018]

[10] Filipczyński L, Pawłowski Z, Wehr J. Ultrasonic Methods of Testing Materials. London, UK: Butterworths; 1966. p. 280

[11] Viktorov IA. Rayleigh and Lamb Waves. Boston, MA: Springer US; 1967. p. 154. DOI: 10.1007/978-1-4899-5681-1

[12] Lamb H. On waves in an elastic plate. Proceedings of the Royal Society A: Mathematical, Physical and Engineering Sciences. 1917;**93**:114-128. DOI: 10.1098/rspa. 1917.0008

[13] Su Z, Ye L. Identification of Damage Using Lamb Waves. London: Springer; 2009. p. 346. DOI: 10.1007/978-1-84882-784-4

[14] Silk MG, Bainton KF. The propagation in metal tubing of ultrasonic wave modes equivalent to lamb waves. Ultrasonics. 1979;**17**:11-19. DOI: 10.1016/0041-624X (79)90006-4

[15] Gazis DC, Herman R, Wallis RF. Surface elastic waves in cubic crystals. Physics Review. 1960;**119**:533-544. DOI: 10.1103/PhysRev.119.533

[16] Zemanek J. An experimental and theoretical investigation of elastic wave propagation in a cylinder. The Journal of the Acoustical Society of America. 1972;**51**:265-283. DOI: 10.1121/1.1912838

[17] Meitzler AH. Mode coupling occurring in the propagation of elastic pulses in wires. The Journal of the Acoustical Society of America. 1961;**33**:435-445. DOI: 10.1121/1.1908685

[18] Gazis DC. Three-dimensional investigation of the propagation of waves in hollow circular cylinders. The Journal of the Acoustical Society of America. 1959;**31**:573-578. DOI: 10.1121/1.1907754

[19] Lowe MJS. A model for predicting the properties of guided ultrasonic waves, and illustration of its application to NDT. In: IEE Colloquium New Applications in Modelling and Inversion Techniques for Non-Destructive Testing. IEE; 1999

[20] Bocchini P, Marzani A, Viola E. Graphical user interface for guided acoustic waves. Journal of Computing in Civil Engineering. 2011;**25**:202-210. DOI: 10.1061/(ASCE)CP.1943-5487. 0000081

[21] Krautkrämer J, Krautkrämer H. Wave Physics of the Sound Field. Berlin Heidelberg: Springer; 1990. pp. 58-92. DOI: 10.1007/978-3-662-10680-8_5

[22] Cawley P, Alleyne D. The use of lamb waves for the long range inspection of large structures. Ultrasonics. 1996;**34**:287-290. DOI: 10.1016/0041-624X (96)00024-8

[23] Lowe MJS, Cawley P. Long range guided wave inspection usage—Current commercial capabilities and research directions. Technical Report, Department of Mechanical Engineering, Imperial College London. 2006. pp.1-40. DOI: 10.1177/058310240

[24] ISO 18211:2016. Non-destructive testing—Long-range inspection of above-ground pipelines and plant piping using guided wave testing with axial propagation. 2016

[25] Kuroishi T, Sakata F. New application of NDE technology guided wave pipe inspection and monitoring system. Journal of The Japan Welding Society. 2006;**75**:220-224. DOI: 10.2207/jjws.75.220

[26] Alleyne DN, Cawley P, Lank AM, Mudge PJ. The lamb wave inspection of chemical plant pipework. In: Review of Progress in Quantitative Nondestructive Evaluation. Boston, MA: Springer US; 1997. pp. 1269-1276

[27] Alleyne DN, Cawley P. The excitation of lamb waves in pipes using dry-coupled piezoelectric transducers. Journal of Non-destructive Evaluation. 1996;**15**:11-20. DOI: 10.1007/BF00733822

[28] Alleyne DN, Cawley P. The effect of discontinuities on the long-range propagation of lamb waves in pipes. Proceedings of the Institution of Mechanical Engineers. 1996;**210**: 217-226. DOI: 10.1243/PIME_PROC_1996_210_316_02

[29] Wilcox P, Lowe M, Cawley P. The effect of dispersion on long-range inspection using guided waves. NDT & E International. 2001;**34**:1-9. DOI: 10.1016/S0963-8695 (00)00024-4

[30] Galvagni A, Cawley P. The reflection of guided waves from simple support in pipes. The Journal of the Acoustical Society of America. 2011;**129**:1869-1880. DOI: 10.1121/1.3543958

[31] Wilcox PD, Lowe MJS, Cawley P. Mode and transducer selection for long range lamb wave inspection. Journal of Intelligent Material Systems and Structures. 2001;**12**:553-565. DOI: 10.1106/N9PB-Y62E-P0Y2-50QF

[32] Lowe PS, Sanderson RM, Boulgouris NV, Haig AG, Balachandran W. Inspection of cylindrical structures using the first longitudinal guided wave mode for higher flaw sensitivity. IEEE Sensors Journal. 2016;**16**:706-714. DOI: 10.1109/JSEN. 2015.2487602

[33] Clough M, Fleming M, Dixon S. Circumferential guided wave EMAT system for pipeline screening using shear horizontal ultrasound. NDT & E International. 2017;**86**:20-27. DOI: 10.1016/j.ndteint.2016.11.010

[34] Zhu L, Wang Y, Sun F. Single torsional guided wave excitation in pipes using magnetostrictive technology. In: 2013 IEEE 11th International Conference on Electronic Measurement & Instruments, ICEMI 2013. Vol. 2. 2013. pp. 872-876. DOI: 10.1109/ICEMI.2013.6743158

[35] Lowe MJS, Alleyne DN, Cawley P. Defect detection in pipes using guided waves. Ultrasonics. 1998;**36**:147-154. DOI: 10.1016/S0041-624X (97)00038-3

[36] Cawley P, Lowe MJS, Simonetti F, Chevalier C, Roosenbrand AG. The variation of the reflection coefficient of extensional guided waves in pipes from defects as a function of defect depth, axial extent, circumferential extent and frequency. Proceedings of the Institution of Mechanical Engineers. 2002:1131-1143. DOI: 10.1243/095440602761609498

[37] Rojas E, Baltazar A, Treesatayapun C. Investigation on damage identification in a pipe using torsional guided waves. In: AIP Conference Proceedings. 2017

[38] Demma A, Cawley P, Lowe M, Roosenbrand AG. The reflection of T(0, 1) mode from cracks and notches in pipes. The Journal of the Acoustical Society of America. 2003;**114**: 611-625. DOI: 10.1121/1.1582439

[39] Løvstad A, Cawley P. The reflection of T(0, 1) guided wave from multiple circular holes in pipes. NDT & E International. 2011;**44**:553-562. DOI: 10.1016/j.ndteint.2011.05.010

[40] Rose JL. Ultrasonic guided waves in structural health monitoring. Key Engineering Materials. 2004;**270-273**:14-21. DOI: 10.4028/www.scientific.net/KEM.270-273.14

[41] Liu Z, Kleiner Y. State-of-the-art review of technologies for pipe structural health monitoring. IEEE Sensors Journal. 2012;**12**:1987-1992. DOI: 10.1109/JSEN. 2011.2181161

[42] Advanced Ionix Technologies. Pipeline corrosion monitoring system [Internet]. Available from: https://ionixadvancedtechnologies.co.uk/ [Accessed: 05/01/2018]

[43] Permasense. Permasense—Experts in remote monitoring solutions [Internet]. 2018. Available from: https://www.permasense.com/ [Accessed: 06/22/2018]

[44] Guided Ultrasonics Ltd. gPIMS [Internet]. Available from: https://www.guided-ultrasonics.com/gpims/ [Accessed: 05/10/2018]

[45] Cawley P, Cegla F, Galvagni A. Guided waves for NDT and permanently-installed monitoring. Insight Non-Destructive Test Cond Monit. 2012;**54**. DOI: 594-601. DOI:10.1784/insi. 2012.54.11.594

[46] Jiang X, Kim K, Zhang S, Johnson J, Salazar G. High-temperature piezoelectric sensing. Sensors (Switzerland). 2013;**14**:144-169. DOI: 10.3390/s140100144

[47] Standards Committee of the IEEE Ultrasonics, Ferroelectrics and FCS. IEEE Standard on Piezoelectricity. Society; 1988. DOI: 10.1109/IEEESTD.1988.79638

[48] Kažys R, Voleišis A, Voleišienė B, Kazys R, Voleisis A, Voleisiene B. High temperature ultrasonic transducers : Review. Ultrasound. 2008;**63**:7-17

[49] Zhang S, Yu F. Piezoelectric materials for high temperature sensors. Journal of the American Ceramic Society. 2011;**94**:3153-3170. DOI: 10.1111/j.1551-2916. 2011.04792.x

[50] Shinekumar K, Dutta S. High-temperature piezoelectrics with large piezoelectric coefficients. Journal of Electronic Materials. 2014;**44**:613-622. DOI: 10.1007/s11664-014-3534-2

[51] Lee H, Zhang S, Bar-Cohen Y, Sherrit S. High temperature, high power piezoelectric composite transducers. Sensors. 2014;**14**:14526-14552. DOI: 10.3390/s140814526

[52] Gotmare SW, Leontsev SO, Eitel RE. Thermal degradation and aging of high-temperature piezoelectric ceramics. Journal of the American Ceramic Society. 2010;**93**:1965-1969. DOI: 10.1111/j.1551-2916.2010.03663.x

[53] Richter D, Sakharov S, Forsén E, Mayer E, Reindl L, Fritze H. Thin film electrodes for high temperature SAW devices. Procedia Engineering. 2011;**25**:168-171. DOI: 10.1016/j.proeng.2011.12.042

[54] Dhutti A, Gan TH, Balachandran W. Effect of electrode configuration on high temperature thickness shear $GaPo_4$ transducer. MDPI Proceedings. 2017;**1**:381-385. DOI: 10.3390/proceedings 1040381

[55] Islam MM, Huang H. Effects of adhesive thickness on the lamb wave pitch-catch signal using bonded piezoelectric wafer transducers. Smart Materials and Structures. 2016;**25**. DOI: 10.1088/0964-1726/25/8/085014

[56] Wandowski T, Moll J, Malinowski P, Ostachowicz W. Assessment of piezoelectric sensor adhesive bonding. Journal of Physics Conference Series. 2015;**628**. DOI: 10.1088/1742-6596/628/1/012114

[57] Lu Y, Michaels JE. A methodology for SHM with diffuse ultrasonic waves in the presence of temperature variations. Ultrasonics. 2005;**43**:717-731. DOI: 10.1016/j.ultras.2005.05.001

[58] Mazzeranghi A, Vangi D. Methodology for minimizing temperature effects in monitoring with acousto-ultrasonic technique. Experimental Mechanics. 1999;**39**:86-91. DOI: 10.1007/BF02331110

[59] Croxford AJJ, Wilcox PDD, Drinkwater BWW, Konstantinidis G. Strategies for guided-wave structural health monitoring. Proceedings of the Royal Society A: Mathematical, Physical and Engineering Science. 2007;**463**:2961-2981. DOI: 10.1098/rspa.2007.0048

[60] Konstantinidis G, Wilcox PD, Drinkwater BW. An investigation into the temperature stability of a guided wave structural health monitoring system using permanently attached sensors. IEEE Sensors Journal. 2007;**7**:905-912. DOI: 10.1109/JSEN.2007.894908

[61] Wilcox PD, Konstantinidis G, Croxford AJ, Drinkwater BW. Strategies for guided wave structural health monitoring. AIP Conference Proceedings. 2007;**894**:1469-1476. DOI: 10.1063/1.2718139

[62] Lee BC, Staszewski WJ. Modelling of lamb waves for damage detection in metallic structures: Part II. Smart Materials and Structures. 2003;**12**:815-824. DOI: 10.1088/0964-1726/12/5/019

[63] Clarke T, Simonetti F, Cawley P. Guided wave health monitoring of complex structures by sparse array systems: Influence of temperature changes on performance. Journal of Sound and Vibration. 2009;**329**:2306-2322. DOI: 10.1016/j.jsv.2009.01.052

[64] Wilcox PD, Croxford AJ, Michaels JE, Lu Y, Drinkwater BW. A comparison of temperature compensation methods for guided wave structural health monitoring. AIP Conference Proceedings. 2008;**975**:1453-1460. DOI: 10.1063/1.2902606

[65] Croxford AJ, Moll J, Wilcox PD, Michaels JE. Efficient temperature compensation strategies for guided wave structural health monitoring. Ultrasonics. 2010;**50**:517-528. DOI: 10.1016/j.ultras.2009.11.002

[66] Harley JB, Moura JMF, Fry FEJ. Scale transform signal processing for optimal ultrasonic temperature compensation. IEEE Transactions on Ultrasonics, Ferroelectrics, and Frequency Control. 2012;**59**:2226-2236. DOI: 10.1146/annurev.ph.20.030158.001231

[67] Konstantinidis G, Drinkwater BW, Wilcox PD. The temperature stability of guided wave SHM systems. Smart Materials and Structures. 2006;**15**:967-976. DOI: 10.1088/0964-1726/15/4/010

[68] Roy S, Lonkar K, Janapati V, Chang F-K. A novel physics-based temperature compensation model for structural health monitoring using ultrasonic guided waves. Structural Health Monitoring. 2014;**13**:321-342. DOI: 10.1177/1475921714522846

[69] Weihnacht B, Klesse T, Neubeck R, Schubert L. Monitoring of hot pipes at the power plant Neurath using guided waves. In: Sensors and Smart Structures Technologies for Civil, Mechanical, and Aerospace Systems. San Diego, CA, USA; 2013

[70] Bagheri A, Pistone E, Rizzo P. Outlier analysis and artificial neural network for the noncontact nondestructive evaluation of immersed plates. Research in Nondestructive Evaluation. 2015;**26**:154-173. DOI: 10.1080/09349847.2015.1022677

[71] Mountassir MEL, Yaacoubi S, Mourot G, Maquin D. Studies on data correction of structural health monitoring using ultrasonic guided waves : Case of study. In: Proceedings 8th EWSHM Conference. Spain: Bilbao; 2016

[72] Buethe I, Mujica L. Damage detection in piping systems using pattern recognition techniques. In: Proceedings 6th EWSHM Conference. Germany: Dresden. p. 2012

Section 2

Power Plants in Different Fuels

Chapter 4

Results of Full Scale Modeling of Electromagnetic Pulse Impact for Lightning Protection of Power Plants

Vladimir Fortov, Alexei Shurupov,
Valentina Zavalova, Alexander Kozlov,
Mihail Shurupov and Nina Shurupova

Additional information is available at the end of the chapter

http://dx.doi.org/10.5772/intechopen.80560

Abstract

This chapter summarizes the results of experimental modeling of lightning impacts that has been carried out several years on the problem of lightning protection of electric power objects, including power plants, primarily in order to increase the stability of their work. The main purpose of the research is to offer the testing facilities and testing schemes of lightning protection. A feature of the models proposed to the attention is the use of the energy of an explosive magnetic generator (EMG). In the first part of the chapter, the investigation connects with direct lightning current impact. For this purpose, a prototype of mobile testing complex on the basis of an explosive magnetic generator (MTC EMG) was developed. The results of MTC EMG field testing for loads with ohmic resistances of 2–10 Ω in the form of current and voltage pulses are presented. The results of an electromagnetic impulse impact in the near field of lightning were modeled experimentally in the second part of the chapter. As a result, the electrical field strength with a rising of voltage front about 100 ns were up to 500 kV/m, and about 0.2 T/μs of the magnetic induction increasing were obtained in the experiments. The paper provides estimates of the techno-economic analysis of the practical application of the development.

Keywords: power plant lightning protection, modeling of pulse lightning impact, explosive magnetic generator (EMG), electrically exploding conductors (EEC)

1. Introduction

With the development and complication of the structure of the energy facilities, the main problem of electric power industry is to ensure stable operation of power plants and transport

of energy to the consumers. In this regard, the role of protection from external influences, especially from lightning, is growing steadily. The numerous experts' statements noted that the ground wires of high voltage line (HVL) supports of stations and cable ways on power plants do not provide the required reliability of the electric grids for the highest voltage classes. Statistics of accidents and breakdowns in the operation of equipment energy indicates a high rate of lightning outages. They ranged from 20 to 50% of the total number of disconnections. The lightning storm outages have negative effect on the station operation, lines, and substation equipment, reducing the switch operational life and causing overvoltage switching on the equipment. Lightning also causes interference in chains of secondary commutation and devices of microprocessor technology, by means of induced electromagnetic fields. Because a lightning refers under the category of natural phenomena which is difficult to study, there is a great interest in full scale modeling effects of lightning. Full simulation of the effects of lightning in some cases is the only source of reliable information on the grounds that it affects on multiple related objects HVL and power plants, as well as to cause nonlinear processes in soils and ground wires when spreading the lightning currents. Understanding of the mechanisms and effects of lightning basic parameters for modeling were taken from work [1].

In the first part of the chapter presents the results of a full scale simulation of lightning currents, affecting directly the grounding devices designed to ensure the safe operation of power facilities. For these purposes have been designed, manufactured, and tested the mobile test complex (MTC EMG). A feature of this complex was the use of a helical explosive magnetic generator (EMG) as a pulse current source. EMG can convert the energy of the explosive in the electromagnetic energy that issues the current pulse in the load. Physical principles of work of explosive magnetic generators are reflected in a lot of classical works. For example, [2] gives the base of physical effects and the methods of generation high level electromagnetic fields. In [3], much attention is paid to EMG with a metal armature, the processes of energy conversion of detonation products into electrical energy pulses, and their efficiency. In [4], various schemes used to connect EMG to loads are discussed. References [5, 6] present the experimental and theoretical work of the Sarov's nuclear center in the direction of lightning simulation using EMG on large grounded objects. EMG using in the experiments to examine spark soil processes [7], allowed us to represent the level of energy and pulse values of generated currents. The ways of transition from theory to practical schemes that use EMG in mobile testing facility were reported by authors in [8] firstly. It demands the reduction of explosive weight that allows realization of EMG, as a consumable item of MTC EMG. The theory of energy transfer from the EMG to high impedance load [9] was used for efficiently transfer energy from the EMG with using transformer circuits. Mathematical modeling of the dynamics of the EMG in a circuit with concentrated parameters allowed choosing the law of inductance output in the operation of EMG to provide a given front of the current pulse in the load without the use of switches. The theoretical background and mathematical modeling of such scheme are described in [10, 11]. In [10], the good agreement of the results of mathematical modeling and experimental measurements is illustrated. This chapter provides more complete results of field tests of MTC EMG. The active inductive load of two types is considered. In the first case, this is the ground loop. In the second case, it is a special model

load. The ground loop forms an active load resistance of 2–4 Ω. In the case of the model load, the resistivity is increased to 10 Ω. The results of field tests showed stable reproduction of pulse values of currents at reliability, safety, and mobility of the complex.

The second part of this chapter presents the results of modeling the effects of high power electromagnetic impulse (EMI), disturbing the stability of energy systems. Such impact is not only on the result of a natural disaster—a thunderstorm, but also occurs at the use of electromagnetic pulse weapons and nuclear explosions. The pulse effect of lightning is accompanied by a change in the induction of the magnetic field in time. In this work, the near field of EMI impact was experimentally modeled by means of a source made on the basis of an explosive magnetic generator. The objects of influence were electronic measuring devices used in the experiment and made in a protected design. The front of the pulse current of EMI source was sharpened by a fast key on the basis of electro-explosive conductors (EEC) placed in the load circuit. The regime of rapid explosion was provided by the intense short-term action of the pulse current on the EEC. Reports collected in the chapter [12] are the basis for understanding the physics of the phenomenon of explosion conductors. The theory of explosion of EEC together with similarity criterion reflecting the relationship of mode of energy release in a conductor during the explosion with its physical properties was used in the selection of parameters of EEC [13–20]. As shown in [14, 15], input in EEC energy sufficient for sublimation of conductors was the main requirement. Criterion for the optimal explosion of conductors in the case of capacitive storage as a pulsed energy source was considered in [17]. We used this approach when we started to simulate the explosion of conductors with a pulse source according to the Marx-Arkadyev scheme. The results were reported at the previous conferences on lightning protection [20]. The use of EMG is reported in this chapter. Two experiments were conducted for the same sources. The first experiment was prepared on the basis of preliminary calculations and was a trial one for the second. The measuring and recording equipment includes: control and measuring equipment, including Rogowski coil, voltage divider, oscilloscopes, and high speed camera HX3 of Japanese production for registration of the rapid process of explosion of the EEC. Evidence of a powerful EMI impact on electronic equipment was the fact that none of the devices could not record the data due to the interference and failure except for a specially designed device. This device was designed for other tasks as a recorder of lightning current. In spite of the use of standard means of protection against electromagnetic interference (metal housing grounded at a common point, isolated power supplies, and shielding), the level of exposure was high.

The results of both experimental and theoretical studies of the models presented were presented at conferences on Interaction of Intense Energy Fluxes with Matter, Elbrus, Kabardino-Balkaria, Russia "Elbrus" and Lightning Protection, St. Petersburg, Russia from 2012 to 2018. One of the presentations of the authors can be found on the conference website [20].

The third part of this chapter is devoted to the importance of full scale lightning simulation for lightning protection systems of power plants in terms of technical and economic indicators. The effectiveness assessments are based on the theory set out in the report at the lightning protection conference held in St. Petersburg in April 2018, a reference to the report is in [21].

2. MTC EMG for full scale simulation of lightning currents

2.1. The principles of MTC EMG creation

During the development of the MTC EMG, several technical solutions were tested. The necessary requirements for the complex are: stable reproduction of pulse values of currents, while in operation for high voltage source, mobility, reliability, and safety. In the circuitry of MTC EMG explosive current breaker in the EMG circuit and closer in the load circuit were excluded, as they have essentially nonlinear characteristics and do not allow reproducing pulses of similar energy. The absence of untriggered discharger in the load circuit relieved the voltage jump when the transformer was in no load operation. In the new circuit, the load is always connected to the secondary winding of the pulse transformer (PT), and the EMG is directly connected to the primary winding of the PT. It gives possible to control the voltage on the load, setting the desired mode of operation of the EMG.

The formation of the front of the current pulse was provided by the design of the EMG. Special attention was paid to the geometry of the final section of the generator. The use of conical geometry in comparison with cylindrical geometry leads to an increase in the liner sliding speed. It is important that in these generators, the increase in the speed of the liner sliding along the spiral is achieved not by using a more powerful explosive, but due to the optimal angle of the cone spiral. For matching the EMG and the load, losses in the primary circuit of the transformer and the inductive-ohmic nature of the load were taken into account. Estimates made with the help of an equivalent circuit of substitution [10, 11] made it possible to obtain a condition for minimizing losses in the primary circuit, depending on the parameters of the circuit. At the same time, the efficiency of the energy transfer of the EMG to the inductive-ohmic load began to depend not only on the coupling coefficient of the pulse transformer windings and the ratio of the load inductance and the inductance of the secondary transformer winding, but also on the ratio of the active resistances of the primary and second transformer windings. In such a scheme, shown in **Figure 1**, the energy is transferred into the load both during the operation of the EMG and after completion, and thus, the pulse transformer is actually the storage of electromagnetic energy. In this case, the dissipation of a part of the energy in the primary circuit after the

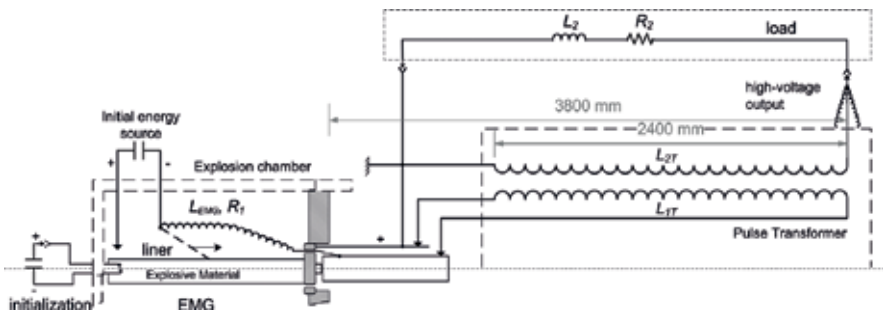

Figure 1. Schematic diagram of the generator of lightning currents with the connected load.

http://dx.doi.org/10.5772/intechopen.80560

termination of the work of the EMG occurs. Estimates showed that when the condition for minimizing losses in the primary circuit is fulfilled, the efficiency of the transfer of energy into the load may exceed 50%.

MTC EMG is located on two KAMAZ vehicles. The lightning current generator, where EMG is the main element and refers to the spiral type, is mounted on the first four-axle base vehicle. The control panel of the test complex is located on the second three-axle base vehicle. The main elements of the lightning current generator are shown in **Figure 2**.

The most important elements of the lightning current generator are the EMG and the pulse transformer (PT). EMG is placed in an explosive protection chamber, which excludes the destruction of the equipment of the complex during the operation. The explosion chamber is capable of withstanding explosions, which correspond to 5 kg in TNT equivalent. Thus, the EMG is the only consumable element of the MTC EMG. To match the EMG with the load, a pulse transformer with a low inductance primary winding is used. The transformer provides a maximum voltage on the primary/secondary windings of 100/1500 kV and a maximum current in the primary/secondary windings of 5000/100 kA. The transformer ratio is 55. The winding coupling coefficient is not less than 0.95. The design takes into account the requirements for limiting weight and increase in strength. The total weight of the equipment does not exceed 80% of the carrying capacity of the vehicle to ensure cross-country capability. The primary and secondary windings are made on one cylinder. High voltage output is

Figure 2. The main elements of the lightning current generator: 1—EMG; 2—explosion protection chamber; 3—pulse transformer; 4—container body; 5—bushing insulator.

carried out through a bushing insulator with a height of about 3 m. The commands between the control panel and the lightning current generator are transferred via fiber-optic communication lines. The measuring complex consists of self-contained recorder oscillograph. Recorders have autonomous power supply and are in a shielded enclosure. The recorder can be placed under any potential.

Most technical solutions are patented. In this scheme, a capacitive storage of electric energy is used as an initial energy source for creating an initial magnetic field in the EMG with an energy of up to 100 kJ. The initialization system is designed to initiate an explosive charge in the generator. The system does not contain electric detonators, which significantly increases the safety of work with explosives.

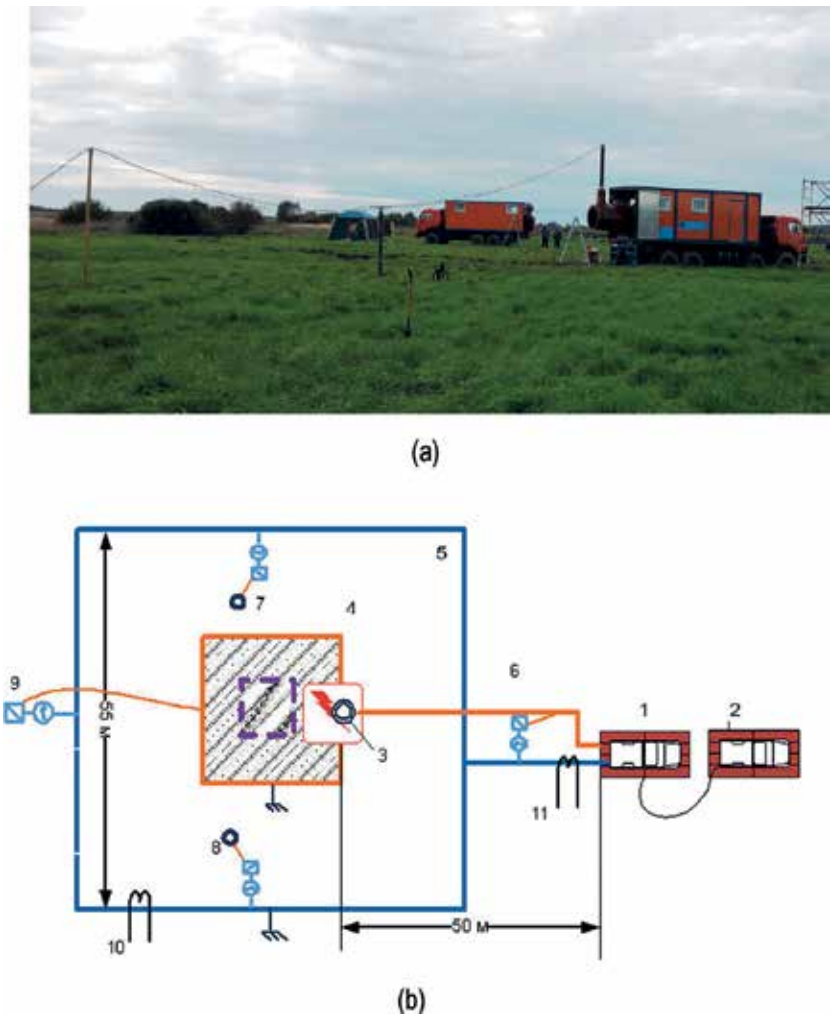

Figure 3. Photo of field tests (a) and experimental diagram (b). 1—lightning current generator; 2—control machine; 3—impulse current input rod; 4—internal input circuit (dashed for the 2nd experiment); 5—ground loop; 6–9—voltage dividers; 10 and 11—Rogowski coils.

http://dx.doi.org/10.5772/intechopen.80560

2.2. The results of the field tests of the MTC EMG on the ground loop

Field tests for an active load of up to 4 Ω were carried out in the east of the Moscow region. The test stand was located on the territory of approximately 70 m × 70 m. The photo of the placement of the MIK VMG and the experimental diagram are shown in **Figure 3**. The load was the ground between two ground loops. Ground loops were made of an aluminum wire with a diameter of 10–12 mm, located at a depth of 0.5 m. The external ground loop was 55 m × 55 m square. The internal ground loop in the first experiment was 15 m × 15 m, which corresponded to a load resistance of 2 Ω, in the second—4 m × 4 m (load resistance—4 Ω). The current was transmitted from the MTC EMG insulator mast to the pulse input rod into the internal circuit via the current transmission line. The total inductance, taking into account the air transmission line, did not exceed 80 μH.

During the tests, the following parameters were recorded: initial current (powering current) of the EMG, current of the EMG (current of the primary winding of the PT), current in the load (current in the secondary winding of the PT), voltage at the MTC EMG output, that is, on inductive-active load, and voltage on the active load.

Rogowski coils were designed to record the derivative of current. They were used without integrators. The current was calculated by software integration of the data, taking into account the sensitivity of each coil. Voltage dividers were used to measure the voltage. The first voltage divider was connected to the high voltage output of the MTC EMG. The second voltage divider was connected to the load. To improve the transient characteristics, low inductance carbon resistors with a total resistance of 20 kΩ were used, which were located in a fiberglass pipe filled with transformer oil. To reduce the effect of parasitic capacitance of the resistor to the ground, when measuring, a pulsed current transformer on a ferrite core with a transformation ratio of 1:55 was used in a divider. This gave a galvanic isolation between the secondary circuit with the oscillograph and the primary circuit with the measured signal. Output voltage ratio was 1:220,000 (~1 MV:5 V).

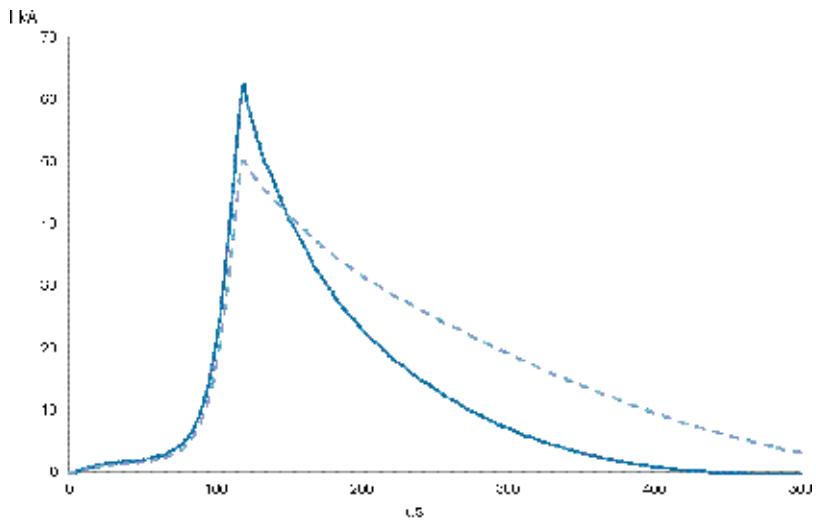

Figure 4. The measured values of the currents in the load for the 1st (dotted line) and 2nd experiments.

Measurement of the resistance of the load (ground) was carried out before the beginning of the experiments. It is assumed that the potential of the outer loop due to its low resistance is zero. This assumption is satisfied (with an accuracy of 0.5%) for the experiment with an internal contour of 4 m × 4 m (experiment no. 2) and about 7% for an internal contour of 15 m × 15 m (experiment no. 1). The main results of the two tests (experiments) are presented in the graphs of **Figures 4** and **5** and in **Table 1**.

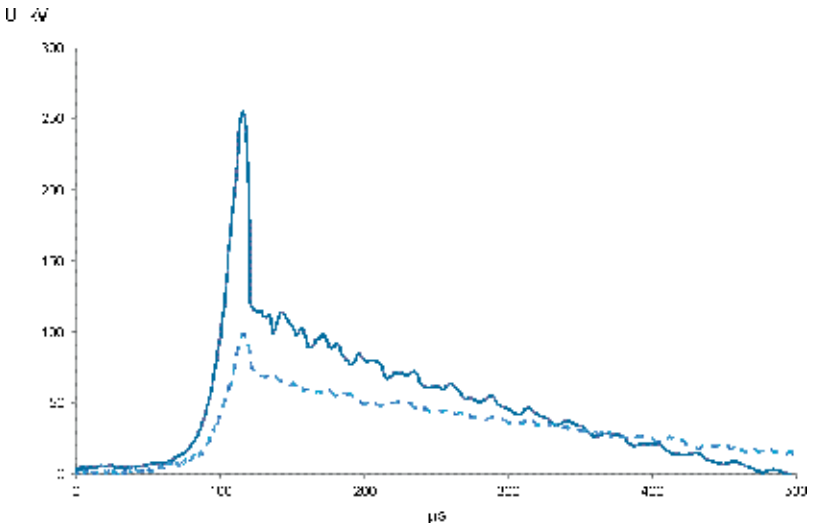

Figure 5. The measured values of the voltage on the load for the 1st (pale color) and the 2nd experiments.

Parameters/experiment no.	**No. 1**	**No. 2**
Initial resistance between current input circuits (active load), Ω	2	4
Load inductance, μH	75	86
Initial energy of EMG, kJ	23	43
Maximum amplitude of the current in the load, kA	50	63
Energy generated by EMG, kJ	900	1500
The maximum amplitude of the output voltage of MTC EMG, kV	220	450
Maximum amplitude of the active load voltage, kV	100	250
Rise time of the current pulse, μs	30	25
Half-amplitude duration of the current pulse, μs	120	80
Energy dissipated in the active load, kJ	500	800
The increase in energy (energy in the active load with respect to the initial energy of the EMG)	21	20

Table 1. Parameters registered in the experiments.

http://dx.doi.org/10.5772/intechopen.80560

Tests of the MTC EMG on the ground loop in the configuration, when the current flowed in the ground between the outer and inner contours, showed a linear increase in the voltage on the load with a decrease in the dimensions of the inner contour. A further increase in the load resistance in the tests became possible when the experimental scheme was changed and the use of model resistance.

2.3. Results of field tests of MTC EMG on model load

MTC EMG field testing on the terminal parameter of the load specified in the development was carried out on a model load with an active resistance of 10 Ω and an inductance of about 150 μH. The tests were carried out on the territory of JIHT RAS, Shatura, Moscow region. Scheme and photo of the experiment are presented in **Figure 6**.

Figure 6a shows a diagram of the connection of the model load to the lightning current generator via a pulse transformer, as well as the location of the Rogowski coils for measuring currents and voltage dividers for measuring the voltage in the circuit. A model load has been developed and manufactured specifically for testing. The active load was modeled by a 10-Ω noninduction resistance.

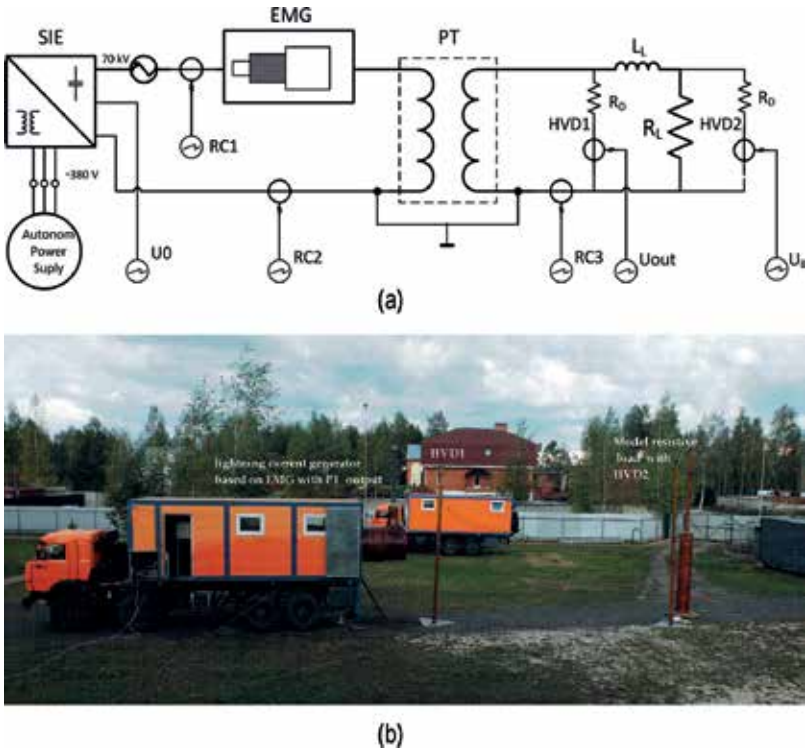

Figure 6. Scheme (a) and the photo (b) of the experiment for model load. SIE—source of initial energy with a capacitive storage; PT—pulse transformer; R_L—resistive (active) load; L_L—inductive load; RC 1… RC 3—Rogowski coils; HVD 1, HVD2—high voltage resistive dividers (1000 kV).

In the foreground of **Figure 6b**, there is a lightning current generator on the first vehicle, on the left—an active load (a noninduction resistor) and two voltage dividers: at the MTC EMG output and on the load. In the background, there is the second vehicle with the control panel.

Parameter	Value
Active load resistance, Ω	10
Load inductance, μH	150
Voltage of the source of initial energy, kV	62
Amplitude value of the powering current, kA	115
The initial energy of the EMG, kJ	73
The maximum derivative of the EMG current, kA/μs	310
The maximum amplitude of the EMG current, kA	6010
Energy generated by EMG, kJ	900
The maximum amplitude of the voltage at the MTC EMG output, kV	810
Maximum amplitude of the voltage on the active load, kV	495
Maximum amplitude of the current in the load, kA	44
The energy produced by the MTC EMG, kJ	1640
Energy dissipated in the active load, kJ	550
The increase in energy (energy in the active load with respect to the initial energy of the EMG)	7
Rise time of the current pulse, μs	37
Half-amplitude duration of the current pulse, μs	50

Table 2. Basic parameters in the tests for model load.

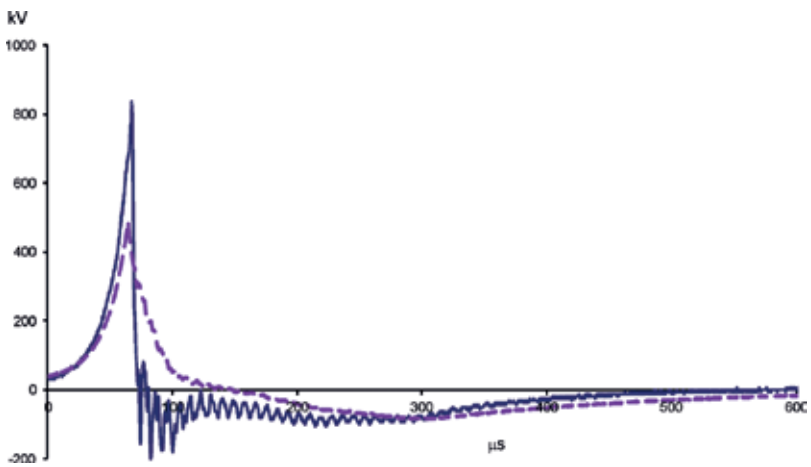

Figure 7. Voltage at the MTC EMG output from the voltage divider no. 1 and on the active load from the voltage divider no. 2.

http://dx.doi.org/10.5772/intechopen.80560

Resistance was installed vertically. The inductive load was modeled by wires connecting the resistive load. To reduce the size, the high voltage connection of the wire for the active load was made in the form of a spiral.

The main results of tests for the model load are presented in **Table 2** and in the graphs of **Figures 7–9**. In these experiments, the signals were recorded on single-channel autonomous oscilloscopes; recording was performed at a given level of the input signal, which explains the time shift of the graphs relative to zero.

As can be seen from **Tables 1** and **2**, the increase in the active load resistance leads to a decrease in the energy transfer efficiency of the load from 55 to 33%, which corresponds to the theory [10, 11]. Thus, the use of MIC HMG for high resistance loads is less effective.

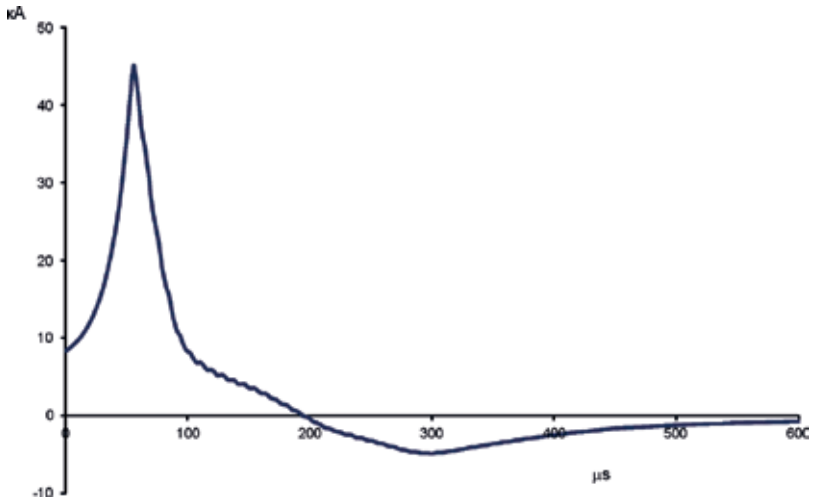

Figure 8. Load current.

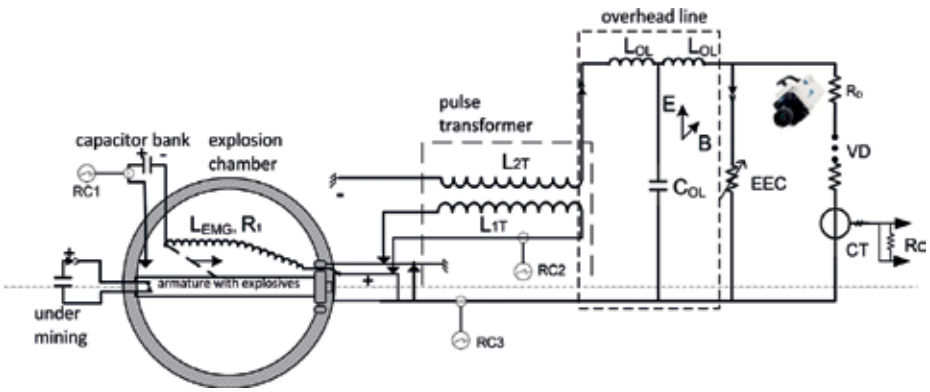

Figure 9. Schematic diagram of an experimental model with a power source based on the EMG. C_{OL} and L_{OL}—are the capacitance and inductance of overhead line; RC1—Rogowsi coil in the EMG circuit; RC2—Rogowsi coil in the load circuit; CT—the current transformer as part of voltage divider.

3. Simulation of electromagnetic pulse effects

3.1. Problem statement

The pulse effect of lightning is accompanied by a change in the induction of the magnetic field in electrically conductive objects in time. The induction effect of the lightning channel is significant at distances commensurate with the length of the lightning channel. Induced voltages arise as a result of such influence on various technical means, for example, overhead transmission lines, grounding devices, etc. Induced voltage leads to the appearance of parasitic currents in the secondary circuits and external power cables due to the conductive coupling. The experimental model based on the EMG is a laboratory setup producing EMI impact on a limited space of 2 m × 2 m × 4 m. The schematic diagram of the electrical control and measuring equipment is shown in **Figure 9**.

The source of the pulse current is a helical-type explosive generator—EMG also. Output of current to the load is carried out through a pulse transformer (PT) and overhead transmission line (OL). The direct and reverse branches of the overhead lines are located on the insulator supports and are common for all experiments. The electrical explosion conductors (EEC) are at the end of the overhead line. General view of an experimental model is represented in **Figure 10**, and the view of EMG assembly is represented in **Figure 11**.

EEC in the EMI models is the key element. The regime of fast explosion is provided by the intense short-term action of the pulse current generated by the source. The rapid increase in resistance in exploding conductors leads to arising of a strong electric field. Together with the

Figure 10. General view of an experimental model with EMG.

http://dx.doi.org/10.5772/intechopen.80560

emerging magnetic field, an electromagnetic disturbance is formed by the EMI effect. The EEC in our models was made from the copper. Copper has a relatively low boiling point and low heat of vaporization. The current reaches the maximum by the end of evaporation if sufficient energy is supplied to the conductor [11]. The selection of EEC parameters, as the number, cross section, and length of the EEC, was carried out taking into account the similarity criteria reflecting the relationship of the character of the energy release in the explosion in the conductor with its physical properties. At the initial stage, the estimates were performed according to the criterion for capacitive energy sources set out in [16], but due to the difference in the pulse current fronts, they were overestimated in terms of the energy required for the explosion of conductors. The main criterion is the ratio of the transmitted EEC energy to the mass of the explosive conductor, which characterizes the initial stage of the explosion. From the balance of the inputted energy and the minimum specific energy required for the explosion, it is possible to estimate the limit mass of the conductors $m = (W_0/\tilde{w})$, where W_0—inputted energy, J; ρ_{cu} —copper density; $\tilde{w} \sim \tilde{w}_m + \tilde{w}_s$, $\tilde{w}_m$—specific melting energy; $\tilde{w}_s$—specific heat of sublimation for copper. Properties of substances were taken from the directory [18], $\tilde{w}_m = 2.13 \cdot 10^5$ J/kg, $\tilde{w}_s = w_v/\rho_{cu} = 5.28 \cdot 10^6$ J/kg ($w_v = 4.7 \cdot 10^{10}$ J/m^3), where w_v is the amount of heat required to convert a unit volume of the conductor material into a metal vapor consisting of neutral atoms. In this regard, the energy $\tilde{w}$ can be interpreted as the minimum specific energy of electrothermal destruction of the conductor material. For a source with a capacitive storage, W_0 is its initial energy, which corresponds to the current action integral calculated for the first quarter of the period. For a source with EMG, W_0 was estimated from the produced energy of EMG, taking into account the efficiency of transmission through the transformer to the load and corrected from the integral of the current action in the load. The total cross section of the conductors was calculated from the energy balance and was associated with the integral of the current: $S_{sum} = \sqrt{(I_d \cdot \rho_e/\tilde{w}/\rho_{cu})}$, where $I_d = \int_0^t I^2(t)dt$—action integral, where ρ_e is the electrical resistivity, which was taken at the melting point. The current in the load for the first experiment was initially modeled numerically; it was supposed that the conductor is torn at the maximum value of the current. Further, the rate of input of the critical energy density in the adiabatic approximation

Figure 11. EMG assembly, before installation in the explosion protection chamber.

is estimated $dW/dt = j_C^2 \rho_e$, W/m^3, $j_C \sim 3.4 \cdot 10^{11}$ A/м^2, critical current density for copper conductor [3, 11]. The time scale of the explosion of the copper conductor was estimated from the law of conservation of momentum (the equation of motion taking into account the equation of state, at equilibrium of the liquid and gas-plasma phase). Thus, the estimated time of the explosion corresponded to the value of $\tau_в \sim r_0 \sqrt{(\rho_c / p_c)}$, where r_0 is the radius of a conductor and ρ_c and p_c are the density and pressure at the critical point. For copper $\rho_c = 2.27 \cdot 10^3$ kg/m^3, $p_c = 9.04 \cdot 10^3$ atm [18], for conductors 80–120 μm, the time was about 80–110 ns. As shown by experiments, the preliminary calculation gave higher values of the integral of the current than in practice. This was because the front-of-the-model current was steeper. Therefore, two experiments with the same initial energy were carried out. The first experiment was trial for the second one. The analysis of the results of the first experiment allowed us to specify the parameters of the node of the pulse exacerbation in order to control the formation of the voltage pulse.

3.2. Results of laboratory experiments

We use the initial energy source for powering the EMG, it was about 15 kJ (a capacitor bank of 90 μF was charged to 18 kV). An overhead line inductance was 5.5 μH.

In the first experiment, 25 conductors of 120 μm diameter were taken. The full cross-sectional area of the conductors is $28 \cdot 10^{-8}$ m^2. The total mass of all conductors amounted to about 2.5 g. The number of conductors was determined by the requirement to obtain an explosion of conductors at the stage of current growth in the load. The specific energy obtained by the conductors is 12.5/2.4–5.2 kJ/g; it is roughly equal to the energy of the sublimation of copper. The experiment showed, see **Figure 12**, that the current was cut off (and the voltage increased abruptly) at the initial phase of the current rise. The current pause mode does not occur, and

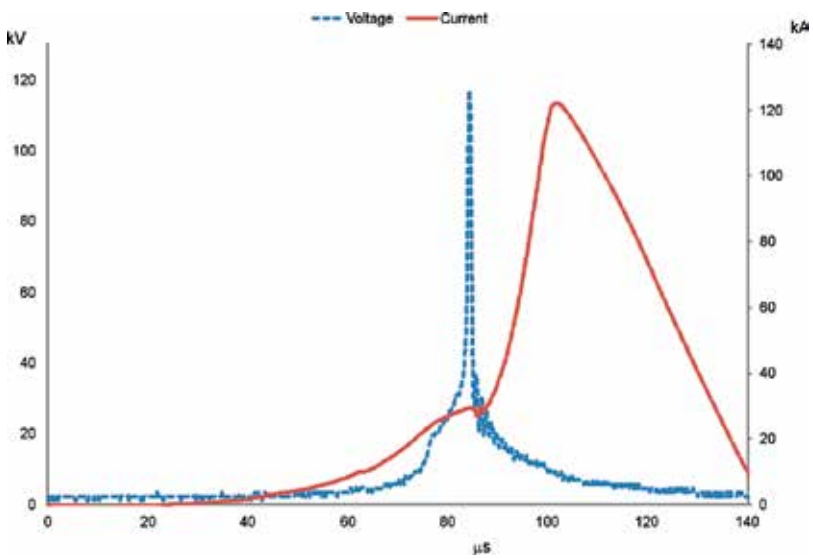

Figure 12. Impulse current and voltage values obtained with the explosion of conductors in the 1st experiment.

the further increase in the current is associated with the transition of the EEC into an electrically conductive plasma state. To achieve higher voltage amplitudes, we need to input more energy. This meant that we need to climb higher along the current curve to the time of the explosion of the EEC. To do this, we need to take more conductors, for input more energy, with a smaller diameter of each to increase the speed of energy input.

In accordance with the described reasoning, in the second experiment, 96 copper conductors with a diameter of 80 μm were taken. The total area of the cross sections of the conductors is $48 \cdot 10^{-8}$ m^2. The total mass of all conductors was about 4.3 g. The initial charging voltage was chosen as in the previous experiment, ~18 kV, respectively, the initial energy was about 15 kJ, as in the previous experiment. The explosion of the EEC occurred at 92 μs, which corresponds to the current drop and voltage peak, as illustrated in **Figure 13**. The maximum value of the current in the explosion was about 70 kA. In the current distribution, see **Figure 13**, we see again a nonpause mode of EEC transition into an electrically conductive plasma state. Further, the current increases again after several periods of high frequency oscillations to a maximum value of 127 kA, **Figure 13**. Then the plasma conductivity decreases due to the expansion of the plasma column, and the current begins to fall. Voltage amplitude at the moment of explosion was about 550 kV, and the electric field strength was about 550 kV/m. Voltage peak occurred approximately 0.5 μs after the explosion of conductors. The front of the voltage pulse was estimated to be approximately 100 ns. Estimates of the current density in the explosion gave a value of about $3 \cdot 10^{11}$ A/m^2. The resistance growth rate was about 16 Ω/μs. The energy inputted in the EVP during the explosion is about 60 kJ. Specific energy was 60/4.3–14 kJ/g, approximately 2.7 times more of sublimation energy of a copper.

Characteristics of high speed camera Memrecam HX-3 (16 Gb, exposition time—200 ns, frame rate of 750,000 frame per second at working special resolution 320 × 24) allowed to fix the

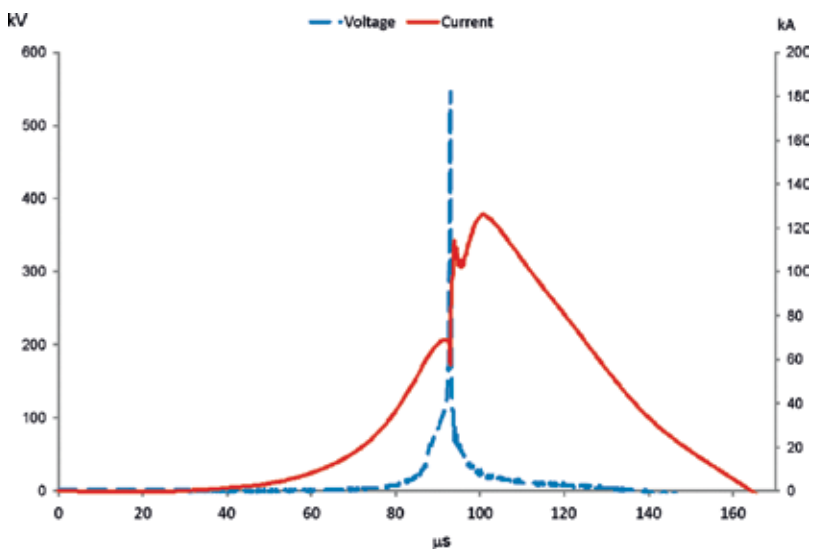

Figure 13. Experimentally obtained impulse current and voltage at the load (EEC).

time of the explosion. Three frames, shot one after another, include: the first frame—before the explosion, the middle frame clearly illustrates the locally glowing area of the exploded conductor, and the next frame—a glowing plasma column formed by the products of the explosion of the EEC. The column has a radius much exceeding the initial radius of the wire, **Figure 14**. The split of the image is connected with the re-reflection from the neighboring conductors. Displayed glow significant attenuated on one-hundredth the frame that corresponds to time over 130 μs after the explosion (~220 μs). At this time, the current almost disappears.

The change of magnetic induction occurring around the EEP at the moment of break was estimated from the Ampere law in the approximation of a single turn solenoid, (N = 1), $\frac{\partial B}{\partial t} = \frac{\mu 0 \cdot N}{2 \cdot \pi \cdot r_{OL}} \cdot \frac{\partial I}{\partial t}$, where $\mu 0$ is the magnetic constant and r_{OL} is a half-height of OL. The maximum value of the current derivative at EEW break was about 170 κA/μs that gives a value of abo ut $\frac{\partial B}{\partial t} = -0.2\mathrm{T}/\mu\mathrm{s}$. The successful use of special devices that measure pulse current at the EMI effect was demonstrated and the obtained curves represented in **Figure 15**. These devices are a new generation of self-contained oscilloscope recorders used for the first time in the

Figure 14. Average frame illustrates of EEC explosion. The top frame is before the explosion and the bottom after the explosion.

Figure 15. Photo of the device for registration of current derivative from the source of powerful EMI action in the near field based on the 4th generation lightning current recorder.

http://dx.doi.org/10.5772/intechopen.80560

measuring equipment of the MTC EMG. Then, they were modified to register the currents of a multicomponent lightning. They have been successfully tested on 220 kV power lines of main electric networks of the South of Russia. In the conditions of strong level of electromagnetic interferences, devices reliably record current derivative and voltages, followed by playback and processing of data on the computer. Analog-to-digital data conversion is 12 bits. The duration of data recording for each component of the lightning current is 600 μs. The temporal resolution of the recorded data is about 100 ns. Further application of this registrar in this research area will be accompanied by an increase in its temporary resolution.

4. Techno economic analysis of the effectiveness of the application of models

There is not a ready-made model of techno economic analysis of the creation project of commercial samples of testing complexes for lightning protection tasks. We took as a basis of the economic expediency of the introduction of system of lightning protection from the point of view of minimizing outages caused by lightning. The analysis is based on the idea of calculating the internal rate of return (IRR) of the protection method, as well as the data on lightning outage presented in the report [21], University of S. Paulo, Brazil. The main numerical indicators for economic calculations and the list of lightning protection services are close to the Russian market. The methodology is based on an analysis of the cost of lightning protection and the benefits of lightning protection. The benefit was regarded as an opportunity to save on the damage caused by the emergency situation both at the power plant itself and the damage caused by the delay in the supply of electricity to consumers, including the payment of fines for regulated direct and indirect losses. It was taken into account what can be represented in monetary terms, excluding social and moral aspects. The simplified calculation did not take into account such aspects as: loss of communication, information, Internet access, reduced mobility of the population, damage to frozen products, disruption of banks, state institutions, etc. The main costs are the measures used to increase the lightning resistance of power plants. These include the improvement of insulation resistance, the use of earthed shielded cables, the installation of arresters in distribution networks, as well as the installation of grounding devices that carry out the removal of lightning currents into the ground. The volume of storm shutdowns was considered as a total number of cases and also with respect to areas with different population densities. Different protection systems with different degrees of complexity were considered. The average costs and benefits for each system were reduced to a unit of time. The obtained input data allowed estimating the values of cash flows and calculating the IRR for each protection system. This rate is equal to the ratio of profit (the amount of losses that can be avoided) to the amount of costs (investments). The following conclusions are made:

- The lightning protection project is effective and appropriate if the final IRR rate is higher than the minimum rate of return for long-term financing, and for Russia, it is about 7% per annum. That is, the energy distribution company should have a positive return on investment.
- Developing countries, where the cost of capital is high, face great difficulties in investing in protection systems, especially in regions with low population density and low income.

If we continue the study of technical and economic analysis in accordance with the proposed methodology in relation to the effectiveness of the implementation of the development of testing systems for our project, we can add the following conclusions:

- We get the amount of benefits for the development of integrated solutions. Each benefit from the selected protection measure can be tested separately. And most importantly, it is possible to get the best comprehensive solution in the application of several protection measures. In theory, such solutions are difficult to obtain because the overall protection solution is not simply the sum of individual measures. For example, for grounding devices that perform the removal of lightning currents, to minimize the resistance of multipath grounding, it must take into account the specific resistance of the soil.
- Developed complex solutions based on the tests can be standardized according to the adopted standards of protection and reproduced in the form of ready-made solutions.
- By using testing complexes in the construction of power plants or scheduled safety inspections, it is possible to reduce the safe level of overvoltage and, accordingly, the number of lightning outages.
- The creation and use of such test complexes are of high importance for developed countries, which have a high level of requirements for the operation of power plants, namely, to the quality and continuity of the energy supplied by them.

The cost of MIC EMG, without the option of EMI impact analysis, is approximately $ 2.3 million per 1 MJ of energy, which is transferred to the load. The evaluation was performed in 2017. As a result of R & D, a sample of testing complex, laboratory test stands, and a set of design and technological documentation necessary for the transition to commercial samples were obtained.

It should be noted that the test complexes based on EMG are a means for testing the existing protection of power stations from lightning. Despite the fact that the basis of EMG work is the physic-chemical law of conversion of chemical energy explosives into electrical energy with an efficiency of not more than 10%, and this tool is able to generate pulsed currents of the mega-ampere level and the electric field intensity of MV/m per microsecond, not achievable by other methods. In the transition from R & D to commercial facility, it requires a detailed calculation, first of all, of the technical and economic effect of the use of testing complex. The powerful impact of lightning is a probabilistic process for the power plant, but the level of destruction is much higher than any other losses. To calculate this effect, it is necessary to take specific parameters to improve lightning protection, applying to the technique described in work [22, 23], and calculate energy and exergy efficiencies. The return on investment in such complexes is likely to be correctly compared with the level of return on capital from long-term investments. There is a direct connection with the economic development of the country, which can afford high tech equipment.

5. Conclusion

Field tests of MIC EMG demonstrated stable reproduction of pulse values of currents during operation: its mobility, reliability, and safety. For the range of loads with active resistance from

1 to 10 Ω and inductance of 70–150 μH, the amplitude values of the currents ranged from 70 to 40 kA. Thus, the efficiency of application of MIC EMG for modeling lightning currents at low resistance loads such as grounding at electrical substations and power plants has been confirmed. The practical application of MIC EMG will allow increasing the level of lightning protection of strategically important energy facilities both at the stage of their building construction and during preventive inspections.

Laboratory testing of the generator of powerful EMI impacts on the basis of the EMG and electro explosive conductors in the load circuit confidently registered voltage pulses with the front of about 100 ns and the amplitude of the electric field strength of about 500 kV/m. The growth rate of the magnetic field intensity in the near field reached 0.2 T/μs. In practice, the use of such a facility will allow to solve the problem of optimizing the location of the elements of grounding devices in order to equalize the potentials in the grounding systems and to identify parasitic connections in electrical circuits, including those induced in the secondary circuits of underground utilities.

The tests of the described system samples showed the readiness of the development for the transition to commercial development. This chapter of the techno economic analysis of the development provides an approach to assess the profitability of the complex depending on the location of the power plant and the required level of lightning protection.

Author details

Vladimir Fortov, Alexei Shurupov, Valentina Zavalova*, Alexander Kozlov,
Mihail Shurupov and Nina Shurupova

*Address all correspondence to: zavalova@fites.ru

Joint Institute for High Temperatures of the Russian Academy of Sciences (JIHT RAS),
Moscow, Russia

References

[1] Bazelyan EM, Raizer YP. Physics of Lightning and Lightning Protection. Moscow: Fizmatlit; 2001 (in Russian)

[2] Knoepfel H. Pulsed High Magnetic Fields. Amsterdam: North-Holland; 1970

[3] Fortov VE. Explosive Generators of Powerful Pulses of Electric Current. Moscow: Nauka; 2002 (in Russian)

[4] Altgilbers LL, et al. Magnetocumulative Generators; 2000. DOI: 10.1007/978-1-4612-1232-4

[5] Vilkov YV, Kravchenko AS, Saitkulov MM, et al. Instruments and Experimental Techniques. 2012;**55**:580

[6] Vilkov YV, Kravchenko AS. Instruments and Experimental Techniques. 2006;**49**:523

[7] Vilkov YV, Kravchenko AS, Selemir VD, Terehin VA. Instruments and Experimental Techniques. 2011;**54**:375

[8] Shurupov AV, Dudin SV, et al. In: Proceedings of the 12th International Conference on the Generation of Megagauss Magnetic Fields and Related Experiments; 13-18 July 2008; Novosibirsk. 2008. p. 298

[9] Herlach F. Explosive-driven energy generators with transformer coupling. Journal of Physics E: Scientific Instruments. 1979;**12**(5):421-429

[10] Shurupov AV, Kozlov AV, Zavalova VE, Bazelyan EM, et al. Mobile testing complex based on an explosive magnetic generator. Journal of Applied Mechanics and Technical Physics. 2015;**56**(1):158-165. DOI: 10.1134/S002189441501023X

[11] Shurupov AV, Kozlov AV, Zavalova VE, Shurupov MA, Fortov VE. The sources of pulse current based on explosive magnetic generators for mobile testing facility. IEEE Transactions on Plasma Science. 2016;**44**(10):1956-1960. DOI: 10.1109/TPS.2016.2566929

[12] Chace WG, Moore HK. Exploding Wires. New York: Plenum Press; 1962

[13] Oreshkin VI, Barengol'ts SA, Chaikovsky SA. Numerical calculation of the current specific action integral at the electrical explosion of wires. Technical Physics. 2007;**52**:642-650

[14] Borisevich SL, Cherkas SL. Technical Physics. 2012;**57**:1380-1386

[15] Pikuz SA, Tkachenko SI, Barishpol'tsev DV, et al. Technical Physics Letters. 2007;**33**:651-654

[16] Khishchenko KV, Tkachenko SI, et al. International Journal of Thermophysics. 2002;**23**: 1359-1367

[17] Khainatskii SA. Condition for realization of an optimum regime of the electric explosion of conductors in liquid media. Technical Physics Letters. 2009;**35**:299-301

[18] Grigoryev IS, Meilihov EZ. Fizicheskie Velichini: Spravochnik. Moscow: Energoatomisdat; 1991 (in Russian)

[19] Bushman AV, Fortov VE, Kanel' GI, Ni AL. Intense Dynamic Loading of Condensed Matter. Washington: Taylor & Francis; 1993

[20] Zavalova VE. Results of Electromagnetic Pulse Impact Simulation for the Purpose of Energy Facilities Lightning Protection [Internet]. 2018. Available from: http://en.rclp2018.com/presentations/

[21] Bernal PSM, Piantini A, Parente V. Cost-Benefit Analysis of Lightning Protection Systems in Distribution Networks [Internet]. 2018. www.rcgi.usp.br. Available from: http://en.rclp2018.com/upload/iblock/a30/a30575f09c84c12796cd2e47ba331d9f.pdf

[22] Taner T, Sivrioglu M. Energy-exergy analysis and optimisation of a model sugar factory in Turkey. Energy. 2015;**93**(1):641-654

[23] Taner T, Sivrioglu M. A techno-economic & cost analysis of a turbine power plant: A case study for sugar plant. Renewable and Sustainable Energy Reviews. 2017;**78**:722-730. DOI: 10.1016/j.rser.2017.04.104

Chapter 5

Hybrid Power Plants: A Case Study

Eduarda Moreira Nascimento,
Júnio de Souza Damasceno and
Sabrinne Kelly Souza

Additional information is available at the end of the chapter

http://dx.doi.org/10.5772/intechopen.80034

Abstract

Energy can be treated as an essential element for the development of society. Therefore, aspects like process' efficiency and environmental impacts must be considered when choosing the supply source. In Brazil, an event showed the fragility of a system that relies on in only one source to attend their necessities; a truckers strike made the whole country stop. The energy sector has a similar situation; more than 60% of Brazilian energetic matrix is represented by one source, hydroelectric power plants. The availability of solar radiation and wind in Brazil makes it possible to diversify its energetic matrix. Thus, the aim of this study is investigating the potential of hybrid solar-wind power plants in two basins of Minas Gerais—Brazil, São Francisco Basin and Jequitinhonha Basin, as well as compare their viabilities in order to address social issues. By analyzing INMET database and economic factors, the study has shown that it is feasible to implement renewable power plants in the basins of the study area, whether individually (solar or wind energy) or hybrid system. It shows in addition that hybrid system should be prioritized, since it presents lower cost, when compared to solar power plant, and more reliability due to seasonality of both sources.

Keywords: hybrid power plants, solar, wind, feasibility, São Francisco Basin, Jequitinhonha Basin

1. Introduction

Energy plays a very important role in society's development, thus it is present in almost every activity [1]. The author in [2] discussed one of the principal forms of energy, which is the electrical one and it can be obtained by a bunch of ways:

a. Work transformations generated by mechanical energy from waterfalls and/or wind force.

b. Thermal energy from the Sun which can be directly used as thermoelectric source or used on a photovoltaic way by means of panels.

c. From heat (combustion, geothermal energy, sun, nuclear fission) through the use of thermal machines.

Some aspects are crucial when talking about energy. One is related to the environmental impacts associated to the energy production and that should always be the smallest possible [3]; another one is the exergy, "measures the ability of a source to produce useful work" [4], which will, in a second moment, be converted into electrical energy. Therefore, as some have been discussing, the production of energy must focus on efficiency [5].

In Brazil, the year of 2018 was tagged by an event that showed the fragility of a system that relies on only one source to attend their necessities. A truckers strike made the whole country stop [6]. The situation of energy supply is quite similar. **Figure 1** shows the Brazilian energetic matrix, where it is possible to see that more than 60% of Brazilian energetic matrix is represented by one source, hydroelectric power plants[1]. Although hydroelectric energy can be considered a renewable source, it cannot be treated as a sustainable source[2] [7, 8]. When talking about sustainability, we are debating something that can endure over time, meeting the present generation needs without compromising the future generations' needs [9]. It matters to find alternative resources to meet these requirements.

Renewable energy sources are playing an important role in the supply of energy for electricity, transport, heat, among others. It currently attends a range between 15 and 20% of world's total energy demand. There is a bunch of alternatives of renewable energy resources, such as

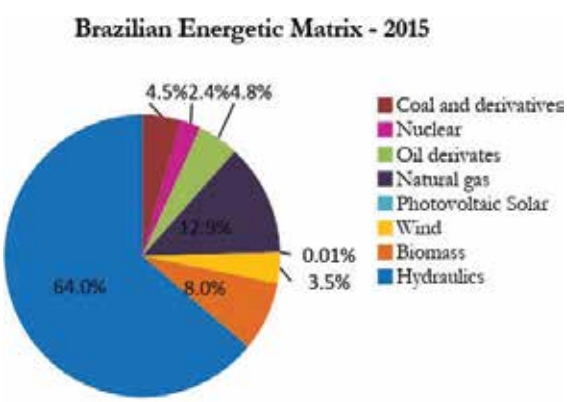

Figure 1. Brazilian Energetic Matrix—2015 [10].

[1]In the world, about 20% of the energy supply is due to its source [8].
[2]The construction of a dam involves several social and environmental impacts, such as land flooding, people displacements, reduction on biodiversity, sedimentation, and so on [8].

biomass, geothermal, solar, modern bio-energy, wind, and it has been particularly favorable for more remote areas, such as rural areas [7, 8, 11].

Despite various options, two of them have excelled: solar and wind resources. The market of wind power and solar photovoltaic are being the most dynamic, with high rates of average growth [12, 13]. All around the world, for both, solar and wind sources, the availability of them is higher than the utilization's necessity [14, 15].

For photovoltaic generation capacity field, Brazil is compared with desert areas—which are the best places in terms of solar radiation—such as Dangola, city in Saudi Arabia desert [16] as well as in the wind field, Brazil has lack of capacity of production [15]. Despite of this quantity of "feedstock," these systems are dependent of a series of natural variables, and a hybrid system that combines these two elements seems to be the ideal arrangement.

In Brazil, municipalities attended by the electricity service have a great representativeness, over than 95% of the total residences [17]. Nevertheless, speaking about rural areas, its coverage percentage is quite lower, reaching about 89.7%. The biggest energy lacuna is seen at the northern region, with something like 24% of rural households without electricity, followed by Northeast (7.4%) and Central West (6.8%) rural areas.

The municipalities of Jequitinhonha and São Francisco river basins have advanced positively in public services in the last few years. The energy sector has advanced considerably by increasing access to electricity from traditional sources to rural families in the region, reaching more than 90% of residencies.

Thus, this chapter has the objective of investigating the potential of hybrid solar-wind energy exploration in Minas Gerais, especially in the Jequitinhonha and São Francisco river basins, which is the most economically underprivileged region of the state, and with good natural characteristics, proposing a cost estimate based on the electricity consumption of each municipality.

1.1. Solar energy

1.1.1. The solar resource

The solar energy that hits the Earth's surface as sunlight is about 10,000 times superior as the humanity gross demand [18]. In this context, exist two basic "technologies that convert sunlight into useful forms of energy". The first is the solar photovoltaic (PV) models/panels that directly convert sunlight into electricity. The second is a thermal system where the thermal energy coming from the Sun produces steam, and this last one is used to produce electricity. This thermal energy can still be used directly for water heat and/or industrial processes [8, 14].

1.1.1.1. Photovoltaic energy

The main uses of photovoltaic energy are observed for commercial purposes, residences, and public buildings; however, despite what one might think, these locations have great representativeness in energy consumption scenario. In Brazil, this value is 40% [19]. PV panels, which

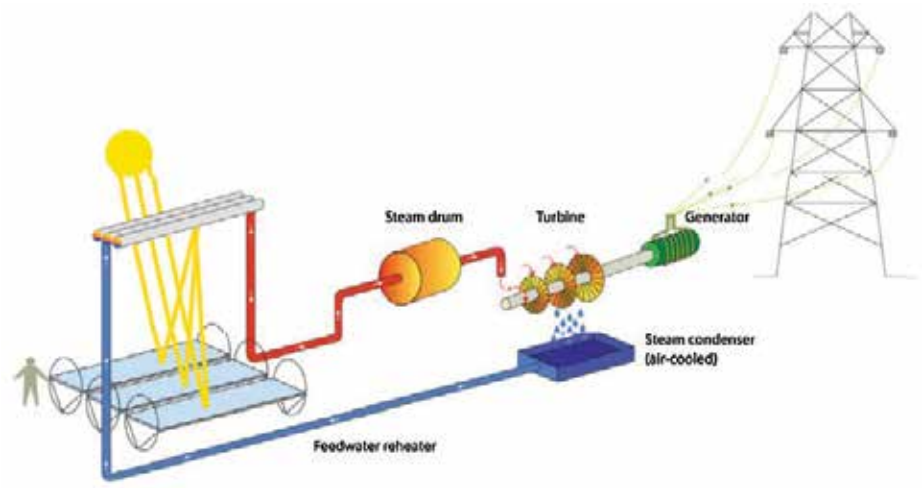

Figure 2. Solar thermal conversion system [24].

can be installed in series or parallel to generate direct current (DC), are used for this system, and they come in two different crystal structures: a polycrystalline and monocrystalline. The first one is usually less efficient because it is composed of just one crystal, making it cheaper; the last one has high efficiency, but it costs a bit more. Panels should not be chosen only based on its price, but many factors have to be put into account such as brand, physical size, durability, certifications. Moreover, the efficiency of PV panels depends on incoming solar radiation intensity, inclination of PV panels, wind speed, among others [19–22].

1.1.1.2. Thermoelectric use

The way of producing power, where thermal energy becomes electricity, happens in two processes, the creation of steam and the use of that steam to turn on a turbine, which generates electricity as we can see in **Figure 2**. Because of the turbines boundaries, this method has a low efficiency, about 25% [8, 23].

1.1.1.3. The Brazilian potential

Brazil has natural characteristics that favor the use of solar energy. It is located at latitude range with high incidence of solar radiation [14]. According to the solarimetric atlas [16], the northern region of Brazil has solar radiation compared with the best regions of the world, and its values of daily solar radiation, monthly average is 8–22 MJ/m^2, can be seen in **Figure 3**.

1.2. Wind energy

1.2.1. Windy resource

Seeking for technologies that minimize negatives impacts on the energy generation, the windy resource has gained attention. Beyond a production with no pollution during the power generation, it is widely available [8, 25]. "Wind energy is the kinetic energy contained

http://dx.doi.org/10.5772/intechopen.80034

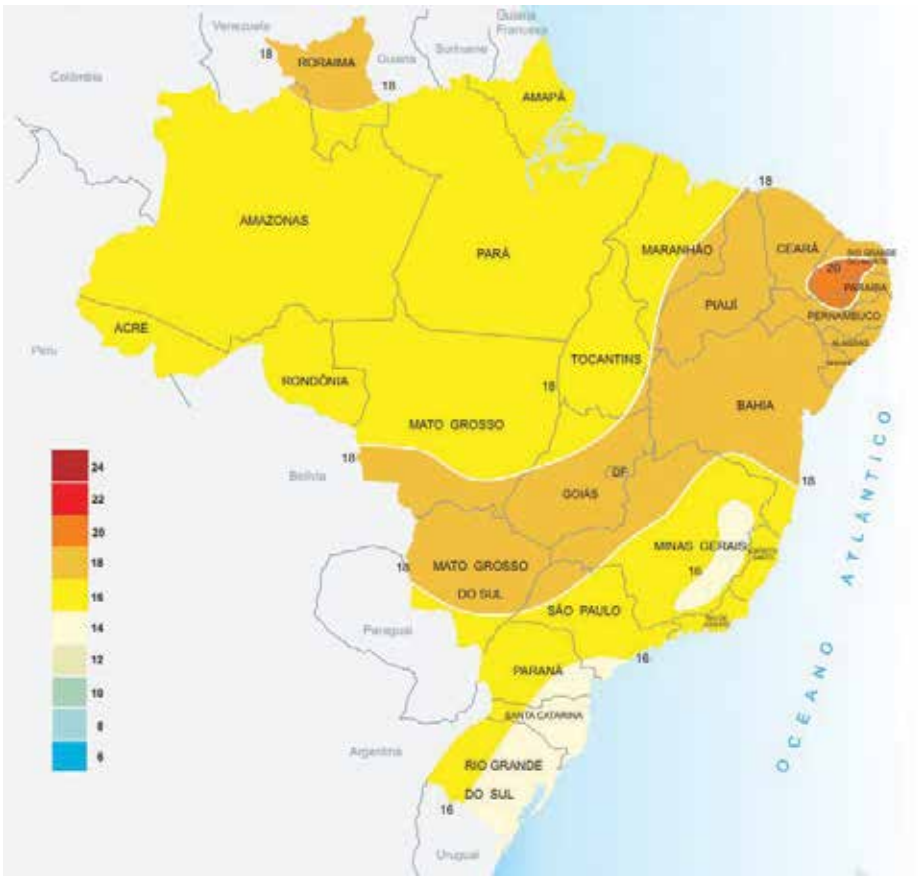

Figure 3. Daily solar radiation, monthly average–MJ/m² dia [21].

in the moving air masses." Nevertheless, for this source to be considered technically feasible, its density must be higher or equal to 500 W/m², at a height of 50 m, requiring a minimum wind speed of 7–8 m/s [15, 24]. According to World Meteorological Organization, these special conditions are only found in 13% of the Earth's surface [26].

1.2.2. Principles of technology

In order to obtain energy from the wind, some turbines are responsible to capture and transform the kinetic energy of the air mass into mechanical energy. Then, a generator is applied and converts the mechanical energy into electricity. A standardization has been established for turbines design as follows: horizontal rotation axis, three shovels, active alignment, induction generator and non-flexible structure [15, 24].

1.2.3. Brazilian and global scenario

The world's capacity of energy production is about three times higher than the energy consumed all around the world in 2004; this value is 53,000 TWh/year, and the estimation of

consumption for 2020 is 27,326 TWh/year. Talking about Brazil, the majority of the studies speak of wind potential values of 60,000 MW [15].

1.2.4. Conflict points: economics and land use

Wind power generation system does not require any type of fuel for its operation, which represents an advantage. However, the equipment cost seems to be a problem. In addition, it requires special accommodating characteristics, such competing demand for land use.

For economics, the biggest issue is related to the investment cost (I_d), simulations ran by [27] has shown that investment cost is guide by the following equation:

$$I_d = C_s \cdot Ne \tag{1}$$

where C_s is the unity investment cost and Ne is the installed power. As wind generator represents the main part of C_s, its value is not as high as other types of energy. For land use, off-shore is an alternative [8].

1.3. Hybrid exploration

A hybrid renewable energy system (HRES) supply consists of two or more power generation technologies combined to enhance the system efficiency, and it can be considered a "modern environmental friendly solution." The HERS can come either in stand-alone or in grid connected mode, showing itself as good option for remote locations [7, 28].

Renewable energy sources such as solar and wind are dependable of natural/climatic characteristics that are not easy predictable; therefore, the combinations of these two sources can increase the system effectiveness twice [29–31]. Another system that has gained attention is fuel-cell generation system, which demonstrates high efficiency and low pollution [32]. However, considering that these cells require pure hydrogen, and therefore, equipment to purify the fuel, it is not going to be used in this study, but its potential can be considered in future studies.

Figure 4 shows the scheme of a common solar-wind hybrid system.

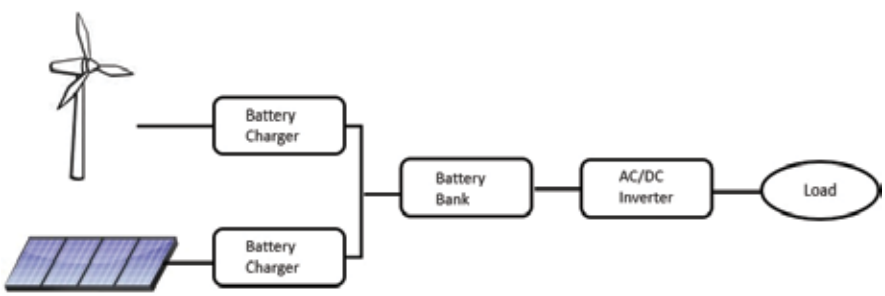

Figure 4. Diagram of a solar-wind hybrid system [11].

http://dx.doi.org/10.5772/intechopen.80034

2. Methodology

2.1. Study area

Municipalities from two basins compose the study area: São Francisco and Jequitinhonha.

The São Francisco River Basin has great importance in the political, economic and social scenario of the country, considered the route of national integration through the connection between the Southeast, Midwest and Northeast regions of Brazil. The basins cover an area of 638,576 km^2, which corresponds to 8% of Brazil and 40% of the state of Minas Gerais. The São Francisco River born in Serra da Canastra in the state of Minas Gerais, covering 2863 km and contributing to the regional development of 521 municipalities in the states of Minas Gerais, Goiás, Bahia, Pernambuco, Sergipe, Alagoas and the Federal District [10, 31]. The vegetation in the region includes the transition area of Cerrado and the Caatinga with small fragments of Atlantic Forest with significant structure, complexity, and forest density. However, in the State of Minas Gerais, 96% of the Atlantic Forest and 75% of the Cerrado were deforested in their historical occupation process [17].

The São Francisco Basin presents distinct socioeconomic patterns that cover areas of high wealth and areas of high population density, as well as areas of intense poverty and well-dispersed populations, with rural population in the upper São Francisco with approximately 26% of the total basin [33, 34]. The basin has multiple uses, 77% of total demand for irrigation and 12% for hydroelectric power supply [35].

The Jequitinhonha River Basin has an area of approximately 70,315 km^2, and 65,660 km^2 (93%) is located in the state of Minas Gerais. The basin is bordered in the west by the São Francisco river basin. The Jequitinhonha river has its source in the Serra do Espinhaço, covering 920 km [36]. The basin is characterized by significant climatic heterogeneity, acting in a dynamic way with the physical and biotic means that are determinant for significant geoenvironmental features, including ecological and cultural patterns that influence the modalities of the use of natural resources [9]. The vegetation is composed of cerrado, fields and transitional vegetation of the Atlantic Forest and Caatinga [33].

The region has a high poverty rate with high exodus to large centers and more than two-thirds of the population occupying the rural area. The main human activities are related to agriculture, mining and garimpo [37].

Municipalities were chosen from these two basins based on the social perspective as well as renewable resources availability, and also considering if the city had National Meteorological Institute (INMET) station, so that it would be possible to analyze the real date. From São Francisco Basin, the cities were: Curvelo, Espinosa, Montes Claros, Ouro Branco, Pirapora, Pirapora, and Três Marias. From Jequitinhonha Basin: Águas Vermelhas, Almenara, Belmonte, Capelinha, Diamantina, Itaobim, Rio Pardo de Minas, and Salinas (**Figure 5**).

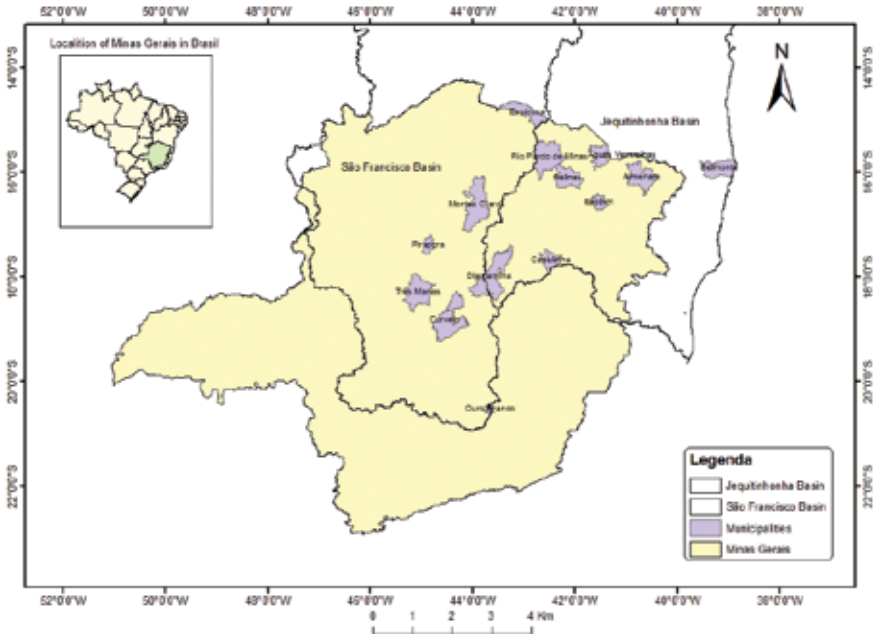

Figure 5. Representation map of municipalities location [11].

2.2. Energy consumption

Understanding energy consumption and need of each municipality is crucial to a successful work and that reveals the reality; therefore, based on the approach used by [38], average residential energy use [10] and residential coverage [17] data were collected.

2.3. Hybrid potential

For the hybrid potential, bibliographic research and INMET (National Meteorological Institute) database were used in order to understand the natural resources available (solar radiation and wind) and how those renewable energy works [39].

Renewable energy resources, solar and wind, were studied through bibliographic research, as well as, their availability on the municipalities what compose the study area. The main bibliographies used were solar and wind atlases of Minas Gerais and Brazil [40–43]; but also, the study counted on interview with expert in the field of energy [44, 45]. The cities were chosen focusing on the social aspect and solar/wind availability.

INMET database, which contains radiation and wind velocity records for fourteen municipalities that compose the study area (Águas Vermelhas, Almenara, Belmonte, Capelinha, Curvelo, Diamantina, Espinosa, Itaobim, Montes Claros, Ouro Branco, Pirapora, Salinas, Rio Pardo de Minas, and Três Marias), provided real date necessary to validate this work. From these data, the means of radiation and velocity of the winds were taken for each of the municipalities for

all months of the year, considering a period of 3 years of data for each municipality. Since the data from INMET database were provided in different metric system of those used in energy system, adjustments, conversions and weight were made on it.

Kruskal-Wallis nonparametric variance test and for Dunn's test, the Dunn's test was used in order to comparatively analyze solar radiation and wind velocity data for the municipalities. Dunn's test was used in the BioEstat 5.3 program [46].

2.4. System dimensioning

The dimension and design of a hybrid system are ruled by three factors: energy consumption, efficiency of the equipment, and availability of natural resources. For this project, was defined that the use of each of the renewable resources would follow the criteria of lower price, while meeting the energy demand [47].

Following [38] approach, generic models of photovoltaic and wind power systems were used according to [48] for a close-to-reality system design. The specification is shown in **Table 1**. It is worth mentioning that the amount of equipment required to each location differs, since their energy use, need, and natural resources are different.

Eq. (2) [37] represents the electricity generated by a photovoltaic system. It evaluates the area of the panel in m^2 (A); the efficiency of the panel in percentage (r); average solar radiation (H) and; a performance ratio, which represents the loss coefficient and ranges 0.5 and 0.9 (PR), the standard value of PR is 0.75. The evaluation gets an energy value (E) in kWh.

$$E = A^* r^* H^* PR \tag{2}$$

It is worth mentioning that the photovoltaic-software calculator was used in order to calculate the photovoltaic electric generation. The calculator uses Eq. (2).

For wind power, the equation evaluates density of air, which is given in kg/m^3 (ρ); area of the wind turbine, considering the diameter of the rotors (A); the wind speed (V); aerodynamic coefficient of rotor power (Cp) and; the efficiency of generator and transmission set (η), Eq. (3).

$$P(Watts) = 12\varrho ArV3Cp\eta \tag{3}$$

Equipment	Nominal power/capacity	Cost (RS)	Lifespan (years)
PV module	1 kW	1500	25
Wind generator	10 kW	1000	20
Battery bank	1 kWh	70	10
Inverter	2000 Wp	800	20

Table 1. Equipment specification [47].

When comes to wind sources, it presents different speeds in its vertical profile. Normally, wind turbines are located 30 m above the ground, but wind speed is measured at 30 m from the ground in INMET stations; therefore, Logarithmic Law of the Winds has to be used in order to obtain reliable data of wind speed [49]. The law follows Eq. (4); where velocity (V) of a wanted point (Z) is a function of a velocity (V_{ref}) at a known point (Z_{ref}) and Roughness length in the current wind direction (Z_0). As all the cities of the study area are located in Minas Gerais, Z_0 is assumed 1 m, based on the Atlas of Brazilian wind potential [8].

$$V = V_{ref} \ln(ZZ_0)/\ln(Z_{ref} Z_0) \quad (4)$$

3. Results and discussions

3.1. Energy consumption

In 2014, the energy consumption in Minas Gerais was 10,698 GWh and the number of residences covered by this power was 6,884,946 [17]; thus, the average residential consumption of the state was 1.55 MWh/year or 129 kWh/month. The residential electrical consumption of the studied municipalities is shown in **Table 2**.

Montes Claros, since it is the most populous municipality of the study, is also the one that presents greater consumption of the residential class.

Municipality	N° residencies	Municipality consumption (GWh/year)
Águas Vermelhas	1781	0.23
Almenara	10,168	1.31
Belmonte	723	0.09
Capelinha	52,549	6.79
Curvelo	45,574	5.89
Diamantina	9322	1.20
Espinosa	7109	0.92
Itaobim	6024	9.90
Montes Claros	99,667	0.78
Ouro Branco	10,355	12.87
Pirapora	15,006	1.34
Rio Pardo de Minas	6006	1.94
Salinas	10,156	0.78
Três Marias	8176	1.31

Table 2. Energy consumption of the studied municipality [10, 31, 37].

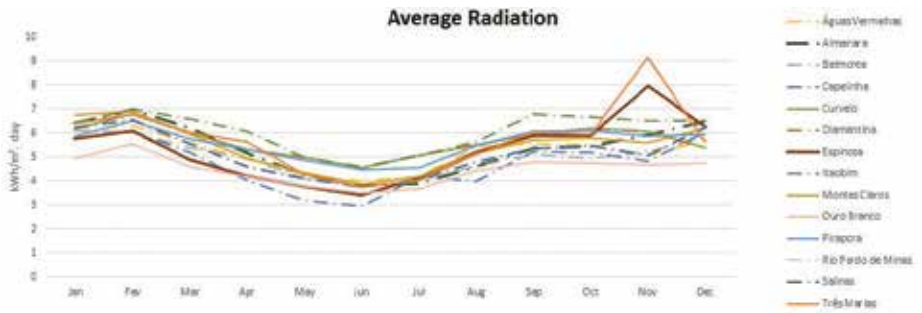

Figure 6. Average radiation for studied municipalities [11].

3.2. Hybrid potential

The hybrid potential is measured by the availability of renewable source, radiation index and wind speed. For photovoltaic purpose, a municipality is considered apt when the average radiation index is 5.5 kWh/m^2 day [25]. The municipalities that compose the study area show the following radiation (kWh/m^2 day [50]), according to analyses of INMET database, Águas Vermelhas 5.6; Almenara 5.5; Belmonte 5.0; Capelinha 4.7; Curvelo 5.7; Diamantina 5.3; Espinosa 6.2; Itaobim 5.6; Montes Claros 5,7; Ouro Branco 4.5; Pirapora 5.9; Rio Pardo de Minas 5.2; Salinas 5,9 e; Três Marias 5,7 (**Figure 6**). Regarding the basin, for Jequitinhonha Basin, Belmonte and Capelinha are not able to receive a photovoltaic system, and for São Francisco Basin, Ouro Branco is not able to support this sort of system in the parameters of this study. Another important factor for this study is daytime radiation (insolation), which is shown in (**Figure 7**), the pattern is that radiation increases during the day until reaches the highest values at 15 h (3 p.m.), showing slitting smaller values at 16 h (4 p.m.), when they start to decrease again. The decrease factor revealed to be faster than the increase. For wind energy, the turbines are activated when the winds reach a speed of 3 m/s. For the study area, the municipalities that have shown feasibility for the implementation of wind energy system are Diamantina, Espinosa, Ouro Branco, Rio Pardo de Minas, and Três Marias (**Figure 8**). The municipalities that have both solar and wind potential are Espinosa and Três Marias

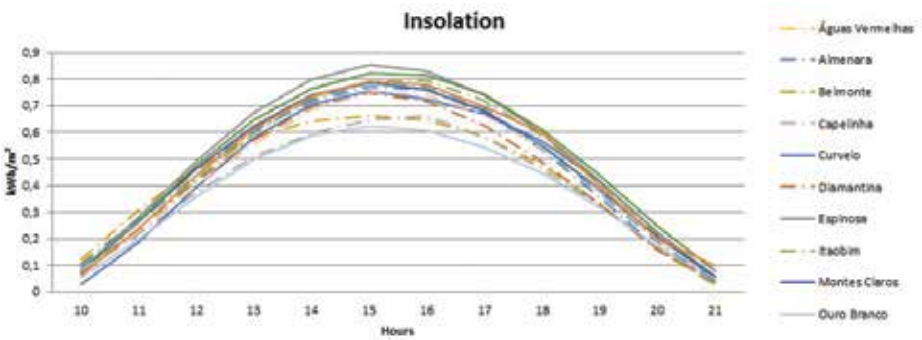

Figure 7. Average insolation for studied municipalities [11].

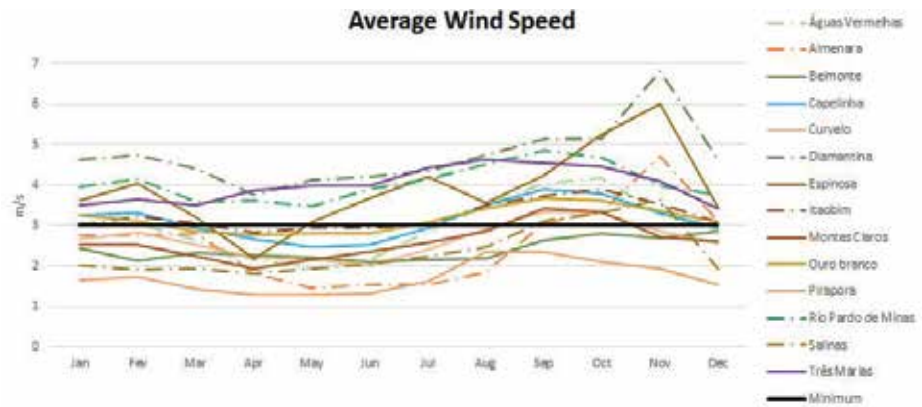

Figure 8. Average wind speed for studied municipalities [11].

(both of them from São Francisco Basin); therefore, they are able to receive a hybrid system. These data were corroborated by the variance test that indicated a significant difference of these municipalities in relation to the others that were analyzed ($H = 72.0573$; $p < 0.0001$). It is worth mentioning that the Logarithmic Law of the Winds were applied to every municipality considering 30 m from the ground, which means that some of the cities would be able to receive this system at higher altitudes; however, it would be so much expansive that would be economically unfeasible.

Of the municipalities eligible for the hybrid system, only Espinosa has no wind availability during 24 h of the day (**Figure 9**).

3.3. System dimensioning

Dimensioning a system depends on the demand and resource available. For this study, dimensioning follows the principle of supplying 100% of cities demand for residential category.

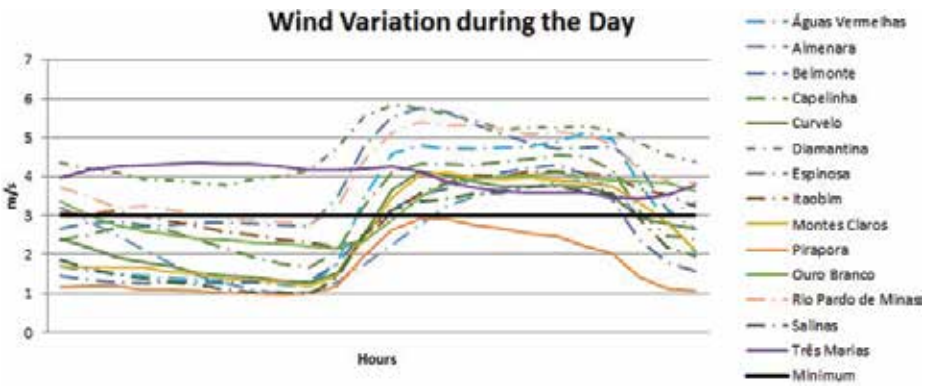

Figure 9. Average wind behavior during the day for studied municipalities [11].

The representation of each part of the hybrid system will be done by "f" as the photovoltaic portion and (f-1) the wind part. For municipalities where wind average was not enough to carry a wind system, (f-1) is equal to zero; therefore, the entire demand will be supplied by f (photovoltaic system). The size of "f" also differs among cities, for the difference of demand as well as solar radiation and wind speeds [38].

Analyses from INMET databases have shown that some municipalities have potential for solar system (Águas Vermelhas 5.6; Almenara 5.5; Curvelo 5.7; Itaobim 5.6; Montes Claros 5.7; Pirapora 5.9; and Salinas 5.9), other for wind system (Diamantina, Ouro Branco, and Rio Pardo de Minas), and two of them for hybrid system (Espinosa and Três Marias). Just Belmonte and Capelinha revealed to be incapable to comport any of the system in the parameters of this study.

For the hybrid-system-municipalities (Espinosa and Três Marias), (f-1) is different from zero. For Diamantina, Ouro Branco, and Rio Pardo de Minas, "f" is equal to zero and for all other (f-1) is equal to zero, except for Belmonte and Capelinha, which did not meet the minimum standards considered in this study.

A simulation of prices, amount of equipment for each municipality is shown in **Table 3** following the specifications and prices (considering batteries and inverters as well) mentioned in Section 2.2.3 (**Table 1**).

The simulations shown in **Table 3** revels that, when technically feasible, hybrid systems should be prioritized, since they show lower cost and are more reliable considering seasonality of solar

Municipality	Consumption (GWh/year)	N° Panels	N° of wind generators	Estimated cost (R$)
Águas Vermelhas	0.23	1.09	0	1,195,646.15
Almenara	1.31	6	0	6,581,538.46
Belmonte	0.09	—	—	—
Capelinha	6.79	—	—	—
Curvelo	5.89	25.69	0	28,179,953.85
Diamantina	1.2	0	100	423,000.00
Espinosa	0.92	25	90	408,123.08
Itaobim	9.9	44.89	0	49,240,876.92
Montes Claros	12.87	55	0	60,330,769.23
Ouro Branco	12.88	0	1000	4,230,000
Pirapora	1.34	5727	0	6,282,078.46
Rio Pardo de Minas	1.94	0	190	803,700.00
Salinas	0.78	3365	0	3,691,146.15
Três Marias	1.06	40	105	488,026.92

Table 3. Energy consumption of the studied municipalities [11].

and wind resource. The wind resource is the second resource that presents the best initial cost, losing only to hydroelectric power stations [51], which proves the data obtained in this study.

3.4. Environmental and social perspective

Although solar and wind energy represent a sustainable and renewable source of energy, they still have negative impact that have to be considered and mitigated, even if their impacts are small compared to traditional sources [52].

With regard to the environment, the raw material for solar energy is silicon, which has to be mined; therefore, all the mining impact has to be considered and represent the main impact of photovoltaic panels. Even though this is a negative impact, it also represents an advantage for Brazilian market, since the country has large reserves of quality quartz that can generate silicon with high purity, cells and solar modules [53].

For wind energy, the main impact is the death of birds due to collision. It is estimated that collisions with wind turbines kills approximately 20,000 to 37,000 birds per year [54]; however, this number represents only 0.003% of birds death, since other anthropological activities have a major influence on this number, such as building, car, chemicals. For wind energy, there are still noise and visual pollution.

Other impact to be quoted is the land use for both systems, since they require a large area [55].

For social, there is much gain in this sort of energy system. First, these systems do not release pollutant, so they are safer and healthier, the greenhouse gas life cycle for renewable energy, including manufacturing, installation, operation and maintenance and dismantling, is minimal [56]. Substituting fossil fuels for renewable energy can reduce premature mortality and generally reduce health costs [57].

Another benefit is that solar and wind systems do not represent conflict of use of water, since they require little use of water [58]. In addition, they require more labor, so they create more jobs per invested currency, and jobs tend to be created in rural areas, which help to avoid rural exodus [58, 59].

4. Conclusions

In Brazil, the year of 2018 was tagged by an event that showed the weakness of a system that relies on in only one source to attend their necessities; a truckers strike made the whole country stop. The energy sector has a similar situation; more than 60% of its energetic matrix is represented by one source, hydroelectric power plants. So, due to the importance of the energy sector, the energetic matrix needs to be a bit diversified.

The analyses carried on in this study demonstrated that Minas Gerais, more specifically municipalities on São Francisco and Jequitinhonha Basins, shows technical feasibility to receive renewable energy system, whether solar, wind or hybrid system. The economical

analyses also revealed that it is economically viable, nuclear power plants, Angra I and II nuclear plants, with a combined capacity of about 2000 MW, received an investment of R$ 6.576 billion [58], a photovoltaic field of this proportion (2000 MW) would cost about R$8 billion, as shown in this project (see **Table 3**, Pirapora), this option has a close price of what was spent in the nuclear power plants, and it is a cleaner option, free of risk to the population.

Even though hydroelectric plants continue to be more economically viable [44, 45], the use of other source of energy is important in order to protect Brazilian market, diversifying national energy matrix.

After all, the study has shown that hybrid system is a viable alternative for Minas Gerais, specially the basins of São Francisco and Jequitinhonha. In addition, it could represent the crucial change to address social issues in these basins.

Author details

Eduarda Moreira Nascimento[1]*, Júnio de Souza Damasceno[2] and Sabrinne Kelly Souza[3]

*Address all correspondence to: emn2103@gmail.com

1 University Center of Belo Horizonte (Uni-BH), Brazil

2 University of the State of Minas Gerais (UEMG), Brazil

3 University Center of Eastern Minas Gerais (Unileste MG), Brazil

References

[1] Heun MK, Owen A, Brockway PE. A physical supply-use table framework for energy analysis on the energy conversion chain. Applied Energy. 2018;**226**:1134-1162. DOI: 10.1016/j.apenergy.2018.05.109

[2] Reis LB d. Electrical Energy Generation. 2nd ed. rev e actual ed. Barueri, SP: Manole; 2011

[3] Topal H et al. Application of trigeneration with direct co-combustion of poultry waste and coal: A case study in the poultry industry from turkey. Thermal Science. 2017:137-137. DOI: 10.2298/TSCI170210137T

[4] Taner T. Optimisation processes of energy efficiency for a drying plant: A case of study for Turkey. Applied Thermal Engineering. 2015;**80**(5):247-260. DOI: 10.1016/j.applthermaleng.2015.01.076

[5] Taner T, Sivrioglu M. Energy-energy analysis and optimisation of a model sugar factory in Turkey. Energy. 2015;**93**(P1):641-654. DOI: 10.1016/j.energy.2015.09.007

[6] Brazilian President Sends in Army as Truck Protest Paralyzes Country. The Guardian, International Edition, Brazil, 25 May. 2018. Available from https://www.theguardian.com/world/2018/may/25/brazil-protests-latest-temer-clears-trucks-highways-army [Accessed: June 4, 2018]

[7] Diab F et al. An environmentally friendly factory in Egypt based on hybrid photovoltaic/wind/diesel/battery system. Journal of Cleaner Production. 2015;**112**(P5):3884-3894. DOI: 10.1016/j.jclepro.2015.07.008

[8] Herzog AV, Lipman TE, Kammen DM. Renewable Energy Sources. University of California, Berkeley, USA: Renewable and Appropriate Energy Laboratory (RAEL). Available online: https://rael.berkeley.edu/sites/default/files/old-site-files/2001/Herzog-Lipman-Kammen-RenewableEnergy-2001.pdf. Copyright: 2002-2015

[9] Heinberg R. What is Sustainability? The Post Carbon Reader: Managing the 21st Century's Sustainability Crise. In: Richard Heinberg, Daniel Lerch, editors. Healdsburg, California: USA, Watershed Media; 2010. 523 p

[10] IBGE. Brazilian Institute of Geography and Statistics. Censo Demográfico. 2010. Available from: https://ww2.ibge.gov.br/home/estatistica/populacao/censo2010/ [Accessed: October 30, 2018]

[11] Silveira EF, de Oliveira TF, Brasil ACP Jr. Hybrid energy scenarios for Fernando de Noronha archipelago. Energy Procedia. 2015;**75**:2833-2838. DOI: 10.1016/j.egypro.2015.07.564

[12] IEA, International Energy Agency. World energy outlook. In: Renewable Energy Technologies. France: IEA Publications; 2015. pp. 2072-5302

[13] Renewables Information: Overview. In: Renewable Energy Technologies. 2017 edition. France: IEA Publications. Available online: https://www.iea.org/publications/freepublications/publication/RenewablesInformation2017Overview.pdf [Accessed: October 30, 2018]

[14] Galdino MAE et al. O contexto das energias renováveis no Brasil. Revista da Direng. Centro de Pesquisas de Energia Eletrica—CPEE. Rio de Janeiro (RJ), Brazil; 2000. pp. 17-25

[15] Ferreira HT. Energia Eólica: Barreiras a sua Participação no Setor Elétrico Brasileiro. São Paulo; 2008. 111 p. Available from: https://goo.gl/qmXuGp. [Accessed: Jun 6, 2018]

[16] Atlas Solarimetrico do Brasil: Banco de Dados Terrestres. In: Chigueru Tiba et al. editors. Recife: Ed. Universitária da UFPE, Brazil; 2000. 111 p

[17] CODEVASF. Integrated Management of Land Based Activities in the São Francisco River Basin Project. GEF/ANA/OAS/UNEP. Executive Summary of the Final Report. Determination of Land Use in the Upper São Francisco River Basin. Brasília (DF): Companhia de Desenvolvimento dos Vales do São Francisco e do Parnaíba; 2002. 17 p

[18] da Silva Rocha L et al. Potencial de geração de energia fotovoltaica integrada a rede pública de distribuição:um exemplo de Açailândia para o Maranhão. Revista Brasileira de Energias Renováveis. 2014;**3**:107-127

[19] Maouedj R et al. Performance evaluation of hybrid Photovoltaic-Wind power systems. Energy Procedia. 2014;**50**:797-807. DOI: 10.1016/j.egypro.2014.06.098

[20] Fares MA et al. Photovoltaic panels characterization and experimental testing. Energy Procedia. 2017;**119**:945-952. DOI: 10.1016/j.egypro.2017.07.127

[21] El Mays A et al. Improving photovoltaic panel using fined plate of aluminum. Energy Procedia. 2017;**119**:812-817. DOI: 10.1016/j.egypro.2017.07.103

[22] Balo F, Şağbanşua L. The selection of the best solar panel for the photovoltaic system design by using AHP. Energy Procedia. 2016;**100**:50-53. DOI: 10.1016/j.egypro.2016.10.151

[23] El Khashab H, Al Ghamedi M. Comparison between hybrid renewable energy systems in Saudi Arabia. Journal of Electrical Systems and Information Technology. 2015; **2**(1):111-119. DOI: 10.1016/j.jesit.2015.03.010

[24] ANEEL, Agência Nacional de Energia Elétrica. Atlas de energia Elétrica. 2nd ed. Available from: http://www2.aneel.gov.br/aplicacoes/atlas/download.htm [Accessed: June 05, 2018]

[25] Chaurasiya PK, Ahmed S, Warudkar V. Wind characteristics observation using Doppler-SODAR for wind energy applications. Resource-Efficient Technologies. 2017;**3**(4):495-505. DOI: 10.1016/j.reffit.2017.07.001

[26] WOM—World meteorological organization. Available from: https://www.wmo.int/pages/index_en.html [Accessed: June 05, 2018]

[27] Taner T, Demirci OK. Energy and economic analysis of the wind rurbine plant's draft for the Aksaray City. Applied Ecology and Environmental Sciences. 2014;**2**(3):82-85. DOI: 10.12691/aees-2-3-2

[28] Baloglu UB, Demir Y. Economic analysis of hybrid renewable energy systems with V2G integration considering battery life. Energy Procedia. 2017;**107**:242-247. DOI: 10.1016/j.egypro.2016.12.140

[29] James EP, Benjamin SG, Marquis M. A unified high-resolution wind and solar data-set from a rapidly updating numerical weather prediction model. Renewable Energy. 2017;**102**(PB):390-405. DOI: 10.1016/j.renene.2016.10.059

[30] Ludwig D. Wind-solar hybrid plants up to twice as efficient. In: PV Magazine: Photovoltaic Market & Technology. 2013. Available from: https://goo.gl/vSL4mZ [Accessed: June 6, 2018]

[31] Tim T. Solar–wind hybrid power plants approximately twice as efficient. 2013. Available from: https://goo.gl/65S8d [Accessed: 071 June 2018]

[32] Senjyu et al. A hybrid power system using alternative energy facilities in isolated island. IEEE Transactions on Energy Conversion. 2005;**20**(2):406-414

[33] MMA. Caderno da Região Hidrográfica do São Francisco / Ministério do Meio Ambiente, Secretaria de Recursos Hídricos. Brasília: MMA; 2006. 148 p

[34] ANA. Agência Nacional das Águas. Região Hidrográfica do São Francisco. Águas que contribuem para o desenvolvimento de 521 municípios. Available from: http://www2.ana.gov.br/Paginas/portais/bacias/SaoFrancisco. [Accessed: April 27, 2016]

[35] Ferreira VO, Silva MM. O Clima da Bacia de Rio Jequitinhonha, em Minas Gerais. Subsídios para a Gestão de Recursos Hídricos. Revista Brasileira de Geografia Física. 2012;**2**:302-319

[36] Ribeiro EM, Galizoni FM, Silvestre LH, et al. Agricultura familiar e programas de desenvolvimento rural no alto jequitinhonha. RER. 2007;**45**(4):1075-1102. DOI: 10.1590/S0103-20032007000400012

[37] Nascimento EM, Souza JD. Hybrid power plants: Viability for cities in Minas Gerais. 2017;**21**(5). DOI: 10.4186/ej.2017.21.5.37

[38] EPE, Empresa de Pesquisa Energética. Statistical yearbook of electricity 2014 baseline year. Brasília: Ministério de Minas e Energia; 2015. 230 p

[39] INMET–National Institute of Meteorology. Database. Belo Horizonte, MG. Uni-BH student, Mar 20. 2016. Database made available via email by institute officials to Eduarda Moreira Nascimento

[40] CEMIG, Energetic Company of Minas Gerais. Solarimetric Atlas of Minas Gerais. Belo Horizonte (MG), Brazil; 2012. 80 p. ISBN: 978-85-87929-50-1

[41] do Amarante OAC, Silva FdJLd, Andrade PEPd. Wind Atlas: Minas Gerais. Belo Horizonte (MG), Brazil; 2010. 84 p. ISBN: 551.5185098151

[42] CRESESB, Reference Center for Solar and Wind Energy. Atlas of Brazilian wind potential. Brasília. 2001. Available from: https://goo.gl/7q2iSh [Accessed: April 01, 2016]

[43] Pereira EB, et al. Brazilian Atlas of Solar Energy. São José dos Campos. 1st ed. 2006. Available from: https://goo.gl/vhlZLw [Accessed: April 01, 2016]

[44] Lopes BM, Belo Horizonte MG. Uni-BH student. 2016. Interview granted by the employee of CEMIG to Eduarda Moreira Nascimento

[45] Silva CHF. Belo Horizonte MG. Uni-BH student. 2016. Interview granted by the employee of CEMIG to Eduarda Moreira Nascimento

[46] Ayres M et al. BioEstat 5.3: Aplicações Estatísticas nas Áreas das Ciências Biológicas e Médicas. 5th ed. Belém-PA: Publicações Avulsas do Mamirauá; 2011. p. 361

[47] Silva ET, Torres EA, Costa CA. Energização em comunidade isolada em sistema híbrido eólico e solar-fotovoltaico e irradicação da miséria: Estudo de caso de uma comunidade quilombola na Bahia. In: Identidade da Escola Superior de Teologia. Vol. 17, n. 1. 2014. Available from: https://goo.gl/hiKOiZ [Accessed: March 21, 2016]

[48] Photovoltaic-Software, 2013-2016 [Internet]. Available from: https://goo.gl/jZj07G [Accessed: July 15, 2016]

[49] Machado RR. Estudo do Potencial Eólico do Pontal do Abreu—Município De Viamão—RS. 2008. Available from: https://goo.gl/RI4ZUt [Accessed: October 19, 2016]

[50] CEMIG, Energetic Company of Minas Gerais. Wind Energy. s.d. Available from: https://goo.gl/kmV1Tl [Accessed: November 10, 2016]

[51] Jaber S. Environmental impacts of wind energy. Journal of Clean Energy Technologies. 2013;**1**(3):251-254. DOI: 10.7763/JOCET.2013.V1.57. Available from: https://goo.gl/oyfMs8 [Accessed: April 13, 2016]

[52] National Research Council. Ecological Effects of Wind-Energy Development. In: Environmental Impacts of Wind-Energy Projects. 2007. pp. 48-90. Available from: https://goo.gl/Nm8fYA [Accessed: October 3, 2016]

[53] EPE, Empresa de Pesquisa Energética. Análise da Inserção da Geração Solar na Matriz Elétrica Brasileira. Nota técnica. 2012. Available from: https://goo.gl/ofcaFm. [Accessed: March 03, 2016]

[54] MME, Ministério De Minas E Energia. Desenvolvimento de Estudos para Elaboração do Plano Duodecenal (2010-2030) de Geologia, Mineração e Transformação Mineral. 2009. Available from: https://goo.gl/Nm8fYA [Accessed: October 4, 2016]

[55] EA, Energy Analyses. Renewable Energy Costs and Benefits for Society RECABS. 2007. Available from: https://goo.gl/xP2YJL [Accessed: September 20, 2016]

[56] Machol B, Rizk S. Economic value of U.S. fossil fuel electricity health impacts. Environment International. 2013;**52**:75-80. DOI: 10.1016/j.envint.2012.03.003. Available from: https://goo.gl/d3ek4U [Accessed: April 20, 2016]

[57] Eletronuclear. Balanço Anual (2007). 2008. Available from: https://goo.gl/yQ3UdX. [Accessed: October 22, 2016]

[58] IPCC, Intergovernmental Panel on Climate Change. IPCC Special Report on Renewable Energy Sources and Climate Change Mitigation. 2011. Available from: https://goo.gl/OQsHrO [Accessed: September 27, 2016]

[59] UCSUSA, Union of Concerned Scientists. Benefits of Renewable Energy Use. 2013. Available from: https://goo.gl/Uf0DDN

Chapter 6

Nuclear Fusion Power Plants

Shutaro Takeda and Richard Pearson

Additional information is available at the end of the chapter

http://dx.doi.org/10.5772/intechopen.80241

Abstract

Nuclear fusion, the process that powers the sun and the stars, is heralded as the ultimate energy source for the future of mankind. The promise of nuclear fusion to provide clean and safe energy, while having abundant fuel resources continues to drive global research and development. However, the goal of reaching so-called "breakeven" energy conditions, whereby the energy produced from a fusion reaction is greater than the energy put in, is yet to be demonstrated. It is the role of ITER, an international collaborative experimental reactor, to achieve breakeven conditions and to demonstrate technologies that will allow fusion to be realized as a viable energy source. However, with significant delays and cost overruns to ITER, there has been increased interest in the development of other fusion reactor concepts, particularly by private-sector start-ups, all of which are exploring the possibility of an accelerated route to fusion. This chapter gives a comprehensive overview of nuclear fusion science, and provides an account of current approaches and their progress towards the realization of future fusion energy power plants. The range of technical issues, associated technology development challenges and future commercial opportunities are explored, with a focus on magnetic confinement approaches.

Keywords: nuclear fusion, power plant, plant design, plant operation, environmental impact, sustainability, DEMO

1. Introduction: a brief history of nuclear fusion

Under enormous pressures and temperatures, two or more atomic nuclei are able to overcome the coulombic barrier and, through the quantum tunneling effect, join together to create a heavier nucleus, and to release enormous amounts of energy in the process. This reaction is called *nuclear fusion*. It is the process that combines lighter elements to create heavier elements, from which the energy released is what powers the sun and the stars [1]. Nuclear fusion has

the potential to provide almost limitless energy for mankind, as its primary fuel sources are abundant [2], there is no risk of a runaway reaction or meltdown, and no long-lived high-level radioactive waste or harmful greenhouse emissions are produced (see Section 5) [3]. As such, the possibility of creating a star on earth and harnessing the energy from the fusion reaction is heralded as the solution to all of mankind's energy problems [4]. The aim of this study is to provide an overview of current development efforts into nuclear fusion as an energy source.

Figure 1 illustrates the binding energy of atomic nuclei and shows the differences between the easily confused nuclear *fusion* and nuclear *fission* reactions. Nuclear fission involves the splitting of unstable heavy atomic nuclei (illustrated by the leftward arrow on the right-hand side of the figure), whereas fusion involves the fusing of light atomic nuclei (illustrated by the upward arrow on the left-hand side of the figure).

Nuclear fusion was first observed earlier than nuclear fission. In 1934, an experiment involving scientists Oliphant, Harteck and Lord Rutherford, where by bombarding deuterium ions into target compounds containing deuterium, they observed that a new isotope of hydrogen and a neutron had been produced [6]. They theorized that a "*hydrogen transmutation effect*" had taken place [6], and it was later proven that this effect had in fact been the D-D fusion reaction (the reaction between two deuterium isotopes).

Although discovered prior to World War II, efforts to utilize the fusion reaction as a source of energy did not materialize until the 1950s [7]. Meanwhile, scientific understanding of the nuclear fission reaction, and the mechanisms by which energy could be produced from it, lead to rapid commercialization of fission technology in the early 1960s. During the same period, nuclear fusion research was considered slow, and was considered as being in "*Purgatory*" [8] due to the relative lack of progress as compared with fission. However, unlike fission, which occurs spontaneously in certain elements in nature and for which the reaction can be easily controlled in manmade reactors, fusion only occurs in stars (and the supernovae of starts) where the intense gravitational pressure and high temperatures allow the fusion reaction to take place. Given

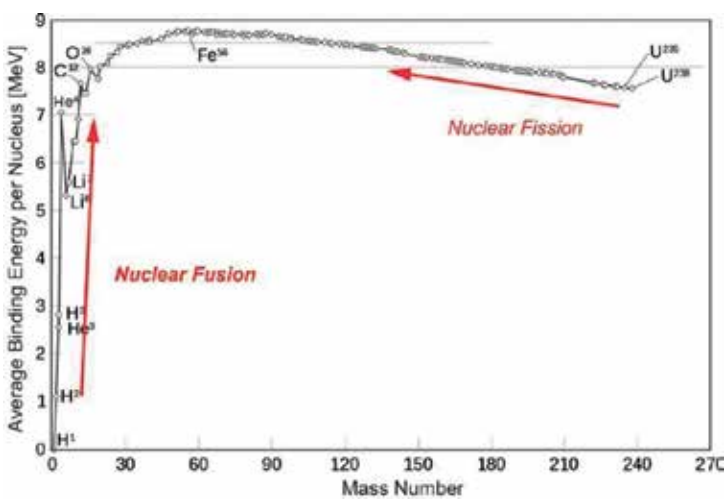

Figure 1. Binding energies of atomic nuclei (from hydrogen to uranium) [5].

http://dx.doi.org/10.5772/intechopen.80241

the extremity of the conditions required, it was immediately clear that the task of mimicking a star and harnessing energy from the fusion reaction on Earth would be a significant challenge.

In 1965, promising experimental results were published by the Soviet Union from a novel nuclear fusion device called a *Tokamak*. A tokamak, which is a Russian acronym for "*Toroidalnaya Kamera Magnitmaya saksial'nym*" (which translates to "toroidal chamber with axial magnetic field"), is a donut-shaped device that was designed for the purpose of confining a high temperature plasma using a magnetic field, which is explained in more detail in Section 3. At first, experimental findings from tokamak experiments were largely ignored by the international fusion research community. However, by the beginning of 1970s the efficacy of the tokamak became apparent, and many countries followed by developing their own tokamak machines. Notable tokamaks around the world include: the Joint European Torus (JET) in U.K. (designed, constructed, and operated by the European Union, and Euratom, starting in the late 1970s and continues operation today), the Japan Torus-60 (JT-60) in Japan (which is now being upgraded to JT-60SA "Super Advanced").

Since the end of the Cold War, focus has shifted towards international collaboration on the development of fusion. Together, the European Union, India, Japan, Russia, United States, South Korea and China are involved in the construction of the ITER tokamak (previously an acronym for International Thermonuclear Experimental Reactor, but now solely referred to as ITER, which is Latin for "*the way*"). A diagram showing the cross-section of ITER is shown in **Figure 2**. Under construction in Saint-Paul-lès-Durance, near Provence, in France, ITER will be the largest fusion reactor in the world to date and is considered the next major step in the path towards fusion energy. The primary objective is for ITER to yield a fusion reaction that produces five times more energy than is needed to sustain the fusion reaction (see Section 2), but it will also demonstrate the scientific and technological feasibility of fusion energy using tokamaks. "First plasma" in ITER (the start of preliminary D-D operation) is currently scheduled to begin in 2025, but the start of full power D-T operation (the reaction between deuterium and tritium), which will allow an attempt at achieving breakeven conditions, has been pushed back almost two decades from the original start date and will now begin in 2035.

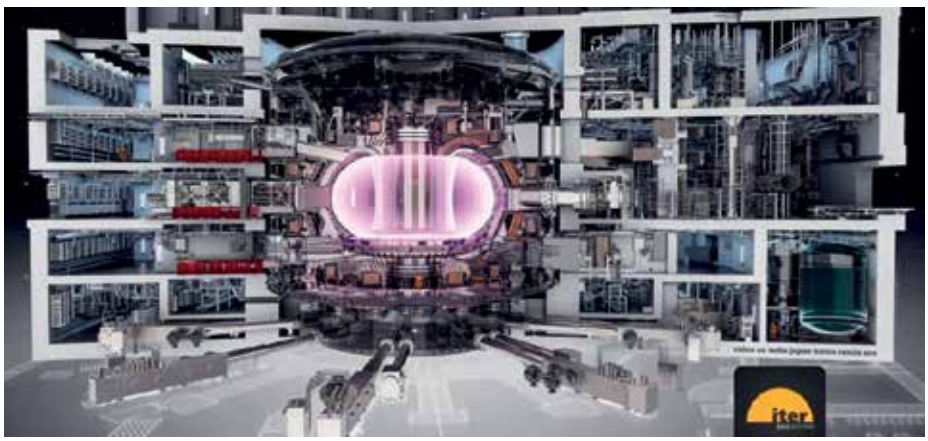

Figure 2. ITER tokamak and plant systems [9].

2. Fundamentals of nuclear fusion science

During the fusion of two or more light atomic nuclei, the mass of the product of the fusion reaction is slightly less than the sum of the reactants. This difference in mass is the conversion of mass into energy, as was theorized by Albert Einstein, and later proven. The relationship between mass and energy is shown in Eq. (1), where E, m and c are the energy released, the mass difference, and the speed of light respectively. In case of a nuclear fusion reaction, the surplus binding energy will be released as kinetic energy of particles, as detailed below.

$$E = \Delta mc^2 \tag{1}$$

As shown in **Figure 1**, a helium-4 (^{4}He) nucleus has the greatest binding energy of any atom lighter than carbon-12 (^{12}C), and as such it is therefore the most stable of the light elements. Therefore, in terms of effectively utilizing energy from the nuclear fusion reaction, and to produce a stable product, it is most desirable to fuse light atoms that result in the production of a helium nucleus. Fusing lighter atomic nuclei has another significant advantage. The lower electric charge of lighter atoms leads to a reduced level of repulsion when interacting with other atomic nuclei, increasing the likelihood that a fusion reaction will occur. Nuclear fusion reactions between the lightest isotopes of hydrogen, deuterium (2D) and tritium (^{3}T), as shown as Eqs. (2)–(4), are therefore the best candidates for the fuel cycle in future fusion reactors [3].

$$^2\mathrm{D} + {}^2\mathrm{D} \rightarrow {}^3\mathrm{T}\ (1.01\ \mathrm{MeV}) + {}^1\mathrm{H}\ (3.03\ \mathrm{MeV}) \tag{2}$$

$$^2\mathrm{D} + {}^2\mathrm{D} \rightarrow {}^3\mathrm{He}\ (0.82\ \mathrm{MeV}) + {}^1\mathrm{n}\ (2.45\ \mathrm{MeV}) \tag{3}$$

$$^2\mathrm{D} + {}^3\mathrm{T} \rightarrow {}^4\mathrm{He}\ (3.52\ \mathrm{MeV}) + {}^1\mathrm{n}\ (14.06\ \mathrm{MeV}) \tag{4}$$

But of the three reactions shown, which offers the best option to be utilized as an energy source? The difficulty of a nuclear fusion reaction can be expressed by the reactivity, which is defined as the probability of a reaction occurring, per unit time, per unit density of target nuclei [10]. Reactivities of nuclear fusion reactions can be obtained by a multiplication of the nuclear cross section σ, and the relative velocity ν [10]. **Figure 3** shows the averaged reactivity $\langle\sigma\nu\rangle$ of the reactions Eqs. (2)–(4), as well as other possible fusion reactions between light atomic nuclei. As is clear, the lower the reactivity, the more extreme the conditions must be for the fusion reaction to occur. The figure shows that the reactivity between atomic nuclei of deuterium and tritium (the D-T reaction) is the most favorable, and it is for this reason that efforts are currently focused on producing a D-T fusion reactor. However, despite the fact that the reactivity of the D-T reaction makes it favorable from a physics perspectives, as detailed in Section 6, due to complications surrounding the long-term availability of tritium, unwanted chemical properties, and the higher energy neutrons produced by the reaction, other fusion fuels that avoid the use of tritium may be preferable. Of these, the D-D fusion reaction, as shown in Eqs. (2) and (3), as well as other aneutronic fusion reactions (reactions not resulting in the production of neutrons), are considered to be the best long-term options for future fusion reactors.

http://dx.doi.org/10.5772/intechopen.80241

Although the D-T fusion reaction requires the lowest kinetic temperature for the fusion reaction to occur, extremely high temperatures in the order of tens of keV are still required. Fusion reactors must be designed to provide and contain the conditions needed for nuclear fusion reactions to occur. In a fusion reactor, atoms of deuterium and tritium are heated to very high temperatures. At high temperatures, the electrons surrounding an atom separate from the nucleus, forming an ionized and electrically conductive substance called a *plasma* (plasma is the fourth state of matter). For fusion to occur, the plasma containing the fusion fuels must reach the thermal (kinetic) energy required, which requires the need to both contain and to heat the plasma. Plasma can be contained by magnetic fields, as it is positively charged. Being electrically conductive, it is also possible to induce a current in the plasma. There are a number of ways fusion plasmas can be controlled, and these are explained in Section 3.

To generate net positive energy from a fusion reaction, the energy released by the reaction must be greater than the energy that is required to induce the reaction. In the case of a fusion reactor,

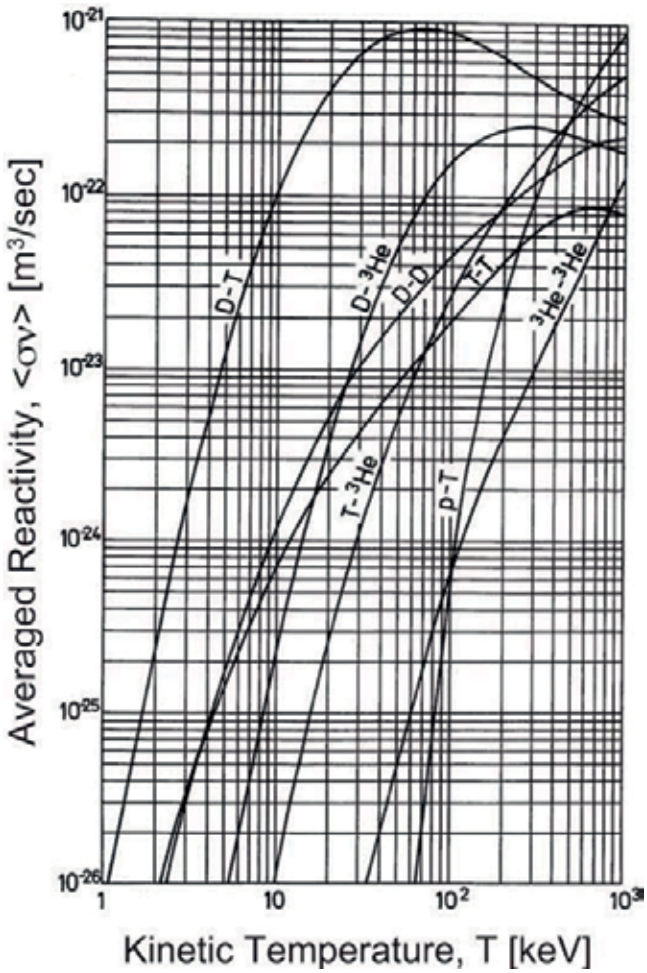

Figure 3. Averaged reactivity <σv> of nuclear fusion reactions between light atomic nuclei [11, 12].

this is the ratio of the energy output from nuclear fusion reactions in the plasma to the energy supplied to sustain the plasma, and is known as the *fusion energy gain Q*, or Q_{fus}. The conditions to achieve Q = 1, the moment at which the energy produced is equal to the energy put in, is known as *scientific breakeven conditions*. In the case of a fusion reactor, auxiliary system power requirements and inefficiencies in the production of electricity mean that scientific breakeven conditions are not sufficient for a commercial fusion reactor. Instead, the ratio of energy production from the fusion reactor must be compared against the total energy consumption of the whole fusion power plant. This is known as the *engineering gain* Q_{eng}. Similarly, the conditions required to achieve $Q_{eng} = 1$ is known as "engineering breakeven," and it is achieving these conditions that is the true goal on the pathway to the realization of fusion energy.

There are three ways to improve the value of Q, in order to get closer to fusion conditions. Firstly, by increasing the rate of the fusion reaction (increasing the output energy) whilst simultaneously reducing the level of external heating needed (decreasing in the input energy), the value of Q can be increased. This is shown by the volumetric *rate of the fusion reaction*, f, as in Eq. (5), where n is the density of the fuel, and $<\sigma\nu>$ is the averaged reactivity. Since $<\sigma\nu>$ is proportional to the square of T, the volumetric rate of fusion reaction f is proportional to n^2T^2, thus when both are increased it leads to an increase in Q. The rate of the fusion reaction is dependent on both the density of the plasma, and on the plasma temperature, and increasing the temperature and density are thus two of the ways to increase Q.

$$f = 0.25\, n^2 < \sigma\nu > \tag{5}$$

The third way to increase Q pertains to the efficiency of a fusion plasma to maintain its high-temperature and high-density plasma conditions. This is known as the *energy confinement time* τ_E, and is expressed by Eq. (6), where W and P_{heat} are the thermal energy and the heating energy of the plasma, respectively [13]. The confinement time τ_E is the first-order delay time constant of the plasma thermal energy when the heating energy $P_{heat} = 0$, and is a measure of how well a fusion plasma can be contained.

$$\frac{dW}{dT} = P_{heat} - \frac{W}{\tau_E} \tag{6}$$

In summary, Q_{fus} is closely linked to the plasma density, the plasma temperature, and the efficiency of contained thermal energy (confinement time). All must be increased to achieve the conditions required for nuclear fusion. These three factors combine as $nT\tau_E$, which is known as *the fusion triple product*, or the *Lawson criterion* [14]. The triple product is used to evaluate the performance of a fusion reactor, and efforts have seen the value of the triple product increase steadily over time, although little improvement has been made in the past two decades.

3. Nuclear fusion reactors

3.1. Approaches to fusion reactors

Although several approaches to controlling and containing a fusion plasma exist, the two primary approaches being explored are based on the concept of *magnetic confinement*, and *inertial confinement*.

http://dx.doi.org/10.5772/intechopen.80241

Magnetic confinement fusion (MCF) reactors are the more advanced of the two approaches, and they utilize magnetic fields generated by electromagnetic coils to confine a fusion plasma in a donut-shaped (torus) vessel. There are two primary types of torus-shaped fusion devices. The *tokamak*, such as ITER (as introduced in Section 1), utilizes magnetic coils arranged around a torus-shaped vessel, which generates a toroidal magnetic field to confine the plasma, and uses a secondary poloidal magnetic field to drive the current in the plasma [13]. Other tokamak variants, such as the spherical tokamak design, which has a lower aspect ratio (the ratio of the outer radius to the inner radius of the torus), exhibits different and potentially better plasma performance but with the tradeoff of increased difficulty in engineering design [22].

Another magnetic confinement concept is the *stellarator*, which uses magnetic coils in a helical configuration around the plasma vessel, creating a spiral-shaped magnetic field which is used to drive the current. The differences between tokamak and stellarator systems are illustrated in **Figure 4**. The stellarator is considered to be a potential long-term solution, and stellarator-based fusion reactors are actively being explored, but like the spherical tokamak may present a great challenge in engineering design [15].

Unlike magnetic confinement approaches, *inertial confinement fusion* (ICF) approaches attempt to externally heat and compress fusion fuel targets to achieve the very high temperatures even higher densities required to initiate the nuclear fusion. For most ICF concepts and approaches, high power lasers are used to compress and heat the fuel.

Recently, a third approach, which exploits the parameter space between the conditions produced and needed for magnetic and inertial confinement, has gained traction in recent years, and is receiving much scientific, and even commercial, attention. *Magnetized target fusion* (MTF), sometimes known as *magnetized inertial fusion* (MIF), looks to exploit the use of higher density plasmas than for MCF approaches, but lower power lasers and other drivers than those used in ICF approaches. MTF may offer a unique route to fusion, and the accelerated development of a number of unique concepts has seen significant support, particularly in the United States of America where the U.S. ARPA-E (Advanced Research Projects Agency-Energy) "ALPHA" program has provided support for exploration into the magnetized target fusion route to fusion [17].

3.2. Progress in reactor development

As described in Section 2, nuclear fusion reactors are often evaluated by their ability to achieve high plasma density n, confinement time τ_E, and temperature T. As such, the history of fusion reactors is best viewed as a history of the improvement of the fusion gain Q on the *Lawson*

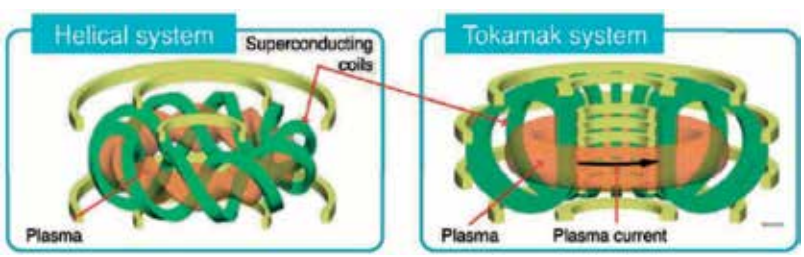

Figure 4. Helical and tokamak magnetic confinement fusion reactors [16].

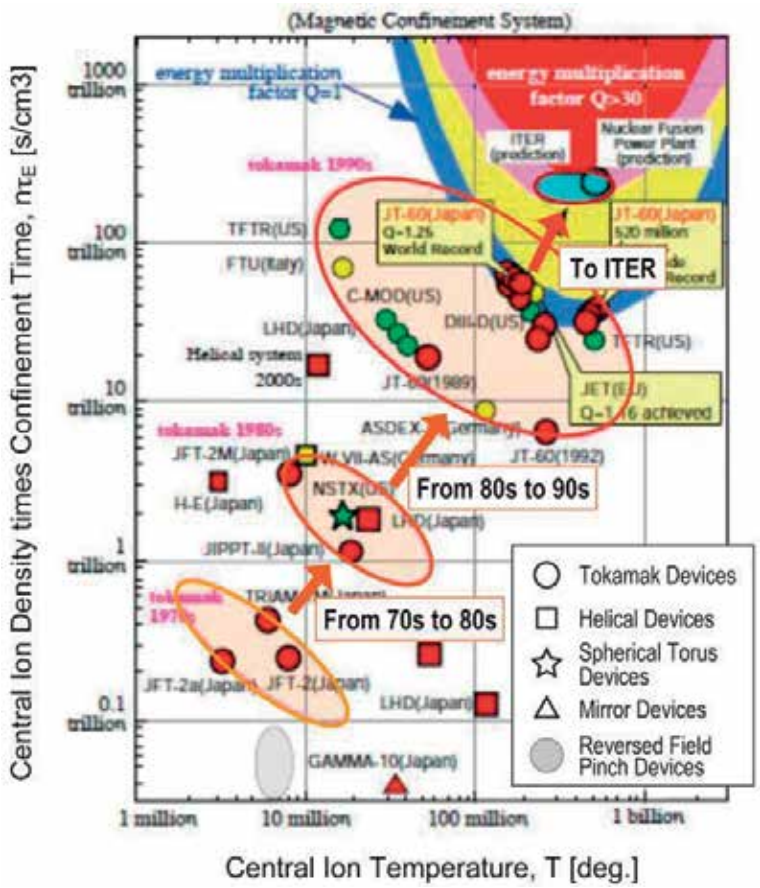

Figure 5. The development of fusion reactors since the 1970s (adapted from [18]).

Diagram. The Lawson Diagram in **Figure 5** illustrates the progress in fusion reactor development, showing progression towards the Lawson criterion, with the central ion temperature (T) shown on the horizontal axis, and the product of plasma density the energy confinement time ($n\tau_E$) shown on the vertical axis. The diagram shows that since the 1970s fusion reactors have seen a steady improvement towards scientific breakeven conditions (Q = 1). However, whilst the scientific community wait on the delayed ITER project to begin operation, progress towards breakeven has stagnated over the past two decades, as all focus has been on ensuring ITER's success, which has diverted effort, resources in the way of both funding and manpower, and time for the exploration of other pathways, and even alternative tokamak concepts.

4. Nuclear fusion power plant design and operation

4.1. Harnessing the energy from the fusion reaction

All information presented here pertains only to the D-T fusion reaction, as the majority of development efforts are based on the D-T fuel cycle. However, it is worth mentioning that aneutronic

fusion fuels, such as the proton-boron-11 reaction, or those involving helium-3, are considered to present promising and viable alternatives for long-term use as fuels for fusion energy. Refer to [19] for a comprehensive overview of the range of potential fuel cycles for future fusion reactors.

The primary energy released by the D-T fusion reaction is in the form of kinetic energy, which is carried by the products of the reaction. Of the two products, the majority of the energy is carried by the neutron (14.1 MeV), with the remainder being carried by the helium nucleus (3.5 MeV). As helium carries a positive charge, it will be affected by magnetic fields of the reactor, and as such the majority of the kinetic energy carried by the helium nuclei from fusion reactions will remain in the plasma, with the energy transferred to the plasma provide a self-heating effect to help sustain the fusion reaction. However, the kinetic energy carried by the neutrons, which are uncharged particles, will not remain in the plasma and instead will deposit their energy as heat in the walls of the reactor. Fusion power plant concepts intended for energy production will capture the energy carried by the neutrons in a blanket surrounding the reactor. The heat energy captured by the blanket will be extracted and converted into electricity through a thermodynamic cycle. It should be noted that whilst the energy is transferred by the neutrons, they also have potential to cause significant radiation damage. This is a major issue for future fusion reactors and must be designed for (see Section 5.1).

4.2. Energy production

The *Rankine cycle* is a closed steam turbine system used to generate electricity by converting energy from a heat source. A standard Rankine cycle follows a four-stage process. Water enters a *boiler*, for which the energy is provided by a heat source (in this case a fusion blanket which is heated primarily by the energy deposited from neutrons), where the energy from the heat carried away in the water is hot enough to form a saturated steam. The saturated steam passes through a *steam turbine*, where it expands transferring its energy to a turbine as rotational energy, which is used to turn a generator to produce electricity. Following the expansion through the turbine, the resulting wet steam enters the *condenser*, where it is converted back into the liquid phase. Finally, the liquid water passes through a *pump*, which returns the working fluid from a low-pressure boiler to a high-pressure boiler, and the cycle repeats. Currently, the Rankine cycle, as well as variations of the Rankine Cycle such as the reheat and regenerative Rankine cycle, are widely used at coal, oil and nuclear fission power plants. Due to the similarities in the conditions of nuclear fission reactors in that they produce high-grade heat, fusion power plants of the future are also expected to employ a Rankine cycle.

The *Brayton cycle* is now utilized at many natural gas power plants. As nuclear fusion reactors have the potential to operate at high-temperatures, fusion power plants of the future operating on the Brayton cycle also have the potential to achieve a higher energy production efficiency than systems using a Rankine cycle. Proposals to use fusion in more advanced electricity generation cycles include the possibility of using the *Integrated Gasification Fuel Cell* (*IGFC*) *cycle* or the *Magnetohydrodynamic* (*MHD*) *generator cycle*. In fact, the potential for fusion to produce high-grade process heat opens a number of avenues for future energy generation technology. Novel ideas for process heat applications of nuclear fusion, for purposes such as hydrogen production [20], high-temperature salt water desalination [21], or biomass gasification could facilitate the deep decarbonization of a larger proportion of primary energy markets, allowing fusion technology to be used to better support ever-increasing global energy demand.

4.3. Operation modes

There are two proposed modes of plant operation for electricity production in fusion power plants. The first is *steady-state mode*, which would allow the plant to generate electricity at a constant rate, as is the case in current nuclear fission power plants. Alternatively, fusion power plants could operate in *pulsed mode*, whereby the reactor system alternates between a short plasma burning period (concept designs see burn period range from 30 min to several hours), and a shut-off period (also known as a *dwell period*) to recharge for the next pulse. Some plant concepts based on a pulsed operational mode are designed with thermal reservoirs that use residual heat to enable continued electricity generation during dwell periods. Concepts that cannot manage continuous energy production in pulsed mode are considered intermittent and thus may not be viable as an electricity generating source but may still be useful for process heat applications, as detailed in Section 4.2.

An alternative is to design smaller ("compact") fusion reactors modules, which then operate together in a modular power plant configuration. By designing a power plant so that of a set of fusion reactor modules, some are operational whilst others are in a dwell period, intermittent fusion devices could still prove viable for electricity production. A modular power plant configuration also opens up the possibility of load-following capability and co-generation, by switching on a greater number of modules to provide electricity at times of high grid demand and then switching the output for the purposes of process heat applications at times of low grid demand. This concept is possible with some of the approaches being explored by various fusion initiatives, and is suggested in [22] (see Section 6), as well as by an array of concepts employing the use of fission SMRs (Small Modular Reactors), which share many similarities with the modular fusion power plant concept [21, 23].

5. Challenges to the realization of a nuclear fusion power plant

5.1. Science, engineering and technology

The science, engineering and technology challenges ahead on the route to commercial fusion are vast and wide-ranging. Principally, for magnetic confinement D-T reactor concepts, the primary technical issues that must be overcome are: [15].

- Stable operation of fusion plasmas
- Design and development of a heat exhaust system (known as the divertor)
- Development of neutron-resistant fusion materials
- Development of tritium breeding technology
- Development of reliable magnet systems

For the success of any fusion device, the operation and control of a high-performance plasma is crucial. The development of reliable plasma regimes with mitigation procedures that prevent

http://dx.doi.org/10.5772/intechopen.80241

instabilities and disruptions in the plasma from causing damage to the walls of the reactor are the subject of much current research around the globe and is a primary focus on the ITER project [15]. Further, to handle the heat from the plasma, and to remove the helium "ash" (the alpha particles) that is produced by the D-T fusion reaction itself, a plasma heat exhaust, known as a divertor, is also required. An integrated divertor design must be developed to be effective at handling the intense heat (10 MW/m^2 is the design basis for ITER [15]) and the high neutron loads over the long operational timescales that will be required for a fusion power plant [15, 24]. Divertors are specific to the tokamak approach, but any MCF power plant concept, or perhaps even MTF approaches, will have to consider a power handling and plasma exhaust system.

In addition to materials needed for the divertor, plasma facing materials (sometimes known as the first wall) must also be developed to provide radiation shielding for protection of the magnets, diagnostics and control equipment, as well as workers and the environment (using a bio-shield), whilst simultaneously allowing neutrons through to the tritium fuel breeding blanket where the energy deposited is used to produce electricity and to breed new fuel to sustain the fusion fuel cycle (see below). The requirements of fusion materials differ to those used for nuclear fission reactors. The neutrons from the D-T fusion reaction are of a much higher energy, and with the reduction of nuclear waste and safety in mind, materials for fusion are subject to judicious selection to ensure that long-lived radioactive waste is not produced through the interaction of fusion neutrons with the surrounding reactor structure [21]. In eliminating certain isotopes, the list of materials available for use in fusion reactors becomes significantly limited, thus providing an added challenge on top of an already difficult problem. An example of the trade-offs is apparent when considering the development of Reduced Activation Ferritic Martensitic (RAFM) steels for fusion applications, which upon neutron irradiation better retain their properties and do not produce any long-lived radioactive waste, but instead suffer from other performance limitations and have more of a limited thermal operation range [25].

Neutron resistant materials also play a critical role in the structure of the tritium breeding blanket systems. The tritium breeding systems have two primary purposes: to breed new tritium fuel from D-T fusion neutron interaction with lithium, and to capture and extract the energy carried by the neutrons in the form of heat so that energy can be produced (see Section 4). Challenges in the design of breeding blankets are wide-ranging. Materials selection, the removal of heat and associated thermal hydraulic challenges, as well as the breeding mechanism itself, all present disparate problems but require an integrated solution. To date, no proof-of-concept for tritium breeding technology has been demonstrated, though a range of designs exist, and preliminary testing and computer modeling has been the focus in the absence of experimental data. However, even if breeding technology is developed, issues surrounding the sustainability of breeding blankets may present an additional hurdle, as discussed in Section 5.5 [15, 26].

The final of the core challenges for fusion is in the development of efficient superconducting magnets, which are required to provide the magnetic field to contain a fusion plasma. Until recently, most effort was focused on the use of low temperature superconducting (LTS) magnets, which are capable of carrying the high fields and currents necessary for large scale magnetic confinement fusion reactors, but that are large in size, and must be cooled to liquid helium temperatures (~4 K) at significant cryogenic cost. Recent developments in magnet technology has seen the development of high-temperature superconductors (HTS) which can carry greater currents at

higher field than LTS, and with greater cryogenic efficiency, owing to the operating temperature ("high-temperature" is a misnomer that refers to potential high-performance magnet operation at 20–30 K, rather than 4 K). Development in HTS, which may lead to the development of more efficient smaller fusion reactors as they are capable of operating at higher field [22, 27].

All issues have interdependencies, and an integrated solution is required and being sought for future fusion devices, and in the development approach. See [15, 28, 29].

5.2. Safety

Unlike nuclear fission reactors, nuclear fusion reactors do not have any risk of a runaway reaction or meltdown. In the case of any abnormalities in fusion reactor conditions, such as an abnormal plasma pressure or density spike, the plasma will dissociate and collapse, and the fusion reaction will cease. The level of decay heat in a fusion reactor after the termination of the plasma is very low compared with fission reactors, which must be cooled after shutdown to prevent core melt. In principle, nuclear fusion power plants do not require an Emergency Core Cooling System (ECCS), as even in a Loss of Cooling Accident (LOCA) the plasma inside the reactor would dissociate due to the influx of impurities from the reactor vessel walls as the surfaces heat up due to the lack of coolant available. In such an event, once the plasma has dissociated, all that remains is residual decay heat, for which studies suggest that the small temperature increases do not lead to melting, and therefore decay heat in a fusion power plant is considered as a low safety risk [30]. Despite this, consideration of such accident scenarios will still be made based on the rigorous method of Probabilistic Risk Assessment (PRA) [30].

Nuclear fusion power plants will not produce high level or transuranic radioactive waste like that produced by fission power plants. However, nuclear fusion power plants will still produce large quantities of intermediate level waste as a result of the existence of high energy neutrons and the in-vessel tritium-contaminated (tritiated) dust that becomes embedded in the reactor walls and components. Radioactive waste from fusion is unavoidable, even with efforts to develop materials such as RAFM steels to reduce the radioactivity and quantities of waste from the reactor structure. Another important example of the impossibility of avoiding the production of radioactive waste from fusion is in the selection of breeding blanket materials, as the neutron irradiation of lead, a crucial breeding material (neutron multiplier) can result in the production of the isotope polonium-210, which is a strong alpha emitter. As such, both issues present a challenge, as the waste from fusion power plants will remain significantly radioactive for a number of decades, perhaps even presenting a higher level of radiological risk than the waste produced in fission reactors in the short-term, and tritiated materials will require novel handing techniques [31]. While the risks associated with radioactive materials in the long-term are considered to be lower than those associated with waste produced from fission reactors, which can last for millions of years, it is likely that a similar level of regulation and licensing will be required to ensure that plant design and waste handling is fit for purpose, safe, and factored in to design and costing.

5.3. Nuclear proliferation and security risks

Nuclear fusion power plant concepts are generally considered to have a lower risk of nuclear proliferation. Nuclear fusion power plants will not handle any currently designated

special nuclear materials. Currently safeguarded are: ^{239}Pu, ^{233}U and enriched uranium (^{235}U). However, it is not inconceivable that weapons-grade ^{239}Pu or ^{233}U could be produced using the neutrons from a fusion reactor by replacing the blanket materials with natural uranium or thorium [32]. Moreover, tritium, the primary fuel for fusion, can be used to boost the yield of thermonuclear fission and fusion weapons, and thus careful accountancy of the fuel will be required [33]. While the nuclear proliferation and security risks regarding nuclear fusion power plants are significantly lower than those required for fission power plants, it is likely that stringent safeguarding for fusion power plants will be required. These must be developed in accordance with International Atomic Energy Agency (IAEA) recommendations.

5.4. Environmental impacts

Although fusion power plants will release small quantities of tritium to within already defined limits, they will not produce greenhouse gases or other air pollutants [34]. As a result, the environmental impacts associated with nuclear fusion power plants will instead be primarily attributed to construction, operation and maintenance, including fuel supply chains, and waste disposal. Environmental Life Cycle Assessments (LCA) suggest that life cycle greenhouse gas emissions of nuclear fusion electricity generation will be somewhere between 6 and 12 g CO_2 equivalent per kWh of electricity production. This is in line with recent renewables estimates [35], and current light water nuclear power plants (5.7 g/kWh), and an order of magnitude lower than for coal power plants (270 g/kWh) [36–38].

5.5. Sustainability

The fuels of nuclear fusion power plants are deuterium and tritium. Deuterium is an isotope of hydrogen with the isotopic ratio of 150 ppm, or 1 part in 6700 atoms of hydrogen. As such, deuterium is abundant in seawater and can be extracted using well-established separation processes. Tritium, on the other hand, does not occur in nature in any significant quantity, and is only produced by commercial purposes as a by-product in heavy water CANDU fission reactors. Tritium is a radioactive isotope, decaying with a half-life of 12.3 years, and with supply coming only from CANDU reactors, supply is severely limited, as a global stockpile of only around 30 kg is available for commercial use worldwide (and the same stockpile must supply ITER with almost 20 kg). That commercial fusion reactors require 55.6 kg of tritium per year per GW (thermal) for operation, future fusion power plants cannot depend on an external supply of CANDU tritium (or otherwise) for commercial operation. Instead, tritium is expected to be produced by neutron interaction with lithium, specifically the isotope lithium-6, in breeding blankets, under the reaction shown in Eq. (7).

$$^{6}\mathrm{Li} + \mathrm{n} \rightarrow {}^{4}\mathrm{He}\ (2.05\ \mathrm{MeV}) + {}^{3}\mathrm{T}\ (2.75\ \mathrm{MeV}) \tag{7}$$

The quantity of tritium produced in the breeding blanket must be greater than that used by the fusion reactor, and therefore the reactor must have a TBR (tritium breeding ratio) above 1 in order to achieve "tritium self-sufficiency". Therefore, although the fuel itself that is required for fusion is tritium, the consumable fuel for a fusion power plant is in fact lithium.

On lithium and deuterium sources alone, it is estimated nuclear fusion power plants could provide the electricity needs of humanity for tens of millions of years (from 14 million [2]

to 23 million years [38]). This leads us to the consideration that the resources for nuclear fusion are '*virtually unlimited*.' Current terrestrial deposits of lithium are estimated at 53 million tons [39]. Given that a nuclear fusion power plant with an electrical output of 1 GWe requires between 10 and 35 tons of lithium over its operational lifetime [2], 2500 1 GWe fusion power plants would require up to 90,000 tons, notwithstanding competition for lithium from advanced technologies such as large scale battery storage. However, it is more complex when considering that many fusion breeder concepts rely on the use of lithium-6 rather than natural lithium. Lithium-6 has an isotopic abundance of only 7.5%, and therefore to obtain 90,000 tons of lithium-6, a total of 1.2 million tons of natural lithium would be required. Even so, this is only around 2% of the current known terrestrial deposits, and a backstop also exists in the form of seawater in which the abundance of lithium and some other key minerals is relatively high. Thus, although production cost would likely increase, lithium could be procured from seawater in the future [40, 41]. Even with competition for lithium, resources appear plentiful for the purposes of fusion, particularly since technological advancements towards D-D and aneutronic fuel cycles may eventually avoid the need for tritium production altogether.

However, resource limitations do exist with other critical materials required for future nuclear fusion reactors. There are potentially significant issues in the supply of helium gas for the cryogenic cooling systems, beryllium for the tritium breeder blanket, and some critical metals that are required for construction of the fusion reactor structure.

Helium resource is expected to be of limited availability for future fusion reactors, and thus improving the efficiency of cooling systems, as well as efforts to reduce and recycle the overall helium inventory, is needed to ensure longevity of the current supply [42]. As above, the lack of tritium available from external sources necessitates the inclusion of a tritium breeder blanket, which will mean lithium as the primary fuel. However, as even enriched lithium-6 tritium breeder blankets are expected to be insufficient to achieve a TBR > 1, beryllium will be used as a neutron multiplier in order to increase the neutron yield and give a higher TBR. Total current global deposits of beryllium are estimated at 100,000 to 150,000 tons, and the quantity of beryllium required per reactor is in the order of 400 tons per GWe. Therefore, current beryllium deposits would be far insufficient to support 2500 GWe of installed fusion reactors using beryllium as the neutron multiplier in the tritium breeder blanket [2]. Fortunately, lead-based tritium breeder blankets, which also provide neutron multiplication and as such offers a substitution option, are also being explored as lead is abundant and cheap. Structural materials, such as vanadium and niobium, are not abundant and although recycling or even extraction from seawater may be possible, alternative metals for alloying should be sought for longer-term fusion reactors.

6. First-Of-A-Kind fusion power plants

6.1. DEMO projects

In anticipation of the successful demonstration of the technical feasibility of nuclear fusion power plants based on the tokamak approach in ITER, many nations around the world are now proposing *Demonstration Nuclear Fusion Power Plants* (*DEMO*) designs. DEMO will be

based on design, engineering and operational experience of ITER, and is expected to be the First-Of-A-Kind (FOAK) commercially viable fusion power demonstrator in the world (even though it may never produce power to the electricity grid).

SlimCS is a DEMO power plant proposed by JAEA (Japan Atomic Energy Agency, later reformed into QST in 2016). SlimCS will have a fusion thermal output of 2.95 GW and an electrical output of 1 GW, and it will assess the economic viability of a large-scale fusion power plant. The reactor is of similar size to ITER, with a major radius of 5.5 m, and an aspect ratio of 2.6 [43]. The Japanese government publicly announced that the decision to construct a DEMO reactor will be made in 2030s, in order to realize the commercialization of fusion energy by the middle of the twenty-first century. As this puts the SlimCS schedule in the same timeframe as the operation of ITER, it is uncertain as to what extent ITER will inform SlimCS.

The European Union has a dedicated team within EUROfusion which is focused on developing the design of a European version of a DEMO fusion device, *EU DEMO*. Similarly, EU DEMO is considered to be the last step before the full-scale commercial roll-out of fusion energy technology. EU DEMO is primarily designed to be a pulsed machine but is expected to deliver long pulse durations with only a short dwell time. The expected fusion thermal output is currently envisaged to be in the order of 2 GW, with electrical output at 500 MW, but the design is only in at a conceptual stage [44, 45].

6.2. Innovative approaches by private companies

Due to delays and cost overruns in ITER, questions have been raised over the viability of the ITER pathway as being the best route to fusion energy. This has led to increasing uncertainty over future involvement and project funding, most notably from the United States of America. Such issues with the ITER project have not helped to shift the longstanding perception that commercial fusion is "always 30 years away" [46]. However, alternative fusion energy concepts are also being developed in parallel to the ITER project and are slowly increasing in technological maturity. And such activities have become the subject of increased international interest over recent years. Delays to the public fusion program, combined with novel ideas, disruptive technologies, and an injection of private funding has led to the birth of a number of private-sector start-ups, all looking for a faster route to fusion [47]. Both *Tokamak Energy Ltd* in the UK, and *Commonwealth Fusion Systems*, a spin-out company from MIT in the US, are developing tokamak variants that operate on alternative high-performance plasma regimes that make use of the benefits of HTS magnets [22, 27].

Non-tokamak reactor concepts are looking to explore entirely different configurations and are considering different ways of initiating, heating and sustaining plasmas. The ARPA-E ALPHA program in the United States of America, which has supported a number of start-ups exploring the physics space between inertial and magnetic confinement fusion, with the vision that it may lead to an "easier" route to fusion. This approach is intended to support a number of promising concepts, to spread the risk of failure and therefore at the same time to increase the chances of success [17, 47]. *General Fusion*, a Canadian-based start-up company is developing a reactor based on an entirely novel acoustically-driven system, which will operate in pulse mode [48]. *TAE Technologies* (formerly Tri-Alpha Energy), a US-based start-up, is exploring the possibilities

of liner-driven proton-boron11 fusion, opting to avoid the complications that arise from the D-T fuel cycle, and are already looking at medical applications as a potentially important market [49]. Indeed, of further interest is that *Lockheed Martin* also has an internal "Skunkworks" team dedicated to developing a novel fusion reactor approach. Although few details have been released, the reactor concept is that of a magnetic cusp device, and although patents have been filed, progress towards the realization of fusion energy of the magnetic cusp device is largely being kept secretive [50]. Numerous other fusion start-ups exist, all with the goal of delivering commercial fusion energy. Whether or not these efforts are on the road to success remains to be seen, but a "new fusion race" and the competition it brings is expected to spark technological advancement in a multitude of areas that will likely benefit all in the fusion community, and those outside it, in the pursuit of the holy grail: commercially viable fusion energy.

7. Conclusions: the road to a nuclear fusion power plant

Nuclear fusion has received frequent cynicism, with the longstanding quip that it is "always 30 years away," in reference to the fact that since the 1970s fusion scientists have continually predicted that fusion energy will take 30 years to become commercial [46]. It appears that this has always been the case, and critics say it always will be. With this in mind, it could appear disingenuous to make the same statement here at the current time, but the realization

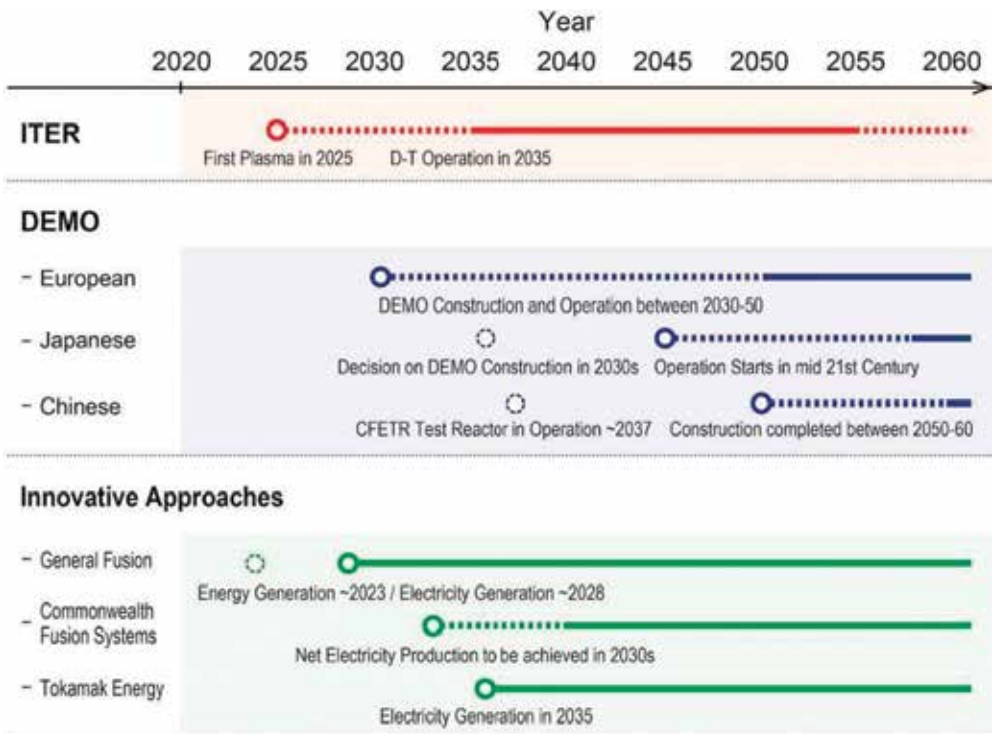

Figure 6. Current timeline for the commercialization of nuclear fusion energy [15, 22, 27, 43, 44, 48].

of a commercial fusion power plant is expected in around 30 years' time. To conclude this overview study, **Figure 6** provides a summary of current efforts, showing key concepts and expected milestones, on the pathway to commercial nuclear fusion energy.

The result of this review study highlights the current plans for the development of fusion to deliver on the promise of fusion energy. Current plans to realize fusion power are continuously updated, however should be treated with caution, as they are subject to uncertainties, unknown obstacles to technological progression and resource limitations in funding and manpower; all of which may limit the ability to achieve future goals in a timely manner. At the current time, however, it is expected that fusion energy will become a reality in less than 30 years. Every effort to ensure this timescale is realized should be made so that fusion can fulfill its potential and make the much-needed impact in global energy.

Acknowledgements

The authors would like to thank the Open University for their support of this work.

Conflict of interest

A proportion of author Richard Pearson's research is sponsored by Tokamak Energy Ltd., UK.

Author details

Shutaro Takeda[1]* and Richard Pearson[2]

*Address all correspondence to: takeda.shutarou.55r@kyoto-u.jp

1 Kyoto University, Kyoto, Japan

2 Open University, Milton Keynes, UK

References

[1] Burbidge EM, Burbidge GR, Fowler WA, Hoyle F. Synthesis of the elements in stars. Reviews of Modern Physics. 1957;**29**(4):547. DOI: 10.1103/RevModPhys.29.547

[2] Bradshaw AM, Hamacher T, Fischer U. Is nuclear fusion a sustainable energy form? Fusion Engineering and Design. 2011;**86**(9-11):2770-2773. DOI: 10.1016/j.fusengdes.2010.11.040

[3] Ueda Y, Inoue T, Kurihara K. Intelligible seminor on fusion reactors—(1) Introduction to fusion reactors. Journal of the Atomic Energy Society of Japan. 2004;**46**(12):27-34

[4] Armaroli N, Balzani V. The future of energy supply: Challenges and opportunities. Angewandte Chemie International Edition. 2007;**46**(1-2):52-66. DOI: 10.1002/anie.200602373

[5] Browne E, Dairiki JM, Doebler RE. Table of Isotopes. Fort Belvoir, VA: National Standard Reference Data System; 1978

[6] Oliphant M, Harteck P, Rutherford L. Transmutation effects observed with heavy hydrogen. Proceedings of the Royal Society of London Series A, Containing Papers of a Mathematical and Physical Character. 1934;**144**(853):692-703. DOI: 10.1098/rspa.1934.0077

[7] Arnoux R. Who invented fusion Saint-Paul-lès-durance: ITER Organization [Internet]; 2014. Available from: https://www.iter.org/newsline/-/1836 [Accessed: 2018-06-01]

[8] Braams CM, Stott PE. Nuclear Fusion: Half a Century of Magnetic Confinement Fusion Research. Boca Raton, FL: CRC Press; 2002. DOI: 10.1088/0741-3335/44/8/701

[9] ITER. ITER Tokamak and Plant Systems [Internet]. 2016. Available from: https://www.iter.org/album/media/ [Accessed: 2018-06-02]

[10] Atzeni S, Meyer-Ter-Vehn J, Meyer-ter-Vehn J. The Physics of Inertial Fusion: Beam Plasma Interaction, Hydrodynamics, Hot Dense Matter. Oxford, UK: Oxford University Press; 2004

[11] National Physical Laboratory. Kaye&Laby. Tables of Physical & Chemical Constant, Chapter 4, Section 4.7 [Internet]. Available from: http://www.kayelaby.npl.co.uk/atomic_and_nuclear_physics/4_7/4_7_4.html [Accessed 2018-06-04]

[12] Torrisi L. Ion acceleration and DD nuclear fusion in laser-generated plasma from advanced deuterated polyethylene. Molecules. 2014;**19**(10):17052-17065. DOI: 10.3390/molecules191017052

[13] Kamada Y. Intelligible seminor on fusion reactors—(2) Introduction of plasma characteristics for fusion reactor design. Journal of the Atomic Energy Society of Japan. 2005;**47**(1):45-52

[14] Lawson JD. Some criteria for a power producing thermonuclear reactor. Proceedings of the Physical Society Section B. 1957;**70**(1):6. DOI: 10.1088/0370-1301/70/1/303

[15] Donné AJH, Federici G, Litaudon X, McDonald DC. Scientific and technical challenges on the road towards fusion electricity. Journal of Instrumentation. 2017;**12**(10):C10008. DOI: 10.1088/1748-0221/12/10/C10008

[16] Nuclear Fusion Research in the World—The Frontier of Nuclear Fusion Research: NIFS/SOKENDAI Department of Fusion Science [Internet]. Available from: http://soken.nifs.ac.jp/wp/en/about/ [Accessed 2018-06-04]

[17] ARPA-E. ALPHA Program Overview United Stated Department of Energy [Internet]. 2015. Available from: https://arpa-e.energy.gov/sites/default/files/documents/files/ALPHA_ProgramOverview.pdf [Accessed 2018-06-10]

[18] Kikuchi M. A review of fusion and Tokamak research towards steady-state operation: A JAEA contribution. Energies. 2010;**3**(11):1741-1789. DOI: 10.3390/en3111741

[19] Stott P. The feasibility of using D–3He and D–D fusion fuels. Plasma Physics and Controlled Fusion. 2005;**47**(8):1305. DOI: 10.1088/0741-3335/47/8/011

[20] Nuttall WJ. A trip to 'Fusion Island' [Internet]. 2005. Available from: https://www.theengineer.co.uk/issues/31-october-2005/a-trip-to-fusion-island/ [Accessed 2018-06-10]

[21] Pearson RJ, Bluck MJ, Murphy ST. A symbiotic approach to compact fission and fusion reactors. ANS Transactions. 2017;**117**(1):378-381

[22] Sykes A, Costley A, Windsor C, Asunta O, Brittles G, Buxton P, et al. Compact fusion energy based on the spherical tokamak. Nuclear Fusion. 2017;**58**(1):016039. DOI: 10.1088/1741-4326/aa8c8d

[23] Locatelli G, Boarin S, Pellegrino F, Ricotti ME. Load following with small modular reactors (SMR): A real options analysis. Energy. 2015;**80**:41-54. DOI: 10.1016/j.energy.2014.11.040

[24] You JH, Mazzone G, Visca E, Bachmann C, Autissier E, Barrett T, et al. Conceptual design studies for the European DEMO divertor: Rationale and first results. Fusion Engineering and Design. 2016;**109**(111):1598-1603. DOI: 10.1016/j.fusengdes.2015.11.012

[25] Stork D, Zinkle SJ. Introduction to the special issue on the technical status of materials for a fusion reactor. Nuclear Fusion. 2017;**57**:092001. DOI: 10.1088/1741-4326/aa69e4

[26] Abdou M, Morley NB, Smolentsev S, Ying A, Malang S, Rowcliffe A, et al. Blanket/first wall challenges and required R&D on the pathway to DEMO. Fusion Engineering and Design. 2015;**100**:2-43. DOI: 10.1016/j.fusengdes.2015.07.021

[27] Whyte D, Minervini J, LaBombard B, Marmar E, Bromberg L, Greenwald M. Smaller & sooner: Exploiting high magnetic fields from new superconductors for a more attractive fusion energy development path. Journal of Fusion Energy. 2016;**35**(1):41-53. DOI: 10.1007/s10894-015-0050-1

[28] Federici G, Kemp R, Ward D, Bachmann C, Franke T, Gonzalez S, et al. Overview of EU DEMO design and R&D activities. Fusion Engineering and Design. 2014;**89**(7):882-889. DOI: 10.1016/j.fusengdes.2014.01.070

[29] Wu Y, Team F. Conceptual design activities of FDS series fusion power plants in China. Fusion Engineering and Design. 2006;**81**(23-24):2713-2718. DOI: 10.1016/j.fusengdes.2006.07.068

[30] Gulden W, Ciattaglia S, Massaut V, Sardain P. Main safety issues at the transition from ITER to fusion power plants. Nuclear Fusion. 2007;**47**:S415. DOI: 10.1088/0029-5515/47/9/C01

[31] Massimo Z, Kuigi C, Vladimir K, Boris K, Raffaella T. Fusion power plants, fission and conventional power plants. Radioactivity, radiotoxicity, radioactive waste. Fusion Engieering and Design. 2018 (in press). DOI: 10.1016/j.fusengdes.2018.05.049

[32] Goldston RJ, Glaser A, Ross AF. Proliferation Risks of Fusion Energy: Clandestine Production, Covert Production, and Breakout. 9th IAEA Technical Meeting on Fusion Power Plant Safety. Vienna: IAEA; 2009

[33] Gsponer A, Hurni J-P. ITER: The International Thermonuclear Experimental Reactor and the Nuclear Weapons Proliferation Implications of Thermonuclear Fusion Energy Systems. Geneva: Independent Scientific Research Institute; 2008

[34] Perrault D. Safety issues to be taken into account in designing future nuclear fusion facilities. Fusion Engineering and Design. 2016;**109**(111):1733-1738. DOI: 10.1016/j.fusengdes.2015.10.012

[35] Nugent D, Sovacool BK. Assessing the lifecycle greenhouse gas emissions from solar PV and wind energy: A critical meta-survey. Energy Policy. 2014;**65**:229-244. DOI: 10.1016/j.enpol.2013.10.048

[36] Uchiyama Y. Life cycle analysis of power genearation systems. CRIEPI Research Report. 1995;**Y94009**:12-31

[37] Tokimatsu K, Yamaji K, Katsurai M, Hondo H. Energy analysis and carbon dioxide emission of tokamak fusion power reactors. Purazuma, Kaku Yugo Gakkai-Shi. 1998;**74**(1):54-66. DOI: 10.1016/S0920-3796(00)00157-5

[38] Text—Fusion Reactors—Tokamak Reactor Designs and their Basis on Plasma Physics and Reactor Technology. JSPF, editor. Nagoya: JSPF; 2011.

[39] USGS. Lithium 2018 [Internet]. 2018. Available from: https://minerals.usgs.gov/minerals/pubs/commodity/lithium/mcs-2018-lithi.pdf [Accessed 2018-06-10]

[40] Ooi K. Technology on the lihium recovery from seawaer (1) adsorbent for lithium. Bulletin of the Society of Sea Water Science, Japan. 1997;**51**(5):285-288

[41] Nobukawa H. Technology on the lihium recovery from seawaer (2) extraction system and simulation. Bulletin of the Society of Sea Water Science, Japan. 1997;**51**(5):289-292

[42] Nuttall WJ, Clarke R, Glowacki B. The Future of Helium as a Natural Resource. Abingdon: Routledge; 2012

[43] Tobita K, Nishio S, Enoeda M, Nakamura H, Hayashi T, Asakura N, et al. Conceptual Design of the SlimCS Fusion DEMO Reactor. Japan Atomic Energy Agency: Naka; 2010

[44] Federici G, Biel W, Gilbert M, Kemp R, Taylor N, Wenninger R. European DEMO design strategy and consequences for materials. Nuclear Fusion. 2017;**57**(9):092002. DOI: 10.1088/1741-4326/57/9/092002

[45] EFDA. Fusion Electricity: A Roadmap to the Realisation of Fusion Energy. Culham: European Fusion Development Agreement; 2012

[46] Herrera-Velázquez JE. Nuclear Fusion as an Energy Option for the 21st Century. In: Klapp J, Cervantes-Cota JL, Chávez Alcalá JF, editors. Towards a Cleaner Planet. Berlin: Springer; 2007. p. 405-419. DOI: 10.1007/978-3-540-71345-6_25

[47] Pearson RJ, Antoniazzi AB, Nuttall WJ. Tritium supply and use: A key issue for the development of nuclear fusion energy. Fusion Engineering and Design. 2018 (in press). DOI: 10.1016/j.fusengdes.2018.04.090

[48] Laberge M. General fusion development program for acoustic magnetized target fusion. Journal of Plasma Fusion Research. 2017;**93**(1):32-37

[49] Binderbauer M, Tajima T, Steinhauer L, Garate E, Tuszewski M, Schmitz L, et al. A high performance field-reversed configuration. Physics of Plasmas. 2015;**22**(5):056110. DOI: 10.1063/1.4920950

[50] McGuire TJ. Magnetic field plasma confinement for compact fusion power. U.S. Patent No. 9,947,420. 17; 2018

Chapter 7

Flexible Operation of Supercritical Power Plant via Integration of Thermal Energy Storage

Decai Li, Wenbin Zhang and Jihong Wang

Additional information is available at the end of the chapter

http://dx.doi.org/10.5772/intechopen.79735

Abstract

This chapter presents the recent research on various strategies for power plant flexible operations to meet the requirements of load balance. The aim of this study is to investigate whether it is feasible to integrate the thermal energy storage (TES) with the thermal power plant steam-water cycle. Optional thermal charge and discharge locations in the cycle have been proposed and compared. Dynamic modeling and simulations have been carried out to demonstrate the capability of TES integration in supporting the flexible operation of the power plant. The simulation software named SimuEngine is adopted, and a 600 MW supercritical coal-fired power plant model is implemented onto the software platform. Three TES charging strategies and two TES discharging strategies are proposed and verified via the simulation platform. The simulation results show that it is feasible to extract steam from steam turbines to charge the TES and to discharge the stored thermal energy back to the power generation processes. The improved capability of the plant flexible operation is further studied in supporting the responses to the grid load demand changes. The results demonstrated that the TES integration has led to much faster and more flexible responses to the load demand changes.

Keywords: supercritical coal-fired power plant, SimuEngine, thermal energy storage, flexible operation, load shifting

1. Introduction

The current balance between power generation and load demand is mainly managed by regulating the output of fossil fuel power plants [1, 2]. With the rapid increase of power generation from renewable energy, fossil fuel power plants are required to play a more important role

in maintaining load balance and providing the grid frequency control service as they are considered as dispatchable power generation units. Fossil fuel power plants are now required to work more flexible and to respond faster with more frequent start-ups or shutdowns for maintaining power network stability; this can cause two serious issues: low plant efficiency and low load factors. To address these issues, it is essential to explore new technologies and operation strategies.

Currently, approximately 39% of global electricity is generated from hard coal, which however produces a large amount of ash, nitrogen oxide, and carbon dioxide. The supercritical boiler was first developed in the US in the 1950s [3], which was a type of technology with improved efficiency and hence reduced carbon dioxide and toxic emissions per unit of electrical energy generation.

The flexible operation is needed for supercritical coal-fired power plants to stabilize the grid frequency. The flexibility of a supercritical power plant can be achieved by a carbon capture facility, which is used to control capture rates in response to variable load demand and carbon prices [4–7]. A method called 'condensate throttling', proposed in [8], could rapidly increase or decrease the power output of a plant. Additionally, the regulation of extracted steam for high-pressure heater could be used to enhance the primary control reserves and to offer the operational flexibility [9, 10].

The boiler turbine coordinated control is a popular control strategy to regulate power generation in thermal power plants. However, the plant response is slow due to the large delay of the energy transfer from the fuel supply to the water-steam loop [10]. Furthermore, because the thermal inertia of a once-through boiler is smaller than a natural circulation boiler, the capability of offering primary frequency reserve is decreased. This motivates the utilization of TES in supercritical coal-fired power plants, as the TES could provide the additional thermal reserve.

Currently, the TES has been widely used in various thermal power plants for flexible plant operation. Several studies [11, 12] were reported on the integration of TES into combined heat and power (CHP) generations. Also, the study of a combined-cycle gas turbine (CCGT) power plant combined with TES in order to improve the plant flexibility was presented in [13]. Besides, many studies have been reported in the area of solar thermal power plants integrated with TES, in which TES is used for time shifting of energy delivery in an economic way [14, 15].

This chapter presents flexible operation of a supercritical coal-fired power plant via the TES integration. Section 2 describes the structure and operation of a supercritical coal-fired power plant and the simulation platform used for this study. Section 3 discusses the integration strategies of TES with the supercritical power plant. Section 4 presents the improved operational flexibility of supercritical power plant when integrating with TES. Section 5 gives the concluding remarks.

2. Description of a supercritical power plant and simulation platform

A thermal steam power plant generates electricity by transforming various types of energy fuel sources making use of an idealized thermodynamic cycle called the "Rankine cycle." The

Carnot efficiency dictates that the thermal efficiency of a power plant is mainly dominated by the temperature and pressure of the steam entering the steam turbines. Above the critical point for water at 374.15°C and 22.12 MPa, there is no phase transition from water to steam. A sub-critical coal-fired power plant with water/steam working under the critical point typically has an efficiency between 33 and 39%. In comparison, a supercritical or ultra-supercritical power plant can achieve a much higher efficiency of up to 48% [1]. Therefore, supercritical power plants have been extensively developed since the 1950s and constructed worldwide, thanks to the simultaneous development of novel materials and components which can withstand high pressure/temperature and adverse working conditions.

A simplified schematic of a typical supercritical coal-fired power plant is illustrated in **Figure 1**. The pulverized coal from the mill is burnt in the boiler furnace, releasing combustion heat to the feed water coming from the Economizer. During elevation of the water inside the water wall and superheater exchanger tubes, the water is transferred directly to the supercritical steam without evaporation. Unlike a subcritical power plant, a drum is not a necessary component in the so-called once-through boiler and it can be replaced by a smaller steam-water separator acting as the drum's role in the consideration of low load working conditions. A reheater is used to absorb the heat from downstream flue gas and reheat the exhaust steam from the high pressure (HP) turbine before it enters the intermediate pressure (IP) turbine. Several streams of steam are extracted from different locations of HP, IP, and low-pressure (LP) turbines to preheat the feed water.

An industrial 600 MW supercritical coal-fired power plant has been used as a reference plant in this study. The on-site measurement data including temperature, pressure, and mass flow rates of the water/steam at different locations under the nominal power output of 600 MW have been collected and summarized in **Table 1**.

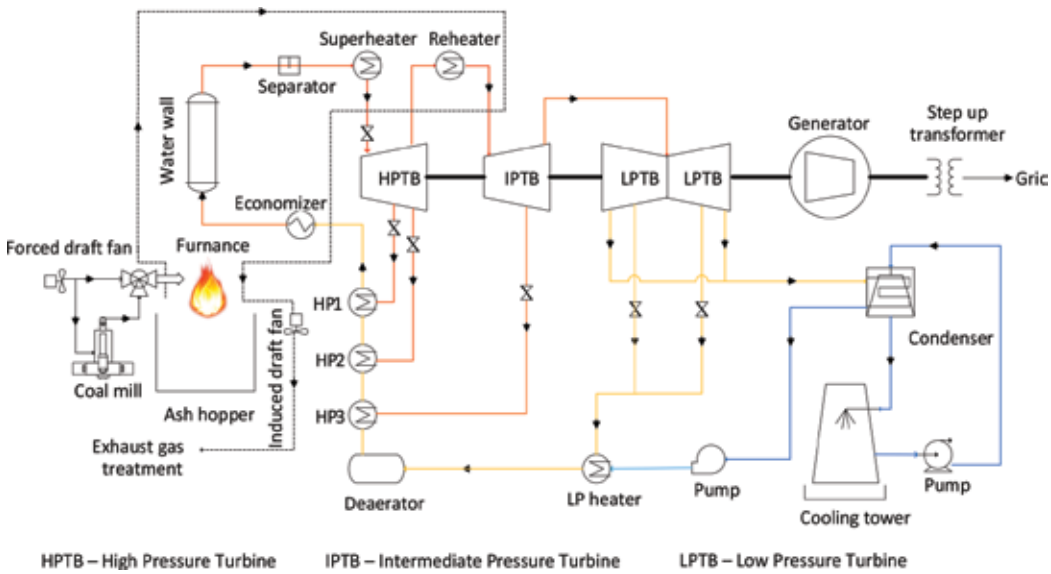

Figure 1. Simplified schematic of a supercritical coal-fired power plant.

	Temperature (°C)	Pressure (MPa)	Flow rate (kg/s)
HP heater inlet	166.86	27.65	484
HP heater outlet	263.49	27.48	484
Economizer outlet	312.63	27.3	484
Super heater outlet/HPTB inlet	562.04	25.1	483.9
HPTB outlet	304.72	4.41	445.9
IPTB inlet	565.66	3.8	406.4
IPTB outlet	354.86	0.9	387.2
LPTB inlet	354.86	0.9	309.2

Table 1. Main water/steam parameters in a 600 MW supercritical coal-fired power plant.

In principle, a power plant model can be established based on the energy and mass conservation equations for different components in the power plant system [9, 16].

Mass balance:

$$\frac{\partial \rho}{\partial t} + \frac{\partial(\rho v)}{dz} = 0. \tag{1}$$

Energy balance:

$$\frac{\partial(\rho h)}{\partial t} + \frac{\partial(\rho v h)}{\partial z} = \frac{\partial p}{\partial t} + Q, \tag{2}$$

where, ρ, v, h, p are the density, velocity, enthalpy, and pressure of the working fluid in the specific control volume respectively, and Q is the heat flow across the boundary of the control volume.

To perform the off-line tests with the optional control mechanism and dynamic responses for a practical power plant, a more detailed and visualized simulation platform called SimuEngine was initially developed by Tsinghua University, China and then further exploited in the University of Warwick, UK. The supercritical power plant model implemented on the SimuEngine can deal with a complex flow net, which represents a typical power plant system consisting of resistance component (such as valves), power components (such as fans), inertia node and source-sink nodes. The joints in a flow net are defined as nodes, while the channels connected with the nodes are defined as branches. Node pressure method is applied to solve the nonlinear flow net equations in order to obtain the nodes' pressure and flow rates of the branches. The simulation results have been verified by the real operational plant data. More detailed descriptions of the fluid network models can be found in previous publications by the authors' group [17, 18].

http://dx.doi.org/10.5772/intechopen.79735

3. TES integration strategies and results

This section presents the integration strategies and simulation results of a supercritical coal-fired power plant with TES. There are three types of TES: sensible heat storage, latent heat storage, and chemical heat storage. The latent heat storage is applied to the hybrid system, as its energy density is higher than sensible heat storage and the cost is lower than chemical heat storage.

3.1. TES charging strategies

TES charging can be realized by extracting steam from different locations of the water-steam loop of the power plant and flowing the extracted steam through heat exchangers to store thermal energy during the off-peak period. In this way, the electrical power output can be regulated while maintaining the constant heat duty of the boiler. This study is conducted to find the answers to the following challenging questions: where the TES can be integrated and how much thermal energy can be extracted without degrading the plant thermal performance? Three heat extraction (TES charging) strategies have been investigated with two optional thermal energy extraction locations, which are Intermediate Pressure Turbine (IPTB) inlet and Low Pressure Turbine (LPTB) inlet. As shown in **Table 1**, the steam temperature at IPTB inlet and LPTB inlet are around 565 and 355°C, and the pressures at these two inlets are around 3.8 and 0.9 MPa, respectively. The simulation results are presented and analyzed in the following subsections.

3.1.1. Extracting steam from IPTB and looping back to the condenser

While the steam extraction point is set at the inlet of the IPTB, the relatively high temperature steam will pass a series of heat exchangers to store the thermal energy contained in the steam. The exhaust steam at the outlet of the TES is mixed with the LPTB outlet steam and enters the condenser. The schematic of this TES charging strategy is shown in **Figure 2**.

The amount of steam extraction is controlled by the valve openings. With different valve openings, the mass flow rate of the steam entering the IPTB and LPTB is changed, as a result, the power output is reduced. The simulation results of the mass flow rates in the TES and the variations of the plant power output with different valve openings are shown in **Figure 3**.

From **Figure 3**, it is clear that the amount of the steam extraction needs to be restricted to a feasible range in order to maintain a stable power output. The simulation study indicates that the maximum flow rate of steam extraction from the IPTB inlet is 80 kg/s, and the relative reduction of the output power is 13.3% in comparison with its rated power.

3.1.2. Extracting steam from LPTB and looping back to the condenser

Instead of the IPTB inlet, the steam extraction at the inlet of LPTB is studied in this section. After the charging process, the steam will flow into the condenser mixing together with the LPTB outlet steam. The schematic of this TES charging strategy is shown in **Figure 4**.

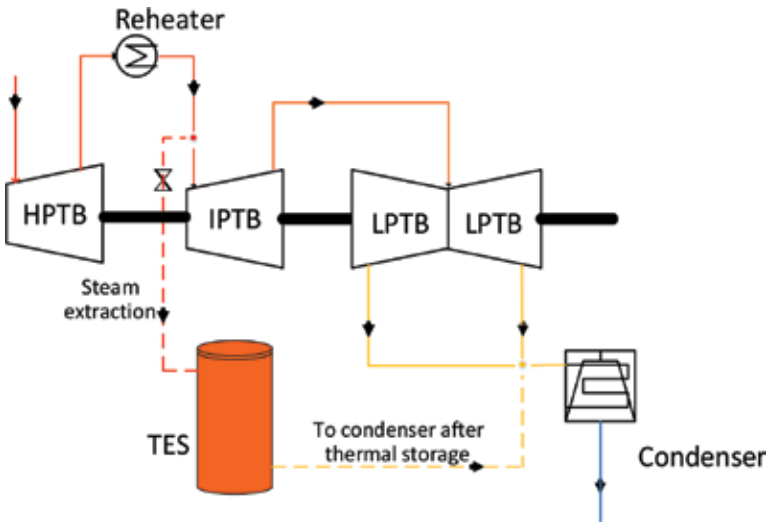

Figure 2. Schematic of the first TES charging strategy.

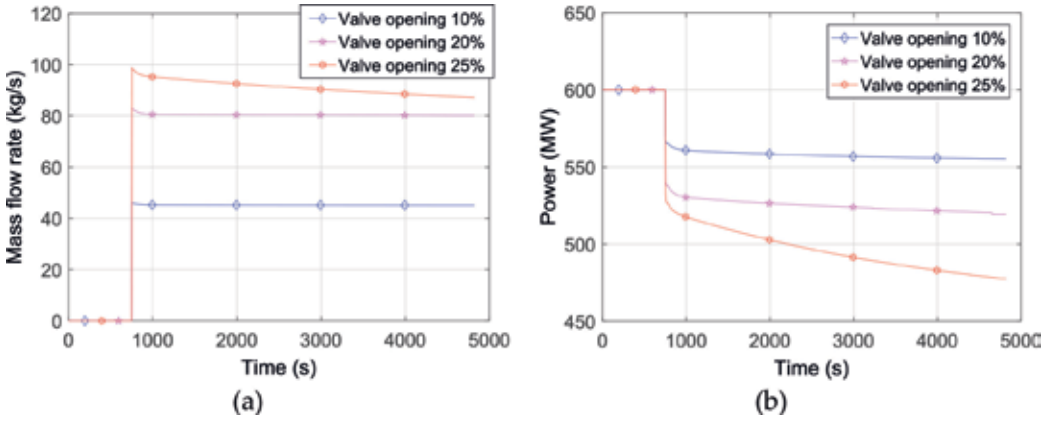

Figure 3. Dynamic responses of mass flow rate in TES and output power: (a) mass flow rate and (b) output power.

The simulation results of the mass flow rates in the TES and plant power output changes with different valve openings are shown in **Figure 5**. The simulation study indicates that in order to maintain a reasonably stable power output, the maximum rate of steam extraction from the LPTB inlet is 56 kg/s (corresponds to the valve opening of 60%), and the relative reduction of the output power is 6.5% (561 MW).

3.1.3. Extracting steam from IPTB and feeding steam back at LPTB inlet

The study reported in this section is to investigate whether the thermal storage can be controlled in order to regulate the temperature and pressure of the exhaust steam at the outlet of the TES. When the temperature of the steam is controlled to have the same value as required

http://dx.doi.org/10.5772/intechopen.79735

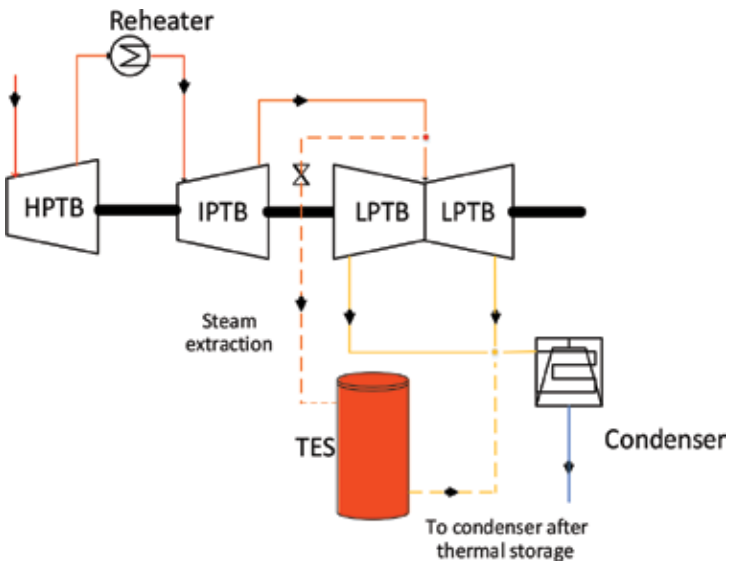

Figure 4. Schematic of the second TES charging strategy.

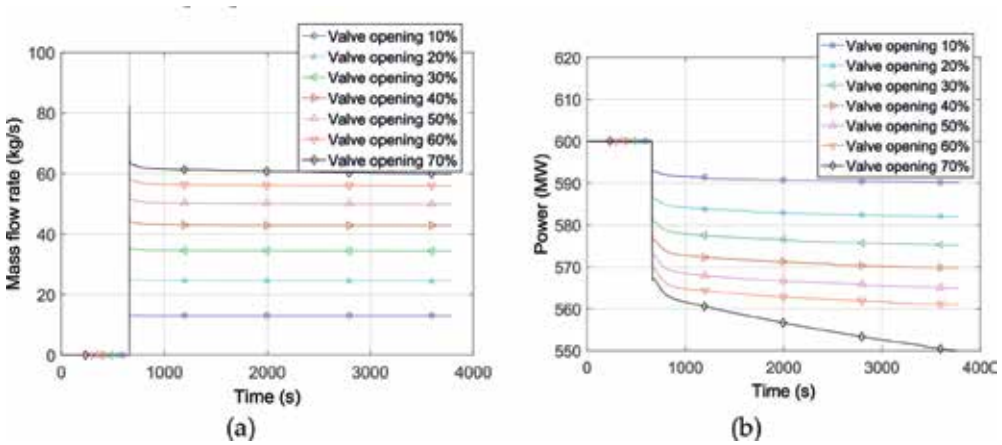

Figure 5. Dynamic responses of mass flow rate in TES and output power: (a) mass flow rate and (b) output power.

by the LPTB inlet, the steam can be fed back to the LPTB inlet directly to mix with the steam coming from IPTB. The schematic of this TES charging strategy is shown in **Figure 6**.

The simulation results of the mass flow rates in the TES and the power output associated with different valve openings are shown in **Figure 7**.

With various operating conditions and application of the above TES charging strategy, the maximum flow rate of steam which can be extracted from the inlet of IPTB is 174 kg/s (corresponds to the valve opening of 60%), and the adjustment range of the output power is 3.9% (576.5 MW). Excess extraction will lead to the steam pressure being lower than the operating

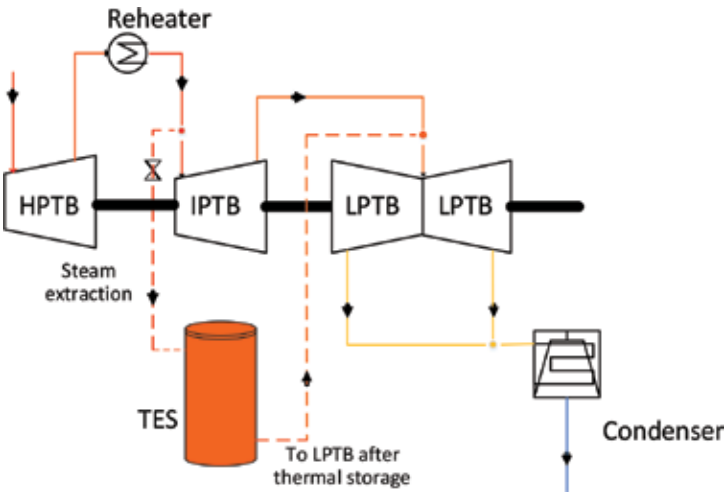

Figure 6. Schematic of the third TES charging strategy.

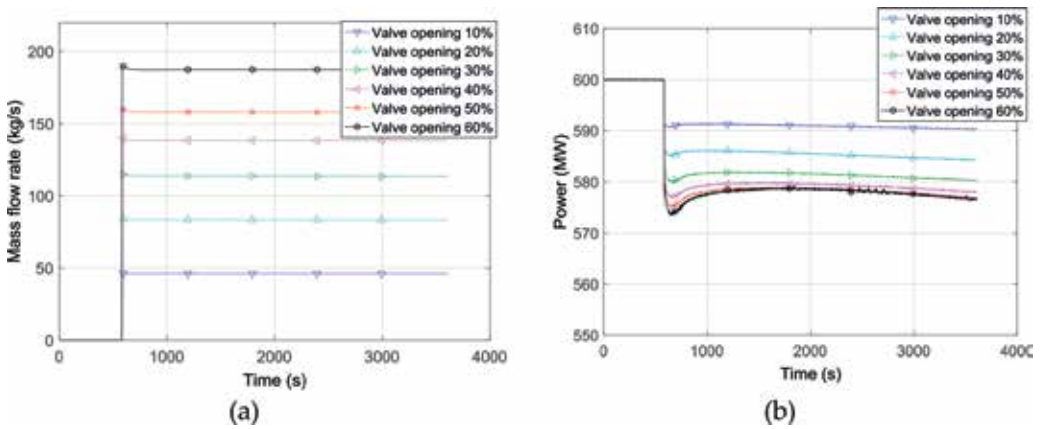

Figure 7. Dynamic responses of mass flow rate in TES and output power: (a) mass flow rate; (b) output power.

pressure required by the IPTB. So this strategy only works with a small range of power regulation. The advantage of this strategy is that the steam can be recycled back to LPTB without modifying the whole system cycle.

3.2. TES discharging strategies

During the electricity peak demand period, the stored thermal energy in the TES will be discharged back to the water steam loop to increase the total electricity generation. Two strategies have been studied: the first one is to use TES to produce high temperature and high-pressure steam, which is then fed into the LPTB inlet; another is to use TES to preheat the feed water instead of using the original preheaters. The simulation study for these two strategies is presented and analyzed in the following subsections.

3.2.1. Using TES to produce additional steam for LPTB

During the TES discharging process, part of the feed water flows into the bottom of the TES section from the deaerator, evaporates into steam and is superheated while it rises along the heat exchanger tubes in the TES, then it leaves the TES in the status of superheated steam. Heat is transferred from the TES to increase the temperature of the water/steam passing through the tubes. The steam is then fed to the LPTB inlet and produces an additional electric power output. As part of the feed water is taken out of the deaerator, more water is needed to be pumped into the deaerator in order to maintain the steam flow rates in the HPTB and IPTB. **Figure 8** shows the schematic diagram of the proposed TES discharging strategy.

Figure 9 shows the simulation results of power output with the heat discharge. With various valve openings, the increased steam flow rate and power output are observed. From the simulation study, the maximum flow rate of the steam generated from the TES is 72.6 kg/s. As a result, the corresponding overall output power is 644.4 MW, which nearly approaches the design limit of the power plant.

3.2.2. Using TES to heat feed water instead of preheaters

In a coal-fired supercritical power plant, part of the steam is taken out from the steam turbines to preheat the feed water, as shown in **Figure 10**. In this supercritical coal-fired power plant, there are three HP heaters and a group of LP heater. The steam taken out from the HPTB is used for No. 1 and No. 2 HP heaters, the extracted steam from the IPTB is used for No. 3 HP heater, and the steam taken from LPTB is used for LP heater as shown in **Figure 10**.

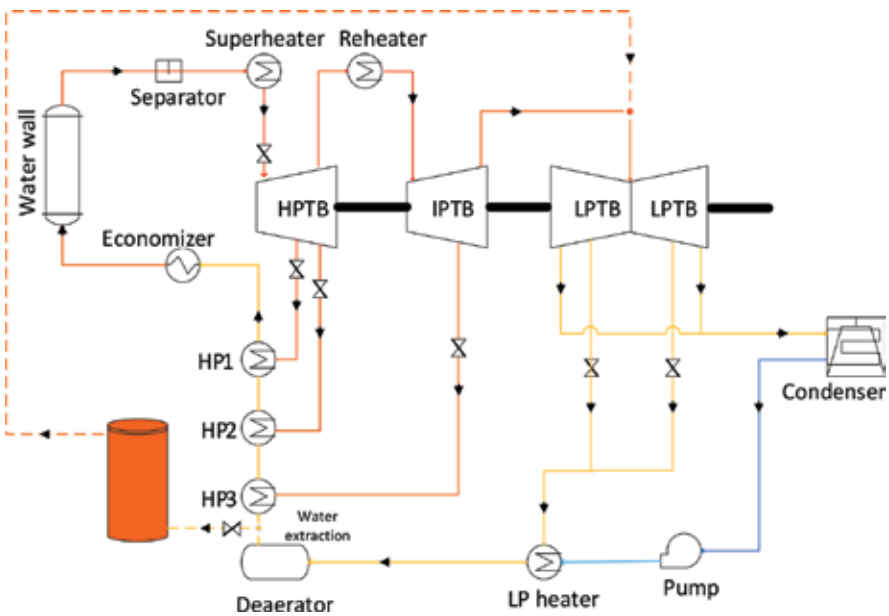

Figure 8. Schematic of the first TES discharging strategy.

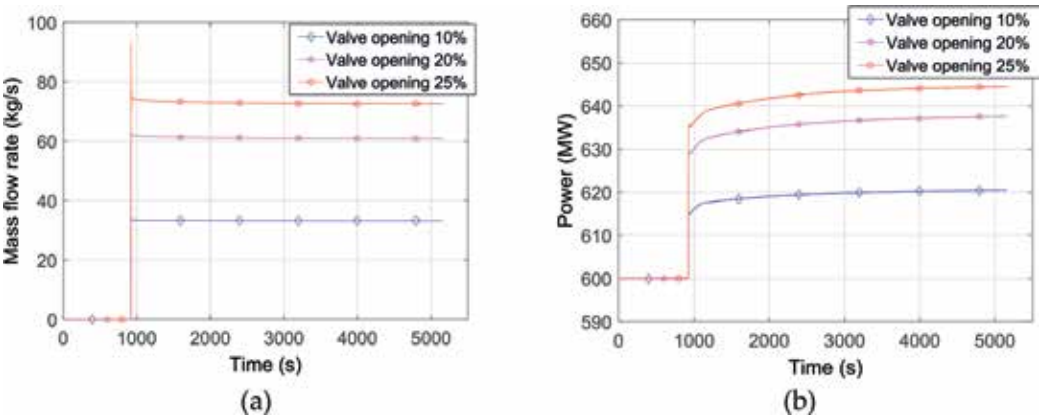

Figure 9. Dynamic responses of mass flow rate in TES and output power: (a) mass flow rate and (b) output power.

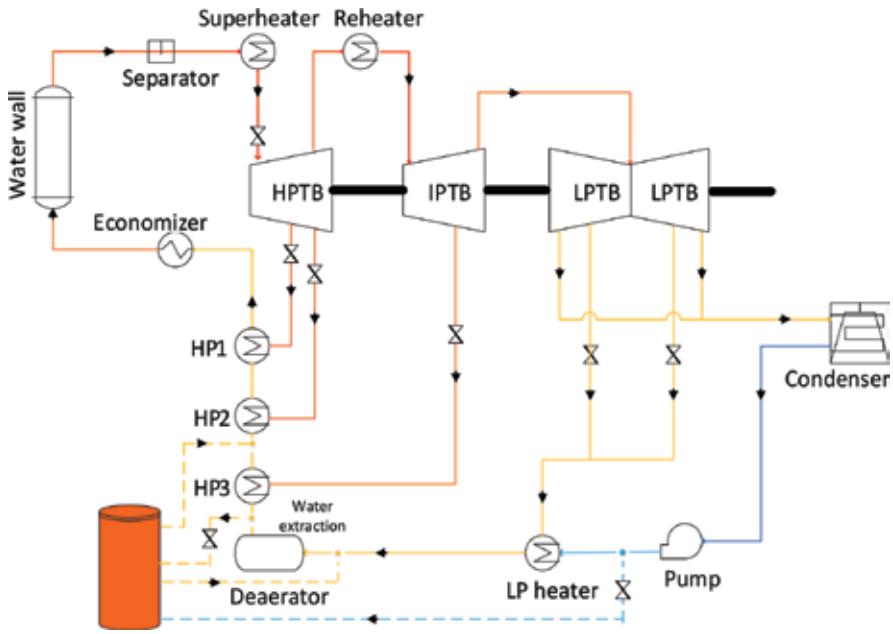

Figure 10. Schematic of the second TES discharging strategy.

The amount of the steam extraction is controlled by regulating valve openings. When these valves are closed, more steam will pass through the downstream turbines and produce more power. However, this operation leads to the decrease of the feed water temperature. With the TES integration, in order to maintain the feed water temperature, the feed water will bypass the preheaters and flow into TES to raise its temperature. Simulation results are shown in **Figure 11**.

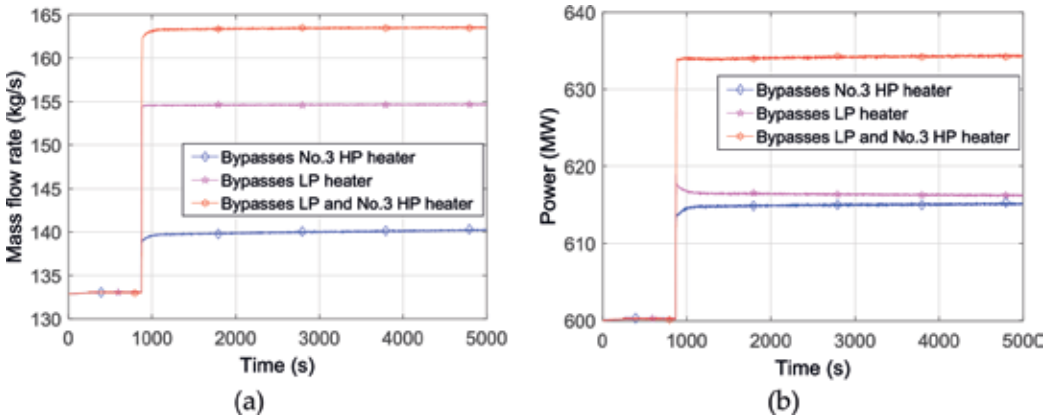

Figure 11. Using TES to heat feed water instead of preheater: (a) mass flow rate and (b) output power.

When the valve used to extract steam for No.3 HP heater is closed, the feed water will bypass the No.3 HP heater and it will be heated by the TES. Accordingly, the output power is increased to nearly 615 MW from 600 MW. When those valves for extracting steam to feed to the LP heater are closed, the feed water will bypass the LP heater and enter the TES for heating. As a result, the output power is increased to around 616.5 MW from 600 MW. When those valves for extracting steam to feed to the LP heater and No. 3 HP heater are closed, the feed water will bypass the LP heater and No. 3 HP heater and be heated by TES. Then the output power is increased to 634 MW from 600 MW. This method requires no plant structure changes so it is more feasible and cost-effective although the power regulation capability is limited to a small range.

4. Improvement in dynamic performance

The simulation results have shown that the power plant could be operated with increased flexibility within a wider range of power output through TES integration. The TES could accumulate or release thermal energy to regulate the plant power output, therefore it offers the enhanced capability in providing the services to load shifting. The dynamic performance of the supercritical power plant with or without TES integration is compared in this section.

The simulation results are shown in **Figures 12** and **13**. The solid line is the power output dynamic responses with the TES integration in action, in which the output power is regulated with the support of TES charging and discharging processes while the amount of feed coal (fuel input) remains the constant. The dashed line represents the power output without TES integration where the power output is directly controlled by changing the flow rate of coal feeding. It can be seen that the power plant integrated with TES shows faster dynamic responses and smoother transitions compared with the power plant without TES.

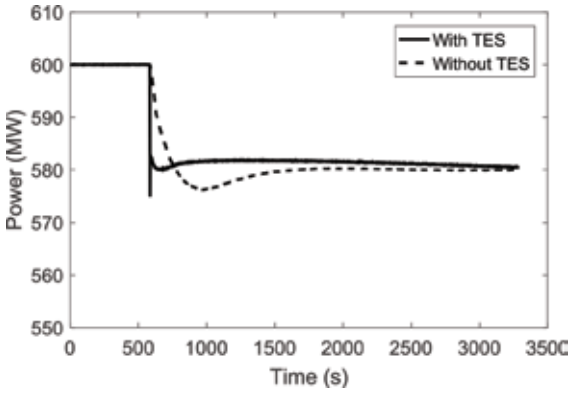

Figure 12. Off-peak period.

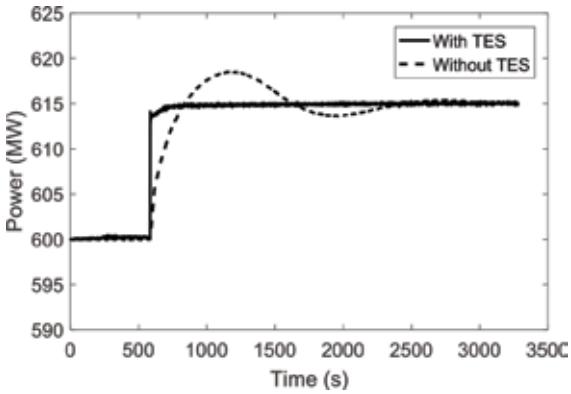

Figure 13. Peak period.

5. Conclusion

This chapter describes the simulation study of TES integration into a supercritical coal-fired power plant for efficient and flexible plant operation. Three TES charging strategies, and two TES discharging strategies were investigated. The simulation results show that it is feasible to extract thermal energy from the water-steam cycle for TES charging during the off-peak time period and to discharge the stored thermal energy back to the power generation process to water steam loop during the peak demand period to boost the power generation. According to the results, following conclusions can be drawn:

1. The flexibility of a supercritical coal-fired power plant can be improved with the TES integration.
2. For the TES charging process, the amount of the steam extraction needs to be restricted to a feasible range in order to maintain a stable power output.

3. For the first TES discharging strategy, the maximum mass flow rate of generated steam is 72.6 kg/s, and the corresponding overall output power is 644.4 MW.
4. For the second TES discharging strategy, the maximum output power is 634 MW.
5. With the TES integration, the supercritical coal-fired power plant presents faster dynamic responses to the load demand changes.

Acknowledgements

The authors gratefully acknowledge the grant support of the UK Engineering and Physical Sciences Research Council (EPSRC, EP/K021095/1, EP/L019469/1 and EP/M01536X/1). The authors wish to thank the China Scholarship Council (CSC) for the PhD scholarship. The authors would like to give our thanks to Mr. Paul Lambart from R-MC Power Recovery Ltd. and Mr. Stuart Simpson from UNIPER for their valuable technical advice. The authors want to give their thanks to the support from China National Basic Research Program 973 (2015CB251301) to enable the collaboration between the UK and China researchers.

Author details

Decai Li, Wenbin Zhang and Jihong Wang*

*Address all correspondence to: jihong.wang@warwick.ac.uk

School of Engineering, University of Warwick, Coventry, UK

References

[1] Kotowicz J, Michalski S. Efficiency analysis of a hard-coal-fired supercritical power plant with a four-end high-temperature membrane for air separation. Energy. 2014;**64**:109-119. DOI: 10.1016/j.energy.2013.11.006

[2] Som S, Datta A. Thermodynamic irreversibilities and exergy balance in combustion processes. Progress in Energy and Combustion Science. 2008;**34**:351-376. DOI: 10.1016/j.pecs.2007.09.001

[3] Narula R, Koza D, Wen H. Impacts of steam conditions on plant materials and operation in ultra-supercritical coal power plants. In: Zhang D, editor. Ultra-Supercritical Coal Power Plants. 1st ed. Cambridge: Elsevier; 2013. pp. 23-56. DOI: 10.1533/9780857097514.1.23

[4] Chalmers H, Gibbins J. Initial evaluation of the impact of post-combustion capture of carbon dioxide on supercritical pulverised coal power plant part load performance. Fuel. 2007;**86**:2109-2123. DOI: 10.1016/j.fuel.2007.01.028

[5] Lucquiaud M, Chalmers H, Gibbins J. Potential for flexible operation of pulverised coal power plants with CO_2 capture. Energy Materials. 2007;**2**:175-180. DOI: 10.1179/174892408X373536

[6] Lucquiaud M, Chalmers H, Gibbins J. Capture-ready supercritical coal-fired power plants and flexible post-combustion CO_2 capture. Energy Procedia. 2009;**1**:1411-1418. DOI: 10.1016/j.egypro.2009.01.185

[7] Lin YJ, Wong DSH, Jang SS, Ou JJ. Control strategies for flexible operation of power plant with CO_2 capture plant. AICHE Journal. 2012;**58**:2697-2704. DOI: 10.1002/aic.12789

[8] Lausterer GK. Improved maneuverability of power plants for better grid stability. Control Engineering Practice. 1998;**6**:1549-1557. DOI: 10.1016/S0967-0661(98)00116-6

[9] Zhao Y, Wang C, Liu M, Chong D, Yan J. Improving operational flexibility by regulating extraction steam of high-pressure heaters on a 660 MW supercritical coal-fired power plant: A dynamic simulation. Applied Energy. 2018;**212**:1295-1309. DOI: 10.1016/j.apenergy.2018.01.017

[10] Huebel M, Gierow C, Prause JH, Meinke S, Hassel E. Simulation of ancillary services in thermal power plants in energy systems with high impact of renewable energy. In: ASME 2017 Power Conference Joint with ICOPE-17 Collocated with the ASME 2017 11th International Conference on Energy Sustainability, the ASME 2017 15th International Conference on Fuel Cell Science, Engineering and Technology, and the ASME 2017 Nuclear Forum; 26-30 June 2017. Charlotte: American Society of Mechanical Engineers; 2017. pp. V002T08A008-V002T08A008

[11] Nuytten T, Claessens B, Paredis K, Van Bael J, Six D. Flexibility of a combined heat and power system with thermal energy storage for district heating. Applied Energy. 2013;**104**:583-591. DOI: 10.1016/j.apenergy.2012.11.029

[12] Pagliarini G, Rainieri S. Modeling of a thermal energy storage system coupled with combined heat and power generation for the heating requirements of a University Campus. Applied Thermal Engineering. 2010;**30**:1255-1261. DOI: 10.1016/j.applthermaleng.2010.02.008

[13] Li D, Hu Y, He W, Wang J. Dynamic modelling and simulation of a combined-cycle power plant integration with thermal energy storage. In: Automation and Computing (ICAC), 2017 23rd International Conference; Huddersfield. New York: IEEE; 2017. pp. 1-6

[14] Kuravi S, Trahan J, Goswami DY, Rahman MM, Stefanakos EK. Thermal energy storage technologies and systems for concentrating solar power plants. Progress in Energy and Combustion Science. 2013;**39**:285-319. DOI: 10.1016/j.pecs.2013.02.001

[15] Tian Y, Zhao C-Y. A review of solar collectors and thermal energy storage in solar thermal applications. Applied Energy. 2013;**104**:538-553. DOI: 10.1016/j.apenergy.2012.11.051

[16] Quoilin S, Aumann R, Grill A, Schuster A, Lemort V, Spliethoff H. Dynamic modeling and optimal control strategy of waste heat recovery organic Rankine cycles. Applied Energy. 2011;**88**:2183-2190. DOI: 10.1016/j.apenergy.2011.01.015

[17] Mohamed O, Wang J, Al-Duri B. Study of a multivariable coordinate control for a supercritical power plant process. In: Automation and Computing (ICAC), 2011 17th International Conference; Huddersfield. New York: IEEE; 2011. pp. 69-74

[18] Draganescu M, Guo S, Wojcik J, Wang J, Liu X, Hou G, et al. Generalized predictive control for superheated steam temperature regulation in a supercritical coal-fired power plant. CSEE Journal of Power and Energy Systems. 2015;**1**:69-77. DOI: 10.17775/CSEEJPES.2015.00009

Edited by Tolga Taner

The main aim of this study is to present power plants for all fields of industry. The chapters collected in the book are contributions by invited researchers with long-standing experience in different research areas. I hope that the material presented here is understandable to a wide audience, not only energy and mechanical engineering specialists but also scientists from various disciplines. The book contains seven chapters in two sections: (1) "Power Plants & Technical Details" and (2) "Power Plants in Different Fuels". This book shows detailed and up-to-date evaluations in different areas and was written by academics with experience in their field. It is anticipated that this book will make a scientific contribution to power plant workers, researchers, academics, MSc and PhD students, and other scientists in both the present and future.

Published in London, UK

IntechOpen

ISBN 978-1-83962-008-9